

Max Planck Institut für Kolloid- und Grenzflächenforschung  
Abteilung für Grenzflächen

---

**Modification of Nanoparticle-Surfaces for Emulsion Stabilization and  
Encapsulation of Active Molecules for Anti-Corrosive Coatings**

**Dissertation**  
zur Erlangung des akademischen Grades  
"doctor rerum naturalium"  
(Dr. rer. nat.)  
in der Wissenschaftsdisziplin "Physikalische Chemie"

eingereicht an der  
Mathematisch-Naturwissenschaftlichen Fakultät  
der Universität Potsdam

von  
Martin F. Haase

Potsdam, den 6. Juli 2011



Published online at the  
Institutional Repository of the University of Potsdam:  
URL <http://opus.kobv.de/ubp/volltexte/2011/5541/>  
URN <urn:nbn:de:kobv:517-opus-55413>  
<http://nbn-resolving.de/urn:nbn:de:kobv:517-opus-55413>

„Die meisten Menschen wollen nicht eher schwimmen, als bis sie es können.“ – Hermann Hesse

# Danksagung

Diese Arbeit wäre ohne das Zutun zahlreicher Menschen nicht auf diese Weise, oder gar überhaupt nicht zu Stande gekommen. Dafür möchte ich mich hiermit bei diesen Menschen bedanken.

Mein Doktorvater, Herr Prof. Dr. Dr. h. c. Helmuth Möhwald gehört zu den Menschen, die das Entstehen dieser naturwissenschaftlichen Arbeit erst ermöglicht haben. Dafür, dass er mir trotz meines ingenieurwissenschaftlichen Fachhochschulstudienabschlusses diese Chance gegeben und dass er mir und Anderen als Betreuer stets eine offene Tür angeboten hat, möchte ich mich herzlich bedanken. Auch meinem Arbeitsgruppenleiter Dr. Dmitry Shchukin möchte ich für diese Möglichkeit danken.

Hätte meine Mutter, Frau Rita Helene Schuth nicht während meiner Schulzeit auf mich und meine Lehrer mit so großem Engagement gewirkt, so wäre diese akademische Laufbahn wahrscheinlich nicht zu Stande gekommen, wofür ich ihr aus tiefstem Herzen dankbar bin. Auch meinem Vater, Herrn Helmut Haase und meinem Stiefvater, Herrn Harald Erwin Schuth bin ich sehr dankbar, da sie mich in schweren Zeiten dazu ermuntert haben, nicht aufzugeben. Meiner Großmutter, Frau Hildegard Haase danke ich ebenso, denn sie freut sich über jeden Anruf und Besuch ihrer Enkel und in ihrem Garten wachsen zudem die leckersten Erdbeeren. Auch meinem Bruder, Herrn Marcus Haase danke ich, da er mir als guter Freund zur Seite steht.

Für die zahlreichen wissenschaftlichen Diskussionen und für sein kritisches Hinterfragen danke ich Herrn Dr. Dmitry Grigoriev. Ebenso Herrn Dr. Klaus Tauer bin ich für Diskussionen und fachlichen Hilfestellungen sehr dankbar. Manche Erkenntnisgewinne wären ohne die vielen elektronenmikroskopischen Aufnahmen von Frau Dr. Brigitte Tiersch, Frau Dr. Tatjana Borodina und Frau Dimitriya Borisova nicht möglich gewesen. Auch für die stets freundliche und hilfsbereite Art von Frau Heidi Zastrow, Frau Annegret Praast, Frau Sabine Siegmund und Frau Anne Heilig möchte ich mich herzlich bedanken. Hätte mir Herr Jan von Szada-Borrryszkowski nicht zahlreiche materialverarbeitungstechnische Hilfestellungen geleistet, so wären einige Experimente dieser Arbeit nicht auf diese Art und Weise zu Stande gekommen. Auch Herrn Dr. Dmitry Fix und Herrn Dr. Matthias Schenderlein danke ich für Hilfestellungen bei software- oder gerätetechnischen Fragen.

Dankbarkeit und Bewunderung bringe ich Förderern und Vorbildern während meiner Studienzeit entgegen: Herr Prof. Dr. Wolfgang Seifert, Herr Prof. Dr. Hans-Dieter Kleinschrodt, Herr Prof. Dr. habil. Rainer Geike, Herr Prof. Ulrich Glinka sowie Frau Prof. Dr. habil. Sabine Enders.

Dr. Juan Jose Giner Casares danke ich für die Freundschaft, welche uns verbindet. Dr. Bernd-Reiner Paulke danke ich für zahlreiche Gespräche und Diskussionen. Herrn Janós Keller danke ich für die gelungene Teamarbeit in unserem musikalischen Labor. Mit Herrn Dr. Martin Hollamby gab es zahlreiche wissenschaftliche Diskussionen, welche mir sehr nützlich waren. Frau Dr. Darya Radziuk danke ich für eine angenehme gemeinsame drei-jährige Zeit in unserem Büro. Herrn Dr. Thorsten Sievers danke ich für Hilfestellungen bei vielerlei labortechnischen Angelegenheiten. Für ihr Verständnis und ihre Anregungen danke ich Frau Julia Schneider. Frau Bettina Borchert danke ich für ihre Versorgung mit verrückter Musik und Herrn Victor Naumov und Herrn Andreas Reimer für die uns verbindende gute Freundschaft.

---

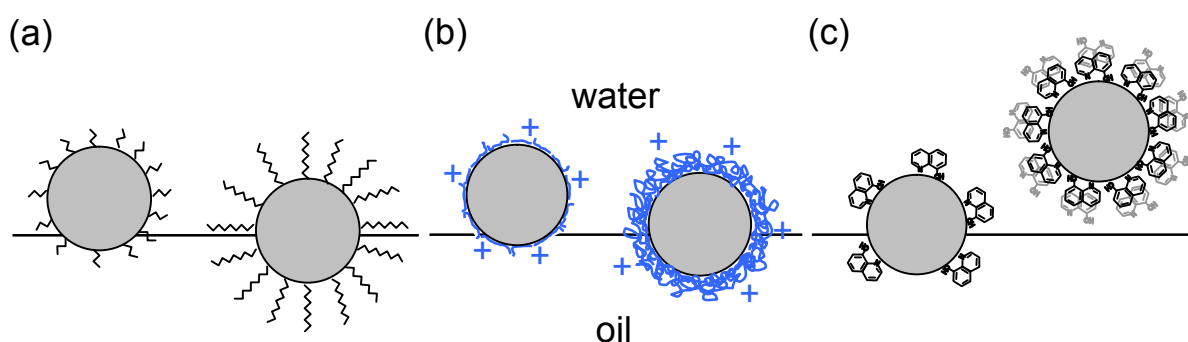
Abstract .....	7
List of Abbreviations .....	10
Introduction .....	11
<b>1 Fundamentals and Literature Survey .....</b>	<b>15</b>
1.1 Solid particles at liquid-liquid interfaces .....	15
1.1.1 The three phase contact angle governs the energy of attachment.....	15
1.1.2 The contact angle determines the preferred emulsion type.....	20
1.1.3 Stability of particle coated emulsion-droplets .....	21
1.1.4 Interactions between interfacially attached particles .....	26
1.1.5 Methods of particle hydrophobization: literature survey .....	29
1.2 Polyelectrolytes .....	32
1.2.1 Dependency of the conformation on the solvent quality .....	32
1.2.2 Determination of the properties of adsorbed films through conformation .....	34
1.3 Anticorrosive coatings .....	34
<b>2 Experimental methods .....</b>	<b>37</b>
2.1 Materials.....	37
2.2 Determination of the 8-hydroxyquinoline partitioning and adsorption .....	37
2.3 Cryogenic SEM.....	39
2.4 Dynamic light scattering and $\zeta$ -potential .....	39
2.5 Contact angle measurements.....	40
2.6 Droplet size measurements .....	41
2.7 Particle attachment onto droplets.....	42
2.8 Polyelectrolyte adsorption procedure.....	42
2.9 Preparation of particle stabilized emulsions, core-polymerization and transfer to the waterborne alkyd-resin.....	44
2.10 Aluminium plates pre-treatment and dip-coating .....	45
2.11 Electrochemical impedance spectroscopy .....	45
2.12 Scanning vibrational electrode technique .....	47
2.13 Confocal laser scanning microscopy.....	48
2.14 Du Noüy ring tensiometry.....	49

---

3	Results and discussion .....	50
3.1	Short Amphiphiles .....	50
3.1.1	Contact angle measurements.....	50
3.1.2	Results of fluid-fluid interfacial tension measurements .....	52
3.1.3	Calculation of the surface energy of the solid.....	53
3.2	Weak Polyelectrolytes.....	58
3.2.1	Characterization of weak polyelectrolyte coated nanoparticles.....	58
3.2.2	Contact angle measurements on PMAA coated alumina plates .....	62
3.2.3	Characterization of nanoparticle stabilized emulsions.....	63
3.3	8-Hydroxyquinoline .....	74
3.3.1	Physicochemical properties 8-hydroxyquinoline.....	74
3.3.2	Properties of silica nanoparticles uncoated and modified with 8-HQ .....	76
3.3.3	Characterization of nanoparticle stabilized emulsions.....	82
3.4	Inhibitor loaded silica/polymer composites .....	92
3.4.1	Bulk polymerization of the 8-HQ and MBTA concentrated monomer-solution .....	92
3.4.2	Polymer and particle size distributions .....	93
3.4.3	8-hydroxyquinoline release in aqueous solution.....	98
3.4.4	Incorporation of the particles in a water-based alkyd resin .....	99
3.4.5	Estimation of the percentage of 8-HQ dissolved in the water-phase of the resin....	101
3.4.6	Passive anticorrosive properties.....	103
3.4.7	Active Anticorrosive properties .....	106
4	Summary and conclusion.....	108
5	References .....	112

## Abstract

Within this work, three physicochemical methods for the hydrophobization of initially hydrophilic solid particles are investigated (see Scheme 1). The modified particles are then used for the stabilization of oil-in-water (o/w) emulsions. For all introduced methods electrostatic interactions between strongly or weakly charged groups in the system are essential. Therefore, in particular the influence of the degree of dissociation of these groups on the properties of the modified particles and the emulsions stabilized by these particles is analyzed.



**Scheme 1.** Wettability of colloidal particles modified with (a) trimethylalkylammonium bromides with different chain lengths, (b) an adsorbed weak polyelectrolyte layer with different thicknesses (c) different amounts of adsorbed 8-hydroxyquinoline

(i) Short chain alkylammonium bromides (C4 – C12) adsorb on oppositely charged solid particles and enable their interfacial activity. Macroscopic contact angle measurements of water droplets under air and hexane on flat silica surfaces in dependency of the surface charge density and alkylchain-length allow the calculation of the surface energy and give insights into the emulsification properties of solid particles modified with alkyltrimethylammonium bromides (Scheme 1(a)). The measurements show an increase of the contact angle with increasing surface charge density, due to the enhanced adsorption of the oppositely charged alkylammonium bromides. Contact angles are higher for longer alkylchain lengths. The surface energy calculations show that in particular the surface-hexane or surface-air interfacial energy is being lowered upon alkylammonium adsorption, while a significant increase of the surface-water interfacial energy occurs only at long alkyl chain lengths and high surface charge densities.

(ii) The thickness and the charge density of an adsorbed weak polyelectrolyte layer (e.g. PMAA, PAH) influence the wettability of nanoparticles (e.g. alumina, silica, see Scheme 1(b)). Furthermore, the isoelectric point and the pH range of colloidal stability of particle-polyelectrolyte composites depend on the thickness of the weak polyelectrolyte layer. Silica nanoparticles with adsorbed PAH and alumina nanoparticles with adsorbed PMAA become interfacially active and thus able to stabilize o/w emulsions when the degree of dissociation of the polyelectrolyte layer is below 80 %. The average droplet size after emulsification of dodecane in water depends on the thickness and the degree of dissociation of the adsorbed PE-layer. A minimum can be found when 15 to 45% of the monomer units are dissociated. The visualization of the particle-stabilized o/w emulsions by cryogenic SEM shows that for colloiddally stable alumina-PMAA composites the oil-water interface is covered with a closely packed monolayer of particles, while for the colloiddally unstable case closely packed aggregated particles deposit on the interface. In both cases the particles can aggregate on the oil-water interface due to their close approach. The vigorous effects of sonication during emulsification are capable of removing such aggregated domains from the interface to the bulk liquid.<sup>1</sup>

(iii) By emulsifying a mixture of the corrosion inhibitor 8-hydroxyquinoline (8-HQ) and styrene with silica nanoparticles a highly stable o/w emulsion can be obtained in a narrow pH window (Scheme 1(c)). The amphoteric character of 8-HQ enables a pH dependent electrostatic interaction with silica nanoparticles, which can render them interfacially active. Depending on the concentration and the degree of dissociation of 8-HQ the adsorption onto silica results from electrostatic or aromatic interactions between 8-HQ and the particle-surface.<sup>2</sup> At intermediate amounts of adsorbed 8-HQ the oil wettability of the particles becomes sufficient for stabilizing o/w emulsions. Cryogenic SEM visualization shows that the particles arrange then in a closely packed shell consisting of partly of aggregated domains on the droplet interface. For further increasing amounts of adsorbed 8-HQ the oil wettability is reduced again and the particles ability to stabilize emulsions decreases. The visualization of droplets shows then non-closely packed particle shells on the interface.

The addition of hexadecane to the oil phase enables the formation of submicrometer sized miniemulsion-droplets upon emulsification. Their size is easily controllable by the silica particle mass-fraction. Subsequent polymerization produces corrosion inhibitor filled (20 wt-%) polystyrene-silica composite particles. Radically initiated polymerization yields polymers with number averaged molecular masses between 40 to 50 kDa. The measurement of the release of 8-

hydroxyquinoline shows a rapid increase of 8-hydroxyquinoline in a stirred aqueous solution indicating the release of the total content in less than 5 minutes. The method is extended for the encapsulation of other organic corrosion inhibitors. The silica-polymer-inhibitor composite particles are then dispersed in a water based alkyd emulsion, and the dispersion is used to coat flat aluminium substrates. After drying and cross-linking the polymer-film Confocal Laser Scanning Microscopy is employed revealing a homogeneous distribution of the particles in the film. Electrochemical Impedance Spectroscopy in aqueous electrolyte solutions shows that films with aggregated particle domains degrade with time and don't provide long-term corrosion protection of the substrate. However, films with highly dispersed particles have high barrier properties for corrosive species. The comparison of films containing silica-polystyrene composite particles with and without 8-hydroxyquinoline shows higher electrochemical impedances when the inhibitor is present in the film. An equivalent electrical circuit representing reasonably the measured data is found to be a series circuit of a resistance with a parallel circuit of a second resistance and a capacitance. By applying the Scanning Vibrating Electrode Technique the localized corrosion rate in the fractured area of scratched polymer films containing the silica-polymer-inhibitor composite particles is studied. Electrochemical corrosion cannot be suppressed but the rate is lowered when inhibitor filled composite particles are present in the film.

By depositing six polyelectrolyte layers on particle stabilized emulsion droplets their surface morphology changes significantly as shown by SEM visualization. When the oil wettability of the outer polyelectrolyte layer increases, the polyelectrolyte coated droplets can act as emulsion stabilizers themselves by attaching onto bigger oil droplets in a closely packed arrangement.

In the presence of 3 mM LaCl<sub>3</sub> 8-HQ hydrophobized silica particles aggregate strongly on the oil-water interface. The application of an ultrasonic field can remove two dimensional shell-compartments from the droplet surface, which are then found in the aqueous bulk phase. Their size ranges up to 1/4<sup>th</sup> of the spherical particle shell.

1. Haase, M. F.; Grigoriev, D.; Moehwald, H.; Tiersch, B.; Shchukin, D. G., Nanoparticle Modification by Weak Polyelectrolytes for pH-Sensitive Pickering Emulsions. *Langmuir*, 2011, 27, (1), 74-82.
2. Haase, M. F.; Grigoriev, D.; Moehwald, H.; Tiersch, B.; Shchukin, D. G., Encapsulation of Amphoteric Substances in a pH-Sensitive Pickering Emulsion. *J. Phys. Chem. C*, 2010, 114, (41), 17304-17310.

## List of Abbreviations

4-VP	4-vinylpyridine	$R_D$	droplet radius
8-HQ	8-hydroxyquinoline	SEM	scanning electron microscopy
$A_{8HQ,silica}$	adsorbed amount 8HQ on silica	SVET	scanning vibrating electrode techn.
AIBN	azo-bis-(isobutyronitrile)	T	absolute temperature
ATAB	alkyltrimethylammonium bromide	U	voltage
C	capacitance	$U_\gamma$	intrinsic surface energy
c.f.pH	critical flocculation pH	V	volume
cfc	crit. flocculation cocentration	$V_M$	molecular volume
CLSM	confocal laser scanning microscopy	w	weight fraction
cmc	critical micelle concentration	$w_i$	interaction parameter (reg sol.theory)
c	concentration, g/ml	$W_{AB}$	interaction energy betw. mol.A and B
D	drop diameter	x	radius of contact line
d	particle diameter	$x_{oil}$	mole fraction oil
DEP	diethylphthalate	Z	impedance
DLS	dynamic light scattering	$z_b$	number of neighboured molecules
EIS	electrochemical impedance spectrosc.		
FRA	frequency response analyzer		
G	free energy	<b>Greek symbols</b>	
GPC	gel permeation chromatography	$\alpha$	degree of dissociation
HD	hexadecane	$\gamma$	interfacial tension
IEP	isoelectric point	$\theta$	contact angle
I	current	$\vartheta$	hexagonal packing factor
k	Boltzmann constant	$\lambda$	wavelength
$l_p$	persistence length	$\mu$	chemical potential
m	mass	$\rho$	density
M	molecular mass	$\tau$	line tension
MBTA	mercaptobenzotriazol	$\varphi$	phase shift
ML	multilayer	$\chi$	chi-parameter
$M_N$	number averaged molecular mass	$\omega$	angular frequency
$M_W$	mass averaged molecular mass		
n	amount of substance	<b>Indices</b>	
$N_{av}$	Avogadro number	0	amplitude value or state 0
$n_C$	number of carbon atoms	a	attachment
p, z	Kaptay functions	c	critical
PAA	poly(acrylic acid)	co	composition
PAH	poly(allylamine hydrochloride)	cont	continuous
$P_{max}^C$	maximum capillary pressure	d	detachment
PDI	polydispersity index	D	droplet
PE	polyelectrolyte	d	dispersive (superscript)
pH <sub>C</sub>	pH value during PE coating	o	oil
PMAA	poly(methacrylic acid)	org	organic
PSE	particle stabilized emulsion	p	particle
PSS	poly(styrene sulfonate)	p	polar (superscript)
r	particle radius	s	solid
R	resistance	sty	styrene
$R_{crit}$	critical drop radius	su	surface
		w	water

### Introduction

An air bubble passing through a suspension can collect solid particles on its surface and retain those on its way. Numerous particle coated air bubbles together will ascend and create a stable foam phase without additional stabilizers. Emulsion droplets can be stabilized against coalescence virtually indefinitely by the deposition of solid particles on the liquid-liquid interface. The droplets can be deformed dramatically, and have grotesque, non spherical shapes. In both cases the particles can be very persistent in resisting removal to the bulk phases and can be virtually irreversibly attached to the interface. A dense particle crust on the interface can be formed and interfacial aggregation may lead to mechanical rigidity of the object. Such observations were published first by Walter Ramsden in 1903<sup>3</sup> and Spencer Umfreville Pickering in 1907<sup>4</sup>. In the abstract of Pickering's paper the pioneer work of Ramsden was acknowledged, but nevertheless the term "Pickering Emulsions" has been established, since then, likely due to the circumstance "*that some of those later scientists did not actually obtain a copy of Pickering's paper, relying on previous citations to it*".<sup>5</sup> Pickering also recognized the importance of the particle wettability by the two immiscible liquids for the type of an emulsion. Depending on whether the oil or the water is the dispersed phase of an emulsion, it is named oil-in-water (o/w) or water-in-oil (w/o) emulsion. In 1923 it was postulated by Finkle, et al.<sup>6</sup> that the liquid with the poorer wettability on the surface of the stabilizing particles becomes the dispersed phase of a particle stabilized emulsion (PSE). This was experimentally confirmed in the paper of Schulmann and Leja in 1953.<sup>7</sup> Surprisingly, only very few articles about the topic followed until it was revitalized by Gelot et al. (1984)<sup>8</sup>, Levine and Sanford (1985)<sup>9</sup> and later Menon and Wasan (1986)<sup>10, 11</sup>. The two latter authors in particular were inspired by the problems that particle stabilized w/o emulsions create during crude oil recovery in petroleum industry. Here, a mixture of crude oil, water and fine inorganic particles are emulsified due to high shear stresses in valves and pipes during the process. Adsorption of asphaltenes and/or resins on inorganic clay and sand particles enables the formation of solid stabilized water-in-oil emulsions<sup>12</sup>, which results in a variety of problems for the oil-refining process, including fouling, corrosion, oil losses or catalyst poisoning.

However, solid stabilized emulsions and foams can also be desirable, as for example in the case of food emulsions like mayonnaise, where egg-yolk particles with sizes of around 1  $\mu\text{m}$  stabilize an oil-in-water emulsion<sup>13</sup>. Another important application of particles at fluid interfaces is the froth flotation of mixtures of fine particles. In this process, air bubbles ascend through an aqueous

suspension and collect selectively only the particle fraction with moderate hydrophobic surface properties. Such surface properties can be natural (coal, graphite) and adjustable by the presence of electrolytes<sup>14</sup> and the pH value<sup>15</sup>, or they can be obtained by selective adsorption of surfactants (frothers) on initially hydrophilic particles (e.g. minerals)<sup>16</sup>.

The two main requirements to obtain a particle stabilized emulsion are “(i) *the particles must be smaller than the droplets and (ii) the particle surface must be partially wettable by both oil and water.*”<sup>17</sup> The attachment of solid particles on liquid-liquid or liquid-gas interfaces is similar to the behaviour of surfactant molecules. Surfactant molecules consist of an oil soluble nonpolar hydrocarbon chain and a water soluble polar head group. This amphiphilic character enables their adsorption behaviour to interfaces between polar and nonpolar fluids. For a solid particle the properties of its outer surface determine the interaction with fluid interfaces. Especially the chemical composition and thereby the compatibility with the two immiscible fluids governs the particle affinity to the interface. Particles can only act as emulsifiers when their surface chemistry and morphology offers wettability for both immiscible liquids. If this is the case and the particles initially dispersed in liquid (a) come into contact with the liquid-liquid interface, then they immerse partially into liquid (b). However, compared to surfactant molecules solid particles do not need an amphiphilic surface with clearly separated hydrophilic and hydrophobic sides (Janus particles) for behaving surface active. Even though hydrophobic and hydrophilic domains are distributed homogeneously over the surface, such an affinity to an interface exists.

During the last decade the ability of different types of nanoparticles to stabilize emulsions has been investigated in many works. Powders or aqueous suspensions of commercial oxide nanoparticles are available inexpensively nowadays. But due to their hydrophilic character they cannot act as emulsion stabilizers themselves. A suitable surface modification is required to render such particles interfacially active. This can be achieved by the reduction of the overall polarity of the surface for instance by the introduction of hydrophobic moieties onto the surface. Therefore, covalent chemistry or more facile physicochemical methods like e.g. the physisorption of organic molecules can be applied. The latter option especially allows reversible surface modifications and enables thereby stimuli-responsive emulsion characteristics. Thus, changes in the external conditions (concentration, pH-value, temperature ...) can enable or disable the emulsification ability of the nanoparticles, which can be interesting for technical applications. It is one aim of this work, to study in particular effects of pH dependent charges on stimuli-responsive emulsification properties of nanoparticles. Those effects can for instance result from the interaction of dissolved organic molecules with a hydrophilic surface. Depending whether the surface attracts these molecules,

adsorption and consequently a change of wettability occurs or not. When a charged surface and/or oppositely charged molecules have a pH dependent dissociation the electrostatically driven adsorption becomes also pH dependent. Thereby this method allows for the stabilization or destabilization of PSE controlled by the pH value (see chapter 3.3).

Also organic polymers with acid or base groups attached to the surface can enable pH dependent emulsification properties of particles. Some research papers have introduced such particles for the emulsification of nonpolar oils in water at neutral to alkaline pH values.<sup>18-20</sup> It is of interest to extend this concept for nonpolar oils also to pH values below 6. Polyelectrolyte (PE) adsorption onto planar and particle surfaces has been an important field of research since a long period of time. The ability of PEs to improve dispersibility of different powders in water has been shown in several publications,<sup>21-23</sup> and since Decher and Hong<sup>24</sup> introduced the layer-by-layer technique, many more applications of polyelectrolyte adsorption have been developed. Novel is the herein introduced approach to use the electrostatically driven adsorption of weak polyelectrolytes on nanoparticles for controlling their emulsification ability (see chapter 3.2).

The changes of the wettability of nanoparticle-surfaces upon modification can be qualitatively represented by their macroscopic flat analogues by means of contact angle measurements. On the basis of this method the different energetic contributions to the wetting phenomena can be obtained and used for the quantitative understanding of a PSE (see chapter 3.1)

Since particle stabilized droplets resemble core shell architectures, they have a high potential to be applied in the field of active molecule encapsulation, e.g. for drug delivery. An economically attractive aspect is the simplicity of the fabrication procedure of such “particle stabilized capsules”. In principle only the components (solid, oil, water) need to be mixed and the application of high shear rates generates capsules with adjustable size. In comparison to surfactant based capsule production no need of subsequent purification from excess surfactants is required since by choosing the right process-parameters all solids self-assemble on the available oil-water interface. As mentioned before the presence of particle hydrophobizing-agents can be required thereby complicating the system. An attempt to compensate for this is the introduction of multifunctional molecules to the system. This is the case when e.g. compartments of the oil or the encapsulated active molecules themselves take over the particle hydrophobization (see chapters 3.3 and 3.4).

Beside the traditional encapsulation of pharmaceuticals for drug-delivery systems another application of active molecule encapsulation has emerged recently: The incorporation of corrosion-inhibitors into micro- or nanometre sized reservoirs in anti-corrosive coatings for metallic substrates. Coatings with such finely dispersed inhibitor reservoirs maintain their barrier properties

against the diffusion of corrosive species and can enhance the long-term protection of the metallic substrate. Furthermore such coatings can potentially have self-healing properties by means of the release of corrosion-inhibitors at damaged sites of the coating. The most prominent corrosion inhibitors are salts of hexavalent chromium, which are used frequently in the industry world-wide. This strongly oxidative ion is inhibiting corrosion efficiently, but is also carcinogenic to humans and animals. It is therefore desired to find substitutions. Potential alternatives can be organic corrosion inhibitors. An attempt for the encapsulation of one typical organic corrosion inhibitor in a PSE is shown in chapters 3.3 and 3.4 and the method will also be generalized for other organic inhibitor molecules.

Another environmental issue in the coating industry is the aim to reduce the usage of volatile organic solvents for resins. Hence, it is of high interest to improve the properties of water-borne coatings to become evenly effective and versatile. One possible way to do so is the addition of PSE-based capsules containing organic corrosion inhibitors to such coatings. In chapter 3.4 an evaluation of this approach by combining different measurement techniques will be applied.

# 1 Fundamentals and Literature Survey

## 1.1 Solid particles at liquid-liquid interfaces

### 1.1.1 The three phase contact angle governs the energy of attachment

Sessile water droplets on solid surfaces under a nonpolar fluid (air, oil) can have different shapes, which are determined by the three phase contact angle  $\theta$ .  $\theta$  depends on the oil-water interfacial tension, the chemical composition and the morphology of the surface. On hydrophobic surfaces, e.g. polyethylene, water droplets have  $\theta > 90^\circ$ , as is the case for droplet (1) in Figure 1(a). By decreasing the hydrophobicity of the surface,  $\theta$  decreases. A droplet with  $\theta = 90^\circ$  can be observed when the surface is wetted equally by water and oil (droplet (2)). A further decrease in hydrophobicity leads to  $\theta < 90^\circ$  (droplet (3), e.g. alumina, silica).

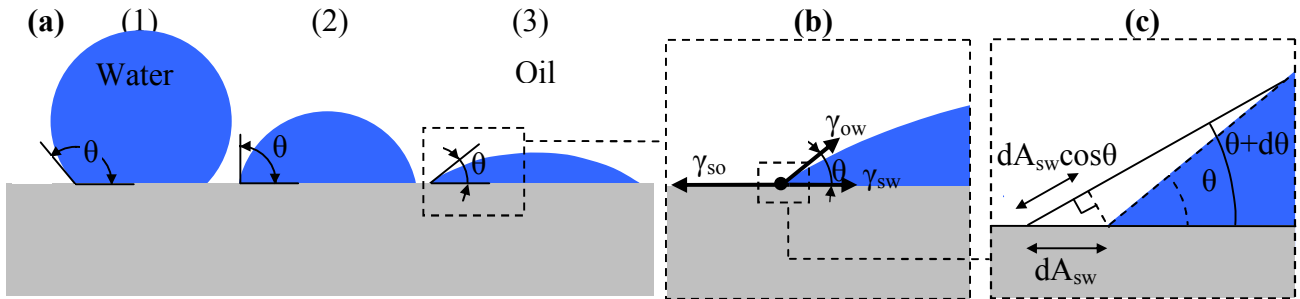


**Figure 1.** (a) Water droplets with different contact angles  $\theta$  under oil on a solid surface. (b) Sectional zoom of droplet (3) including the surface tensions acting on the three phase contact line. (c) geometrical construction of an infinitesimal decrease of  $\theta$ .

In Figure 1(b) the interfacial tensions  $\gamma_{so}$  (solid-oil),  $\gamma_{sw}$  (solid-water) and  $\gamma_{ow}$  (oil-water) are implemented at the three phase contact line, which can be represented by a point for a symmetrical droplet. These surface energies determine the droplets'  $\theta$  which can be derived by considering a droplet with  $\theta$  in equilibrium as shown in Figure 1(c). By decreasing  $\theta$  slightly by  $d\theta$ , an increase of the water-oil surface area  $dA_{wo}$  occurs. Simultaneously, the solid-water contact area increases to the same extent as the solid-oil area decreases. The construction of a right-angled triangle gives the proportionality to the water-solid surface increase  $dA_{sw}$  through

$$dA_{wo} = dA_{sw} \cos \theta \quad (1.1)$$

With the interfacial tensions and (1.1), we can write the energy increment related to the surfaces

$$dU_\gamma = \gamma_{ow} dA_{ow} + (\gamma_{sw} - \gamma_{so}) dA_{sw} = [\gamma_{ow} \cos \theta + \gamma_{sw} - \gamma_{so}] dA_{sw} \quad (1.2)$$

In equilibrium the energy does not change  $dU_\gamma = 0$ , hence the expression in brackets corresponds to the Young equation (1.3) for a sessile water droplet under oil

$$\gamma_{so} = \gamma_{sw} + \gamma_{ow} \cos \theta \quad (1.3)$$

Due to the local approach of the Young equation, it is also applicable for a colloidal particle after attachment to the oil water interface as shown in Figure 2(b). In this case, it is not the movement of the water but the positional change of the particle determining the equilibrium  $\theta$ . Here  $\theta$  is conventionally always measured through the aqueous phase.

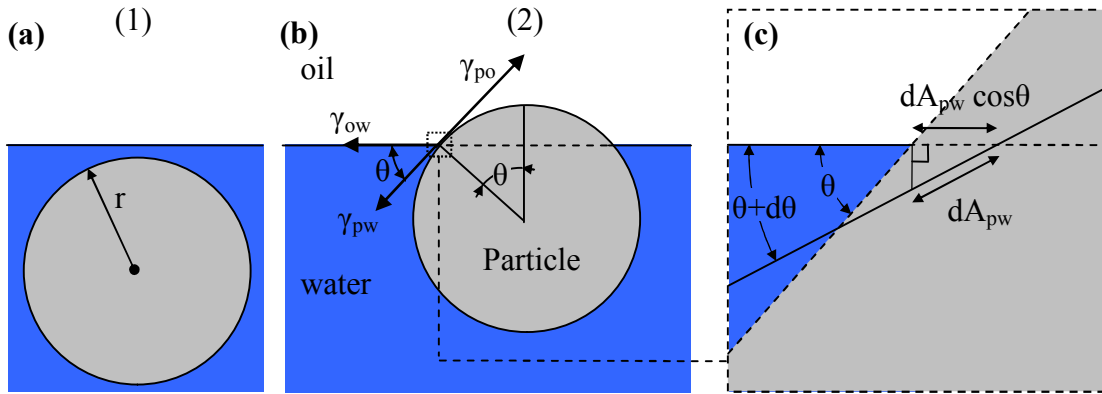


**Figure 2.** (a) Solid spherical particle with radius  $r$  completely immersed in the water phase as state (1). The particle attaches to the oil-water interface and develops the contact angle  $\theta$  in state (2). (c) Zoomed section around the three phase contact point

In Figure 2(b) no deformation of the liquid interface, nor the formation of a meniscus around the particle is assumed. This holds true for smooth particles<sup>25</sup>, particles with size  $< 10 \mu\text{m}$ <sup>26</sup> and in the absence of strong electrostatic interactions across the nonpolar liquid<sup>27</sup>.

When there is no  $\theta$  hysteresis present and effects of line-tension can be neglected, a similar construction as in Figure 1(c) can be done for a particle resting at a water-oil interface. By moving the particle infinitesimally towards the water-phase,  $\theta$  decreases by  $d\theta$  as shown in the zoomed section of the three phase contact line in Figure 2(c). Here the dashed line represents the original

position of the solid surface and the continuous line the new position. Due to the spherical shape of the solid surface, the pictured section of the surface not only moves down but also turns by  $d\theta$ . Because of the infinitesimal dimensions, the surface can be depicted by an even line. A right angled triangle can be constructed to obtain the analogue expression of equation (1.4) by the same derivation as before.

$$\gamma_{po} = \gamma_{pw} + \gamma_{ow} \cos \theta \quad (1.4)$$

In the following the energy of attachment for a colloidal particle on the water-oil interface will be derived without considering the effects of gravity. The derivation was first published by Koretsky and Kruglyakov in 1971<sup>28</sup> and can also be found in other publications<sup>17, 29</sup> and text books<sup>5, 30</sup>.

When the particle is completely surrounded by water (state (1)), the surface free energy can be expressed by

$$G^{(1)} = \gamma_{ow} A_{ow}^{(1)} + \gamma_{pw} A_{pw}^{(1)} \quad (1.5)$$

with  $A_{ow}^{(1)}$  the interfacial area between oil-water and  $A_{pw}^{(1)}$  the area of the particle water interface. When the particle attaches to the oil-water interface in state (2), the particle makes up a surface with the oil-phase  $A_{po}^{(2)}$ , and for a negligible line tension contribution, the surface free energy is given by

$$G^{(2)} = \gamma_{ow} A_{ow}^{(2)} + \gamma_{pw} A_{pw}^{(2)} + \gamma_{po} A_{po}^{(2)} \quad (1.6)$$

The particle-water surface  $A_{pw}^{(2)}$  equals the total surface area of the particle and can be written as

$$A_{pw}^{(1)} = A_p = A_{pw}^{(2)} + A_{po}^{(2)} \quad (1.7)$$

By subtracting equation (1.7) from equation (1.6) and considering equations (1.4) and (1.7), the free energy change due to the particle attachment (a) from the water phase (w) can be written as

$$\Delta G_{aw} = G^{(2)} - G^{(1)} = \gamma_{ow} \Delta A_{ow} + \gamma_{ow} A_{po}^{(2)} \cos \theta \quad (1.8)$$

where  $\Delta A_{ow} = A_{ow}^{(2)} - A_{ow}^{(1)}$  equals the negative area of the oil-water interface occupied by the particle. The first term represents the decrease of surface energy for the fluid-fluid interface, while the latter corresponds to the energy increase of the solid-oil interface. Equation (1.8) can be used for a particle with an arbitrary shape. In the following, a spherical particle attached to the interface (Figure 2(b)) will be considered.  $\Delta A_{ow}$  can be expressed with the particle radius  $r$  as  $\Delta A_{ow} = -\pi(r \sin \theta)^2$  and the particle-oil contact surface is defined as a spherical cap by  $A_{po}^{(2)} = 2\pi r^2(1 - \cos \theta)$  due to the equivalence of the inscribed angle and  $\theta$  (only for flat liquid surfaces) as shown in Figure 2(b). Combining these geometrical expressions with equation (1.8) and employing the trigonometric identity  $\sin^2 \theta + \cos^2 \theta = 1$  yields the free energy of attachment for a spherical particle from the water phase:<sup>28</sup>

$$\Delta G_{aw} = -\pi \cdot r^2 \gamma_{ow} (1 - \cos \theta)^2 \quad (1.9)$$

A similar equation can be obtained for the attachment from the oil phase, which has a plus sign instead of a minus sign in the brackets of equation (1.9). A particle exclusively wetted by water ( $\theta = 0^\circ$ ) does not change the systems free surface energy. By increasing the oil wettability of the particle (increasing  $\theta$ ) the free surface energy of the system is reduced by  $\Delta G_{aw}$  due to the particle attachment. It reaches  $\Delta G_{aw} = -\pi \cdot r^2 \gamma_{ow}$  at  $\theta = 90^\circ$ , which equals the reduction of the oil-water surface energy by the removal of the surface occupied by the particle. Above  $90^\circ$ , the particle is more wetted by oil than water and the surface energy is further reduced by immersing more into the oil phase. From the second power of the radius in equation (1.9) it follows that for bigger particles the reduction of the surface energy is much greater for the same  $\theta$ . When inserting a typical interfacial tension for oil-water of 50 mN/m into equation (1.9) and assuming a partially hydrophobic colloidal particle with  $\theta = 60^\circ$  and  $r = 30$  nm the reduction of  $\Delta G_{aw}$  expressed in the thermal energy  $k \cdot T$  at  $25^\circ\text{C}$  ( $k$  – Boltzmann constant,  $T$  – absolute temperature) equals around - 8600 kT per particle. For comparison, surfactant molecules typically have adsorption energies of the order of 1 - 20 kT and maintain a dynamic adsorption/desorption equilibrium at water-oil interfaces. The deep adsorption energy well of a particle can be interpreted as a quasi-irreversibly adsorbed state and explains why partially wettable colloidal particles form a hexagonally densely packed surface coverage on oil-water interfaces. The interfacial energies upon particle attachment are shown in Figure 3 in dependence of  $\theta$ .

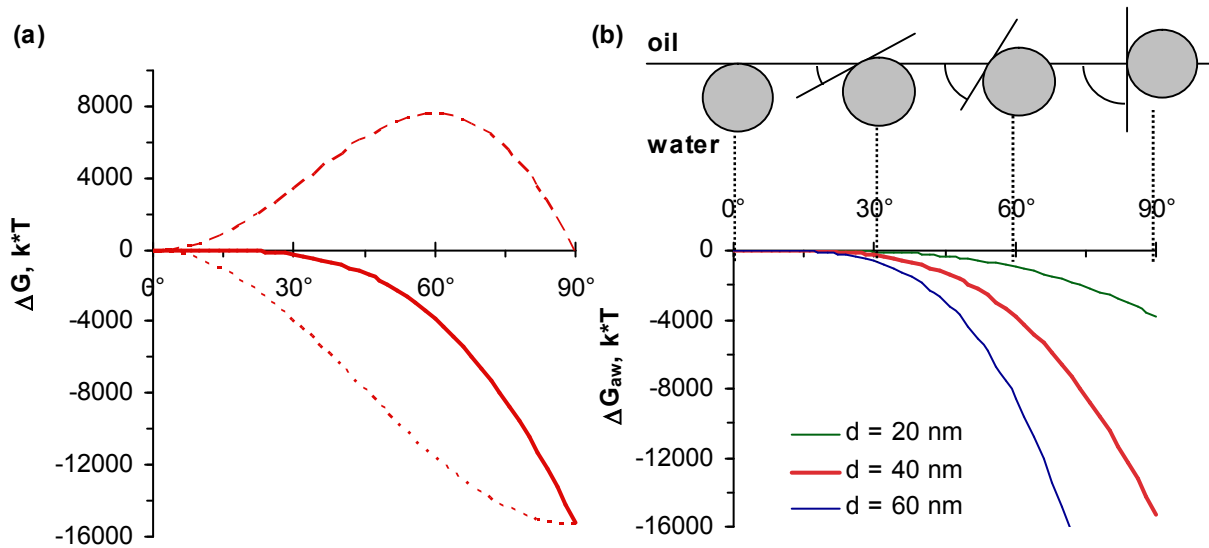


**Figure 3.** Dependence of the interfacial energies upon attachment of a spherical solid particle to an oil-water interface on the contact angle  $\theta$ . **(a)** long-dashed: energy gain of the solid interface, short-dashed: energy reduction of the oil-water interface, continuous: energy of attachment (sum of both) **(b)** energy of attachment for different particle diameters, all curves for  $\gamma_{ow} = 50$  mN/m

As can be seen from Figure 3(a), the interfacial energy for the solid surface is always positive with the exception of  $\theta = 0^\circ$  and  $\theta = 90^\circ$ . Except for  $\theta = 0^\circ$ , the energy-loss upon the reduction of the oil-water surface is bigger at all  $\theta$ . Thus, the energy of attachment is negative and favours particle attachment.  $\Delta G_{aw}$  for particles with  $\theta < 15^\circ$  is comparable to their thermal energy. Once attached, such particles detach rapidly and cannot be used as emulsion stabilizers. The energy gain for the solid surface reaches a maximum at  $\theta = 60^\circ$  and decreases above this value. This is the main reason for the strong decrease of  $\Delta G_{aw}$  above  $\theta > 60^\circ$ . Above  $\theta > 90^\circ$ , the particle is more immersed in oil than in water. Therefore it is not the reduction of the interfacial energy between the two liquids but the one between the water and the hydrophobic particle, which dominates the energy decrease. The more negative  $\Delta G_{aw}$  with increasing particle-diameter (Figure 3(b)) explains the higher emulsion stability for bigger particles. To characterize the stability of an emulsion, the consideration of the energy of detachment  $\Delta G_d = -\Delta G_a$  is useful. When  $\Delta G_d$  is plotted versus  $\theta$ , the detachment to the oil phase  $\Delta G_{do}$  must be considered, too. Because  $\Delta G_d$  is always positive (except for  $\theta = 0$ ) the graph in Figure 3 is mirrored along the  $\theta$ -axis and the consideration of the detachment to oil is obtained by mirroring  $\Delta G_{dw}$  along the vertical line at  $\theta = 90^\circ$ .

Aveyard et al.<sup>31</sup> considered the possible relevance of line tension effects on the energy of attachment  $\Delta G_a$  for nanoparticles. To account for such effects, the Young-equation (1.4) must be

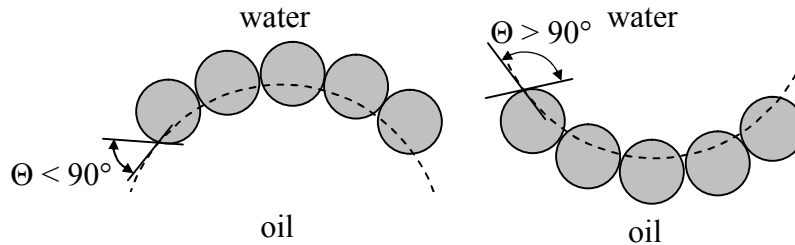
rewritten and the additional term  $2\pi x\tau$  must be included in the sum in equation (1.6). Herein  $x$  is the radius of the spherical contact line of oil-water-solid and  $\tau$  is the line tension. Moreover, macroscopic  $\theta$  (Figure 1) differ from the  $\theta$  for nanoparticles at fluid-fluid interfaces in the presence of line tension.<sup>32</sup> Positive line tensions tend to reduce the length of the contact line, thereby moving  $\theta$  away from  $90^\circ$  ( $\theta$  is reduced for  $\theta < 90^\circ$  and increased for  $\theta > 90^\circ$ ), while for negative line tension the opposite is true. Exact values of  $\tau$  are not known, but it is believed that realistic values lie in the range between  $+1 \times 10^{-10}$  N and  $-1 \times 10^{-10}$  N. For nanoparticles (size  $< 100$  nm), the energetic contribution of the line tension can render  $\Delta G_a$  positive for low values of  $\theta$  and thereby inhibit the particle attachment to the interface. For a given  $\theta$  a critical  $\tau_c$  exists, at which  $\Delta G_a$  becomes zero. The lower the interfacial tension  $\gamma_{ow}$ , the lower  $\tau_c$ , in other words particles attached to oil-water interfaces with low  $\gamma_{ow}$  are more sensitive to line tension effects. This result is obvious because of the smaller energy loss for lower  $\gamma_{ow}$  upon reduction of the oil-water interfacial area due to particle attachment.

The partitioning of particles with  $\theta$  around  $90^\circ$  and of reasonable sizes ( $> 5$  nm) between the bulk phases can be considered to take place exclusively in the phase which has the better wettability on the particles ( $\theta < 90^\circ$  water,  $\theta > 90^\circ$  oil). This results from the high energy (compared with  $kT$ ) that such particles gain upon complete immersion in the phase with the poorer wettability.<sup>31</sup>

### 1.1.2 The contact angle determines the preferred emulsion type

As already mentioned in the introduction, Finke et al.<sup>6</sup> were the first who described correctly, for the case of a closely packed particle layer on a liquid-liquid interface, the preference of the liquid with the poorer wettability on the particles to become the disperse phase of an emulsion. The situation is similar to surfactants, where the geometrical proportions of the hydrophilic and hydrophobic moieties determine the emulsion type. When a liquid-liquid interface curves, the side towards which the interface curves is being compressed, while the opposite side is being stretched. Surfactants with a bulky hydrophobic but a comparably small hydrophilic part force the interface to curve towards the aqueous side, since the smaller hydrophilic parts of the surfactants can be more easily packed upon compression. The same is the case for particles with  $\theta > 90^\circ$  closely packed at an oil-water interface (see Scheme 2).<sup>33-35</sup> The curving towards oil is blocked by the particles, since their major part is immersed in the oil phase. More easy is the curving towards the aqueous phase because of the excess space for the particles. Hence, particles with  $\theta > 90^\circ$  tend to stabilize water-in-oil emulsions while particles with  $\theta < 90^\circ$  stabilize oil-in-water emulsions. But the type of PSE

has been shown for particles with intermediate wettabilities to depend also on the volume fractions of the liquid phases.<sup>36</sup> Theoretical works regarding the preferred emulsion type, considering interfacial bending energies<sup>31</sup>, thermodynamic criterions<sup>37</sup> and capillary pressure effects<sup>38</sup> have been published recently, but will be not discussed here.



**Scheme 2.** Type of an emulsion in dependence of the contact angle.

### 1.1.3 Stability of particle coated emulsion-droplets

Stability in the field of emulsion science denotes the quality of an emulsion to maintain its physical state over long periods of time. Relevant physical properties in this context are the droplet-size distribution and the dispersity of the emulsion. The former is mainly governed by the stability of an emulsion against coalescence and Ostwald-ripening, while the latter depends on the tendency of the emulsion drops to cream or sediment, which is related to the droplet size and can be a result of droplet-flocculation. From a thermodynamic point of view, an emulsion is usually an unstable system, but physical processes occurring during destabilization can be decelerated sufficiently to obtain stability within practicable time periods.

#### 1.1.3.1 Stability against coalescence

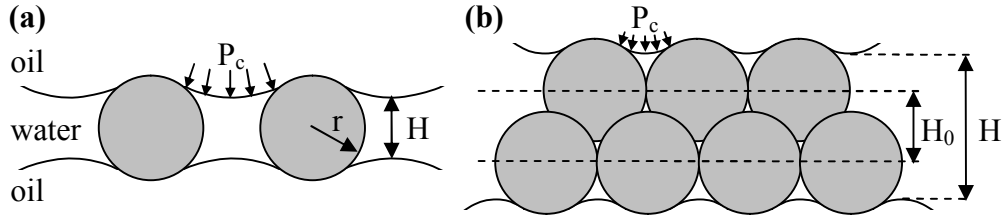
In the last section, the high energy of attachment of solid particles with partial wettability on fluid-fluid interfaces has been discussed. The stability of solid-stabilized emulsions against coalescence is mainly related to this property. Consider a volume of 5 ml oil with a typical interfacial tension against water of  $\gamma_{ow} = 50\text{mN/m}$  completely phase separated in water. By the application of a strong shear flow (e.g. by turbulent mixing) in the presence of monodisperse spherical particles with  $d = 20\text{ nm}$  and  $\theta = 90^\circ$ , monodisperse emulsion droplets with a diameter of for instance  $D = 10\text{ }\mu\text{m}$  are formed. By multiplying the equation for the total volume of the  $N_D$  emulsion droplets  $V = 1/6N_D\pi D^3$  with their surface area  $A_{ow} = N_D\pi D^2$  an area of  $6\text{ m}^2$  is calculated. When the

comparably small increase of configurational entropy is neglected, the interfacial energy of the system will be increased by  $\Delta G_{ow} = \gamma_{ow} A_{ow} = 300\text{mJ}$  (the work which has to be performed is higher due to viscous dissipation during the mixing process). The closest packing of the spherical particles on the newly formed oil-water interface is a hexagonal lattice with a fraction of the area occupied by the particles of  $\pi / (2 \cdot 3^{1/2}) = 0.907$ . Division of the area occupied by the particles ( $5.44 \text{ m}^2$ ) with the particles cross section ( $\pi / 4 \cdot d^2$ ) yields the number of  $1.73 \cdot 10^{16}$  attached particles. Multiplying this number with equation (1.9) gives a total energy of particle attachment  $\Delta G_{aw} = -272.1\text{mJ}$ , which is released as heat from the system. Accordingly, the change of interfacial energy of the system increases by  $\Delta G = \Delta G_{ow} + \Delta G_{aw} = 27.9\text{mJ}$ .<sup>\*</sup> This energy could be released by coalescence, but for this the steric barrier of particles must first be overcome by their detachment from the interface, which requires the huge amount of  $\Delta G_{dw} = +270\text{mJ}$  or  $3800 \text{ kT}$  per particle (see Figure 3). Thus, thermodynamically spoken, the emulsion is in a metastable state, similar to a chemical reaction which first needs the supply of activation energy before the state of lower energy can be attained.

To overcome the steric particle barrier to initiate coalescence, the following mechanism can play a role. When two particle-stabilized emulsion droplets of e.g. oil-in-water come into close contact, a thin liquid film of water forms between them. This concept was first theoretically considered for PSE by Denkov et al.<sup>39</sup>, who introduced the idea of the maximum capillary pressure  $P_c^{\text{max}}$  for two oil droplets, separated by one layer of particles (Scheme 3(a)).  $P_c^{\text{max}}$  is the pressure difference between the inside of the drops and the outside in the water film. Pressing the droplets together (e.g. by centrifugation) can lead to the permeation of oil through the pores of the particle layer(s), accompanied by the formation of a meniscus. The curvature of the meniscus increases as the pressing force increases and thereby the distance between the approaching menisci decreases. At  $P_c^{\text{max}}$ , the two menisci meet and coalescence takes place. It follows that the higher  $P_c^{\text{max}}$ , the higher the pressing force which the liquid film can withstand. Later, Kruglyakov and Nushtayeva extended this concept to a closely packed double layer of particles (Scheme 3(b)).<sup>40, 41</sup>

---

<sup>\*</sup> A more precise calculation, considering also the curvature effects of the emulsion droplets, was introduced by Kralchevsky et al.<sup>37</sup>. Here,  $\Delta G$  is termed “work of formation,  $W$ ” – a calculation with the parameters above yielded  $\Delta G = W = 28.1\text{mJ}$ . The difference of  $\Delta G$  and  $W$  lies below 1 % also for smaller contact angles, e.g.  $30^\circ$ .



**Scheme 3.** Thin water film between two oil droplets separated by **(a)** one layer of particles **(b)** a closely packed double layer of particles.  $P_c$  is the capillary pressure, increasing  $P_c$  decreases  $H$ , film rupture takes place for **(a)**  $H = 0$  and **(b)**  $H = H_0$ .

Previous works related to  $P_c^{\max}$  for PSE were summarized, simplified and if necessary corrected in the paper by Kaptay, who obtained the general formula for a single- as well as a double layer of particles between the droplets:<sup>38</sup>

$$P_c^{\max} = \pm 2p\gamma_{ow}(\cos\theta \pm z)/r \quad (1.10)$$

with  $p$  and  $z$  functions of particle arrangement,  $r$  the particle radius, a plus sign for o/w and a minus sign for w/o emulsions.  $P_c^{\max}$  is sensitive to the particle size, e.g. for a close packed double layer at  $\theta = 60^\circ$  ( $z = 0.405$ ,  $p = 4.27$ )<sup>38</sup>  $P_c^{\max} = 193\text{bar}$  for 20 nm particles, while  $P_c^{\max} = 0.2\text{bar}$  for 20  $\mu\text{m}$  particles. The smaller the particle-size the higher the film-stability. By increasing  $\theta$ ,  $P_c^{\max}$  decreases due to the closer distance between the top of the menisci and so does the predicted stability. For a single layer of particles the parameter  $z$  equals zero and in this case equation (1.10) predicts no stability at all for  $\theta = 90^\circ$  ( $P_c^{\max} = 0$ ). These results are in contrast to the stability dependence following from the increasing  $\Delta G_{asw}$  with increasing  $\theta$  in equation (0.9). To allow for this contradiction, a joint analysis of equation (1.9) and (1.10) was performed by Kaptay and yielded optima for the stability dependence on  $\theta$ , depending on whether a single layer or a double layer of particles is present between the droplets, and on whether an oil/water or a water/oil emulsion is considered.<sup>38</sup>

Some authors have proposed, that the stability of emulsions against coalescence is highest when the particles are weakly flocculated.<sup>42, 43</sup> Tambe and Sharma consider the rheological properties of the particles at the interface as factors for the stability of PSE.<sup>44, 45</sup> In summary it should be remarked, that the mechanisms behind the stabilisation of PSE against coalescence are not yet fully understood.

### 1.1.3.2 Stability against Ostwald-ripening

When the size of emulsion-droplets is reduced, the chemical potential of droplets becomes more sensitive to the addition of molecules or their removal from or to the bulk phase. This fact is related to the bigger surface increase  $\Delta A_{ow} = 2V_M/r$  ( $V_M$  – molecular volume) upon addition of a molecule to the smaller droplet. A bigger surface increase results in a bigger increase of the surface free energy to the chemical potential  $\mu_{su} = \gamma_{ow} \Delta A_{ow}$ .<sup>46</sup> When the oil exhibits a nonnegligible solubility in the aqueous phase, a dynamic equilibrium between dissolution in water and recondensation on oil droplets exists. If furthermore both very small droplets ( $r < 500$  nm) and bigger ones are present, the molecules in the small droplets experience a higher solubility in the continuous phase due to the Gibbs-Thomson effect. This leads to a higher concentration of the dissolved oil near the small droplets and results in a diffusional flow towards the bigger oil-droplets, where the recondensation takes place. As a result, the small droplets disappear and the big droplets grow. There are two common ways to slow down this so called Ostwald-ripening: (i) Ultra low interfacial tensions with non-ionic surfactants decrease  $\Delta G$  upon re-condensation on small droplets, (ii) the reduction of the oil solubility in water. The first approach seems to be less appropriate for PSE, e.g. because the high concentration of surfactants required can lead to undesired surfactant-particle interactions, which can diminish the interfacial activity of the particles.<sup>47</sup> The latter case has been shown to be very effective also for PSE, especially in the field of emulsion polymerization.<sup>48</sup> When small amounts of a solute with negligible water solubility are dissolved in the oil phase, the solubility of the oil is indirectly reduced, too.<sup>49, 50</sup> This can be explained by the built-up of an osmotic pressure counteracting the Laplace pressure of small droplets.<sup>51</sup> An equivalent explanation is the additional contribution of the droplets composition to the chemical potential  $\mu_{co} = R_G T \ln(x_o)$  with  $x_o$  the mole-fraction of the oil,  $R_G$  the Gas-constant and  $T$  the absolute temperature.<sup>52</sup> The total chemical potential is then written as  $\mu = \mu_{su} + \mu_{co} = 2\gamma_{ow} V_M / r + R_G T \ln(x_o)$ . When the chemical potential  $\mu$  equals zero, no further dissolution of oil takes place and droplets with equilibrium compositions and sizes can be obtained. The equilibrium droplet size is obtained for  $\mu = 0$  and the equation for  $\mu$  can be rewritten to

$$r = -\frac{2\gamma_{ow} V_M}{R_G T \ln x_o} \quad (1.11)$$

For the example styrene in water ( $\gamma_{ow} = 34$  mN/m,  $V_M = 114.5$  cm<sup>3</sup>/mol, 298.15K,  $M_{Sty} = 104.15$  g/mol), containing 4 wt-% of water insoluble hexadecane ( $M_{HD} = 226.44$  g/mol,  $x_o = x_{Sty} = 0.981$ ) the equilibrium droplet size equals  $d = 2r = 0.327$   $\mu$ m. Practically spoken, by introducing sufficient

mechanical energy, submicrometer-sized oil droplets can be produced, which can be stabilized for reasonable periods of time by dissolving small amounts of water-insoluble molecules (polymers, longchain-alkanes ...) in the oil phase.

### 1.1.3.3 Stability against creaming and sedimentation

Oil/water emulsions are usually subjected to creaming, since the oil-phase mostly has a lower density than water and the size of the emulsion's droplets lies in the majority of cases above the colloidal dimensions ( $> 2 - 3\mu\text{m}$ ). However, the density of a particle-stabilized droplet is a volume weighted average density of both oil and particles and depends on the droplet-size. Consider monodisperse spherical particles with radius  $r$ ,  $\theta = 90^\circ$  and a spherical oil droplet with radius  $R_D$ . Then the number of closely-packed particles  $N_p$  attached to the oil droplet equals the droplet-area  $A_d$  reduced by the hexagonal-packing-factor 0.907 divided by the cross-sectional area  $A_p$  of one particle  $N_p = 0.907A_d / A_p = 4 \cdot 0.907 \cdot R_D^2 / r^2$ . The volume of the particles  $V_p$  follows by multiplying  $N_p$  with the volume of a single spherical particle  $4/3\pi r^3$ , while the oil volume  $V_D$  equals  $4/3\pi R_D^3$ . The volume weighted average density  $\rho$  is  $\rho = (V_p \rho_p + V_D \rho_D) / (V_p + V_D)$  with the density of the particle  $\rho_p$  and of the oil  $\rho_D$ . By inserting the former relations one yields  $\rho = (3.682r\rho_p + R_D\rho_D) / (3.682r + R_D)$ . A critical droplet-radius  $R_{\text{crit}}$  can be obtained when the droplet-density equals the density of the continuous liquid  $\rho_{\text{cont}} - \rho_{\text{crit}} = 0$ . Rearrangement of the droplet-density yields  $R_{\text{crit}} = 3.682 \cdot r \cdot (\rho_p - \rho_{\text{cont}}) / (\rho_{\text{cont}} - \rho_D)$ . Droplets with a closely-packed particle layer on their surface with a radius  $R_{\text{crit}}$  will neither cream nor sediment.  $R_{\text{crit}}$  depends linearly on the particle size  $r$ , for instance for a n-dodecane ( $\rho_D = 0.75\text{g/ml}$ ) droplet in water ( $\rho_{\text{cont}} = 0.998\text{g/ml}$ ) covered with alumina particles ( $\rho_p = 3.94\text{g/ml}$ ) of  $r=10\text{ nm} \rightarrow R_{\text{crit}} = 0.43\mu\text{m}$  and for  $r=100\text{ nm} \rightarrow R_{\text{crit}} = 4.3\mu\text{m}$ .<sup>†</sup>

---

<sup>†</sup> By considering the fact, that for  $\theta < 90^\circ$  more particles can be attached to the surface of a convex drop and that every attached particle displaces some of the oil, Kralchevsky<sup>37</sup> developed a more complex geometrical description. With his expression for  $N_p$  and an increased drop radius  $R_{12}$ , a calculation for  $\theta = 30^\circ$  and the same parameters as before yielded for  $r = 10\text{ nm} \rightarrow 0.448\mu\text{m}$  and for  $r = 100\text{ nm} \rightarrow 4.48\mu\text{m}$ .

### 1.1.3.4 Stability against flocculation

Flocculation of particle-stabilized emulsion-droplets denotes the formation of interconnected emulsion-droplet-clusters. The increased weight or buoyancy force acting on such flocs leads to an enhanced rate of sedimentation or creaming. For the classification, two cases should be distinguished: (i) the droplet-surface is covered with a non-closely-packed or (ii) with a closely-packed particle monolayer. For o/w emulsions, the first case can e.g. be observed for hydrophilic particles ( $\theta < 50^\circ$ ) with repulsive surface characteristics (e.g. highly charged particles). By the collision of two oil droplets, both covered by non-closely-packed layers of such particles, the particles mainly protruding in water can act as a bridge by being immersed in both droplets simultaneously. This is further facilitated by the unoccupied oil-water interface in non-closely-packed particle layers. By increasing the  $\theta$ , this situation becomes less probable, because (i) particles tend more to form closely-packed-layers and (ii) the thin aqueous film between two emulsion droplets becomes less stable<sup>39</sup>. Emulsion droplets covered by closely-packed-layers have in general a lower tendency of flocculation. Kralchevsky et al. showed this theoretically for o/w emulsions with  $\theta < 90^\circ$ .<sup>37</sup> Two flocculated spherical droplets show a flattening of their contact surfaces. For droplets covered with closely-packed-particle layers this requires positive energies of bending and dilatation, making the flocculation process thermodynamically unfavourable.<sup>37</sup> However, when the colloidal stability of the interfacially attached particles is reduced, flocculation can also occur for emulsion droplets with closely-packed-particle layers. This can be the case e.g. for charged particles due to the addition of salt or the pH adjustment towards the isoelectric point of the particle surface. When there is an excess of particles in the bulk water, such destabilization can lead to the formation of a three-dimensional network of interconnected particles and particle-covered oil-droplets.<sup>53-55</sup>

Often the increase of the  $\theta$  of particles initially dispersed in water (e.g. by introducing nonpolar surface groups) leads also to their reduced colloidal stability. However, there are also exceptions from this rule. Latex particles with  $\theta > 90^\circ$  for instance are often well dispersible in water, due to their charged sulphate surface-groups.<sup>56, 57</sup>

### 1.1.4 Interactions between interfacially attached particles

As for spherical particles in the bulk-phase, the total interaction between two spherical particles attached to a fluid-fluid interface results from the coactions of different forces. The forces can be assumed to act additive when there is no mutual interaction between them. Compared to spherical

particles in the bulk-phase, the major difference in the description of the interaction is their dependence on the  $\theta$ . A particle at a fluid-fluid interface is separated into two spherical caps, one immersed in the polar phase, the other emergent in the nonpolar phase. The surface properties of the particles, as well as the intermediation of the forces, depend on the fluid type covering the surface. In addition to this difference, further forces like capillary forces, which do not exist in the bulk case, can participate in the total interaction. For the description of the total interaction, the use of the Derjaguin approximation<sup>17</sup>, which “relates the force between curved surfaces to the interaction energy between flat surfaces”<sup>58</sup>, simplifies the geometrical considerations.

As for charged particles in the bulk phases, colloidal particles located at fluid-fluid interfaces experience long-ranged repulsive electrostatic double layer forces through the polar phase. For thin to moderate double layers, symmetric electrolytes and a non significant overlap of the double layers the Poisson-Boltzmann equation can be used to describe the repulsive electrostatic interaction across the polar fluid.<sup>59</sup> The short-ranged attractive dispersion (van der Waals) forces act through both fluid phases, but have a higher constant of proportionality (Hamaker constant) in the nonpolar fluid<sup>60</sup>. Both interactions add to the distance-dependent DLVO interaction energy. By increasing  $\theta$ , the particle surface area immersed in the polar phase decreases and so does the double layer repulsion. Simultaneously, the surface in the nonpolar phase increases, and so does the dispersion attraction. Both effects together lead to a decrease of the repulsive barrier of the DLVO theory with increasing  $\theta$  and should induce two-dimensional aggregation of the particles. Unexpectedly, microscopic visualizations of the interfacial behaviour of charged hydrophobic latex particles ( $\theta > 110^\circ$ ) at planar fluid-fluid interfaces have shown that the opposite is true.<sup>61-63</sup> In these studies, well ordered, crystalline arrangements of the hydrophobic particles with well defined spacing have been observed, while for hydrophilic particles unordered, partly aggregated surface coverage has been found. Another repulsive interaction must exist. It is believed, that charged particles attached to an interface between water and a nonpolar fluid can retain water in the form of small droplets or a thin layer on the particle surface on the side exposed to the nonpolar fluid.<sup>61, 62</sup> Through this, the preservation of surface-dipoles (dissociated surface groups + counter ions) or small amounts of surface-monopoles (dissociated surface groups) on the solid-nonpolar fluid interface is possible. Because of the low dielectric permittivity of the nonpolar phase, an electric field generated by the surface mono- and dipoles is long-ranged and can be very strong. The strength of this electrostatic force depends on the amount of such surface groups. The part of the particles' surface-area immersed in the nonpolar phase and accordingly the amount of dipoles and monopoles in this

environment is determined by  $\theta$ . The strength is thus also governed by  $\theta$  and is in particularly relevant for charged hydrophobic particles with  $\theta > 90^\circ$ .

Moreover it has been shown that the charged hydrophobic latex particles even form patches of crystalline order, which remain stable for times of more than 30 minutes when the surface coverage is incomplete.<sup>27</sup> This shows that an attractive force for such particles must also be present. As mentioned earlier, forces like gravity or nonuniform wetting of particles due to their roughness (undulated contact line)<sup>25</sup> can deform the fluid-fluid interface and create a meniscus profile around the particles. Nikolaides<sup>27</sup> was the first to describe such a deformation being the result of the strong interaction induced by surface-monopoles and –dipoles. Such a deformation gives rise to a capillary attraction between the particles, which can be balanced by the aforementioned strong repulsion to yield the well defined spacing between the particles on the fluid-fluid interface.

When the electrostatic interaction between the particles is mainly mediated through the nonpolar phase as in the case described above, the structure of ordered particle monolayers is insensitive to the electrolyte concentration or valency.<sup>63</sup> However, for hydrophilic charged particles ( $\theta < 90^\circ$ ), the electrolyte influences the particle structure significantly, due to the fact that the interaction is then mainly governed by the electrical double layer forces. As in the case of charged particles in the bulk-phase, the increase of electrolyte concentration or valency can lead to strong or even irreversible aggregation due to a decrease of the Debye screening length.

The force between the particle and the fluid molecules results in an entropic interaction influencing the structure of the fluid molecules around the particle and is therefore called structural interaction (also solvation-, hydration- force).<sup>64</sup> A hydrophilic particle attracts water molecules, resulting in a layered structure of water molecules around the particle, which in turn leads to repulsion between approaching particles. The opposite is true for hydrophobic particles attracting each other in water. The hydrophilic interaction should not play a significant role here, since it is only recognizable for particles with very low  $\theta$  and consequently no interfacial activity, while the hydrophobic interaction is detectable when  $\theta > 64^\circ$ <sup>65</sup>. The structural force is a short ranged but very strong interaction.

Another short ranged interaction between the particles attached to a fluid-fluid interface is the solid-elastic force, which results from the mechanical interaction of the particles. However, this interaction should only play a role when the distance between the particles is reduced to the nearest approach, e.g. by compression of a particle covered air-water interface in a Langmuir trough.

When the interaction energies between particles become comparable to the interfacial energies, they must be considered in the derivation of the energy of attachment (equation (1.9)).  $\Delta G_a$  would then become less negative for repulsive interactions or more negative for attractive interactions. Levine

et al.<sup>17, 66</sup> calculated the magnitude of the electrostatic double layer force, the dispersion force and the structural force and compared the results to the energy of attachment of a particle. It turned out that all considered particle interaction forces together make up only a small fraction of the energy of attachment ( $< 0.5\%$ ). Aveyard et al. showed theoretically that for the case of long-ranged electrostatic repulsions mediated through the nonpolar phase, the energy of attachment can become positive for high surface charge densities and high particle coverage on the surface.<sup>31</sup> This result is in agreement with the experimentally observed non-closely packed crystalline assemblies of charged latex particles.<sup>61-63</sup>

### 1.1.5 Methods of particle hydrophobization: literature survey

In addition to several publications by Tambe and Sharma<sup>44, 67, 68</sup> in the mid-nineties, it were mainly the publications of Aveyard and Binks<sup>34</sup> which initiated a flurry of scientific work about solid stabilized emulsions after the turn of the millennium. During the last ten years, many studies have been carried out about theoretical aspects of particles at fluid-interfaces, interactions of surface active molecules with nanoparticles enabling PSE, emulsions stabilized by stimuli-responsive particles, the fabrication of capsules and polymer-particle composites on the basis of PSE, the rheology of PSE, novel materials derived from particle assembly on liquid surfaces and more. The present work mainly deals with the modification of particle wettability. Therefore, in the following an overview of previously published methods is given and their most important effects are briefly summarized.

#### 1.1.5.1 Adsorption of amphiphilic molecules

The modification of the wettability of solid surfaces by the adsorption of amphiphiles has been extensively investigated in the past. The origin of this method comes from the field of froth-flotation, where “frothers” (amphiphilic molecules) are used to increase the affinity of particles to the foam-phase.<sup>69</sup> For hydrophilic surfaces, the polar head groups of amphiphiles can act as anchors for the adsorption on the particle surface, while the hydrophobic tails exposed to the surrounding liquid “hydrophobize” the particle surface. One of the first articles about this method in the field of PSE was the work of Schulman and Leja.<sup>7</sup> They studied the influence of the adsorption of fatty acids and alkyl sulphates on  $\text{BaSO}_4$  on the  $\theta$  in dependency of the chain-length, pH value and amphiphile concentration. Longer alkyl-chain-lengths, as well as higher amphiphile concentrations

(however still below the cmc), resulting in higher adsorption densities, gave higher  $\theta$  of water droplets under oil and air. For sufficiently long alkyl-chains (number of carbons  $n_C \geq 12$ ) and high enough concentrations  $\theta$  was found to be above  $90^\circ$ , and consequently the formation of w/o emulsions was favoured. This effect is possible due to the adsorption of two amphiphiles per Barium surface group, which for fatty acids only takes place at alkaline pH values (when they are fully dissociated), but for alkyl-sulphates it takes place independently of the pH-value.

Several studies have shown that increasing the surfactant concentration leads to the formation of bilayered structures or micellar aggregates of amphiphiles on the particle surfaces.<sup>70, 71</sup> Thus, a re-hydrophilization takes place due to the orientation of the hydrophilic head groups towards the aqueous phase. This was shown for cationic surfactants on negatively charged surfaces<sup>72</sup> as well as for anionic surfactants on positively charged surfaces<sup>73, 74</sup>. Such structural changes of the adsorbed amphiphiles can e.g. be monitored by measurements of the electrophoretic mobility ( $\zeta$ -potential) of the particles. By increasing the surfactant concentration, the absolute value of the  $\zeta$ -potential initially decays due to the compensation of surface charges through oppositely charged head-groups and increases again at a certain surfactant-concentration due to excess charges of the surfactants upon bilayer-formation.<sup>70, 75</sup>

Usually an inversion of the preferred emulsion type does not take place for the modification of particles with single-chain surfactants (except when two surfactant molecules per surface group adsorb)<sup>7, 74, 76</sup>. Binks and Rodrigues<sup>77</sup> have shown that silica particles stabilize o/w emulsions at low di-chain surfactant concentrations, w/o emulsions at intermediate concentrations and o/w emulsions again at high concentrations.

To “hydrophobize” a particle surface sufficiently, the adsorbing amphiphiles do not necessarily have to be able to stabilize an emulsion alone, as it is the case for the afore mentioned systems. Gonzenbach et. al.<sup>78</sup> and later Akartuna et al.<sup>79</sup> showed that inorganic hydrophilic particles can become sufficiently interfacially active by the adsorption of short amphiphiles to stabilize highly concentrated foams and oil-in-water emulsions. For instance with alumina particles modified with adsorbed short chain fatty acids (number of carbons in the chain  $n_C \leq 5$ ), very stable and concentrated o/w emulsions can be obtained.<sup>79</sup> It was shown later that the macroscopic  $\theta$  on the alumina surface results from the adsorption of the fatty acids on all involved interfaces.<sup>80</sup> Li and Stöver obtained pH dependent o/w emulsions on alumina coated silica particles through the adsorption of the potassium hydrogen phthalate, which only contains one aromatic ring as the hydrophobic moiety.<sup>81</sup>

### 1.1.5.2 Emulsion stability by controlling the surface charge of particles

When the surface charge of hydrophilic particles is reduced,  $\theta$  can be sufficiently increased to enable the o/w emulsification ability of solid particles. The silica surface for instance has an isoelectric point (IEP) in the range  $2 < \text{pH} < 3$ . By lowering the pH value into this region, hydrophilic silica nanoparticles without coating can become sufficiently hydrophobic to act as stabilizers for o/w emulsions alone<sup>47</sup> (an advantage of silica particles is that they do not aggregate at the IEP). Another way to reduce the charge of solid particles is the addition of salt. Laponite clay particles are poor emulsifiers, but in the presence of 0.1 M NaCl, the o/w emulsion stability can be significantly improved.<sup>82</sup> A more effective approach to increase the hydrophobicity of negatively charged particles is by specific adsorption of multivalent cations.<sup>83</sup> In the presence of 2 – 5 mM  $\text{LaCl}_3$  the charges of silica nanoparticles are sufficiently compensated and the particles are not too aggregated to stabilize o/w emulsions.<sup>43</sup>

It has been shown by Fujii et al. that the interfacial activity of water-swallowable poly-4-vinylpyridine-silica microgel composite particles can be controlled via the charge of the 4-VP groups.<sup>18</sup> At low pH values, the positive charges render the microgel-particles hydrophilic, but neutralizing the charges by raising the pH value establishes the hydrophobic character of the 4-VP, and consequently o/w emulsions can be stabilized. Another system with similar pH dependent properties has been developed by Amalvy et al..<sup>84</sup> Here the chargeable 2-(dimethylamino)ethyl monomer-groups of copolymer molecules adsorbed on silica govern the interfacial activity of the particles. Again deprotonation at high pH-values enables the o/w emulsification ability.

To stabilize o/w emulsions with hydrophobic particles containing chargeable groups, the opposite of the aforementioned is required: the particle charge has to be increased. Carboxylic acid coated polystyrene particles reside in oil in their uncharged state at low pH-values.<sup>85</sup> Upon raising the pH above a value of 10, the acid groups deprotonate sufficiently to render the particles more hydrophilic to stabilize o/w emulsions.

## 1.2 Polyelectrolytes

### 1.2.1 Dependency of the conformation on the solvent quality

Polyelectrolytes are water soluble polymer-molecules with negatively (polyanions) or positively (polycations) charged monomer-units. The architecture of a polyelectrolyte can be a simple linear chain or a more complicated branched structure. In the following, we will consider mainly the former case. The persistence length of a linear chain polymer  $l_p$  is the “*length over which two parts of the chain keep their orientational correlation*”<sup>86</sup>, in other words: when comparing the end to end distance of the polymer molecule with  $l_p$ , one gets an idea of whether the polymer conformation is stretched or coiled. Compared to uncharged polymers of the same end to end distances, polyelectrolytes can have very high values for  $l_p$ , ranging up to a few hundred nanometers.<sup>87, 88</sup> Such linearly stretched polyelectrolytes with high molecular masses ( $> 10^6$  g/mol) can strongly increase the viscosity of water. The reason for this extended conformation of polyelectrolytes in water is the strong and long-ranged coulombic repulsion between identically charged monomer-units.

Similar to acids or bases, which can have a strong or weak tendency to dissociate, polyelectrolytes are classified as strong or weak polyelectrolytes. Weak polyelectrolytes carry acid or base groups in their monomer-units with  $pK_a$  values in the range of 2 – 10. However, compared to their monomeric equivalents, the acid or base groups in a polyelectrolyte differ in their dissociation behaviour.<sup>89, 90</sup> The reason for this is the coulombic repulsion between neighbouring monomer-units, which tends to suppress the dissociation. For weak polycations the  $pK_a$  is decreased (e.g. allylamine<sup>91</sup>  $pK_a = 9.5$ , poly(allylamine)<sup>92</sup>  $pK_a = 8.7$ ) and for weak polyanions the  $pK_a$  is increased (e.g. acrylic acid<sup>93</sup>  $pK_a = 4.5$ , poly(acrylic acid)<sup>94</sup>  $pK_a = 6.7$ ). When the dissociation of a weak polyelectrolyte is decreased by changing the pH-value, the coulomb repulsion between monomer-groups is also lowered. Through this,  $l_p$  is reduced and the polymer begins to coil and becomes more compact on further charge reduction to finally form a globule at very low dissociation (see Figure 4).<sup>95</sup>

In the uncharged state the monomer-units attract each other, but the entropically driven tendency for high configurational freedom counteracts the compacting of the coil. This process is similar to the demixing of binary liquid mixtures and can also be described with the regular solution theory<sup>86</sup>

$$w_i = z_b N_{av} (W_{AB} - 0.5W_{AA} - 0.5W_{BB}) \quad (1.12)$$

Herein  $w_i$  equals the interaction parameter,  $z_b$  is the number of nearest neighbouring molecules,  $N_{av}$  the Avogadro number,  $W_{AB}$  the interaction energy between monomer-units and water molecules,

$W_{AA}$  and  $W_{BB}$  the respective interaction energies of monomer-units and water-molecules among each other.

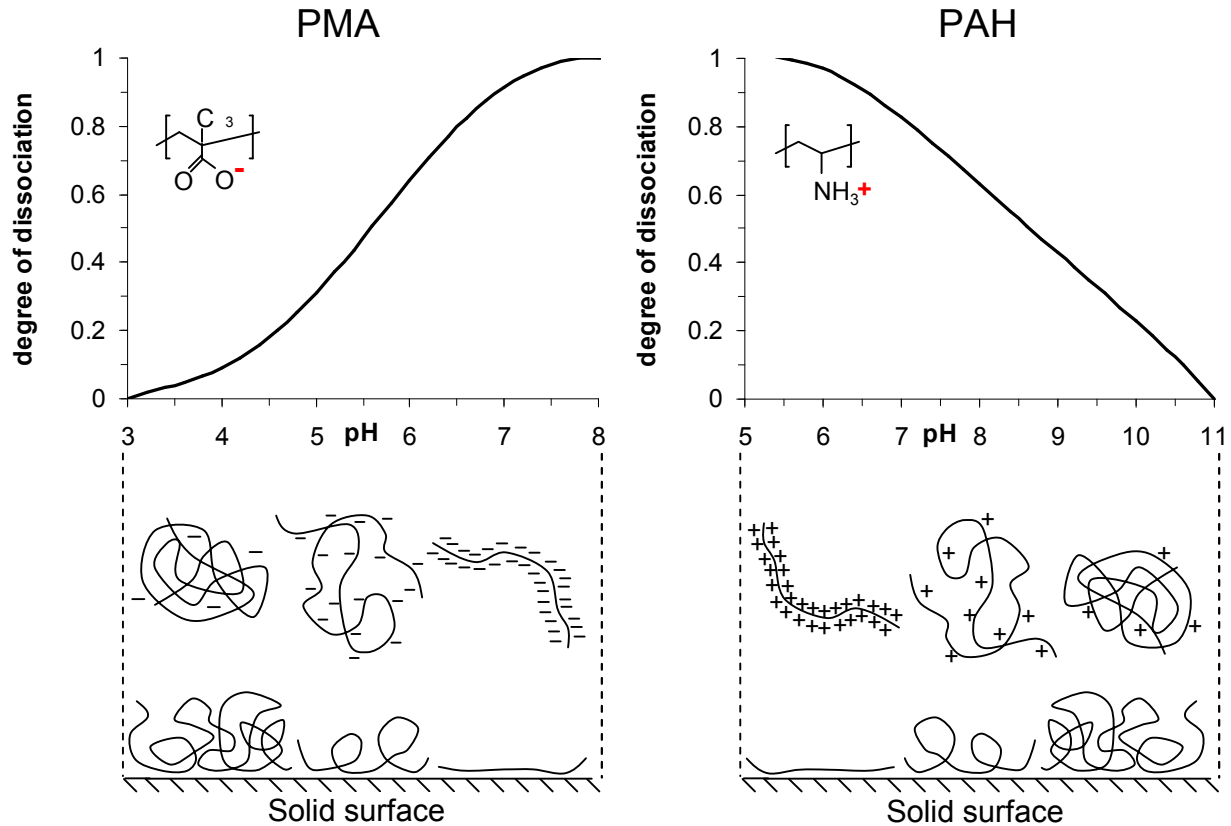


**Figure 4.** Influence of the degree of dissociation of weak polyelectrolytes on the examples of polymethacrylic acid (PMAA) and polyallylamine hydrochloride (PAH) on the adsorption behaviour on solid surfaces.

Although the regular solution theory does not account for electrostatic effects, it can be stated that the initial repulsion of charged monomer-units (large positive  $W_{AA}$ ) changes into an attraction in the uncharged state (negative  $W_{AA}$ ). Furthermore, the solvation of uncharged units by water is reduced and thus  $W_{AB}$  becomes less negative. In chapter 3.2 it will be shown that these effects can be used to control the  $\theta$  of solid particles with adsorbed polyelectrolytes. Accordingly, the attractive interaction energies  $W_{AA}$  and  $W_{BB}$  let  $w_i$  increase and the contact of monomer-units becomes more favourable. For polymers the solvent quality is expressed using the parameter  $\chi = w_i/RT$ . When  $\chi < 0.5$ , the entropy counteracts the compacting force, but for  $\chi > 0.5$ , the polymer becomes more dense.

### 1.2.2 Determination of the properties of adsorbed films through conformation

Weak polyelectrolytes can adsorb strongly on oppositely charged surfaces.<sup>96</sup> In addition to the electrostatic attraction between the opposite charges, the adsorption is also accompanied by an entropic effect. Upon adsorption, huge amounts of counterions are released. This is the case for both the charged polyelectrolyte monomer-units and for the charged surface groups. However, in regimes of very high salt concentrations this entropic effect is lowered and adsorption can even be suppressed.<sup>97</sup> At low or moderate salt concentrations, the adsorption of polyelectrolytes is quasi-irreversible and the polyelectrolyte also remains on the surface upon dilution. This is a consequence of the huge number of contacts between the monomer-units and the surface-groups. Although the energy of adsorption per contact is low (order of  $kT$ ), all contacts together make up an adsorption energy much higher than the thermal energy of the polymer-molecule. The adsorption of a linearly stretched fully charged polyelectrolyte can lead to a compensation of the charges of the surface-groups and the monomer-units, resulting in a neutral surface (Figure 4). When the intrinsic charge density of the polyelectrolyte is higher than that of the surface, charge overcompensation can take place and then the surface obtains the charge of the polyelectrolyte.<sup>98</sup> However, charge overcompensation can also be a result of a coiled polyelectrolyte adsorbing on the surface (Figure 4). The reason is that upon adsorption, the conformation of the polyelectrolyte may not change remarkably, and by this the thickness of an adsorbed polyelectrolyte film is determined. For weak polyelectrolytes this is done by adjusting the polyelectrolytes' charge density via the pH value, which greatly influences the amount of adsorbed weak polyelectrolytes on oppositely charged surfaces.<sup>21</sup>

### 1.3 Anticorrosive coatings

The main objective of organic barrier coatings on metal substrates is to suppress the diffusion of corrosive species (water, electrolytes, oxygen) to the metal surface. To provide an effective barrier, such coatings usually consist of highly cross-linked organic polymers and other additives. Unfortunately, the nonpolar character of the polymers (binders) usually requires the use of organic solvents, which vaporize upon application of the coating, accompanied by the binder cross-linking reactions. However, the aim of both national and international legislation is to reduce the use of such volatile organic compounds in the coating industry. Instead of solvent-borne, the use of water-borne and powder coatings for the protection of metals and other substrates must be expanded. However, water-borne coatings still have several drawbacks and cannot always replace the highly

effective solvent-borne coatings, especially in harsh environments. Drawbacks can be lower barrier properties, the inability of some water-borne coatings to withstand freeze/thaw cycles, the requirement to contain biocides to prevent microbiological degradation and the formation of foam due to high contents of surface active molecules in some of the lacquer formulations.<sup>99</sup>

To improve the corrosion resistance of coatings, the use of inhibitive, barrier and sacrificial pigments in coatings has a long history. In the European Union, inhibitive pigments have in the past mainly been chromates, like strontium chromate. Chromates in their hexavalent form have strong oxidizing power, which makes them very efficient as corrosion inhibitors, but for the same reason they are also strongly mutagenic and carcinogenic to both humans and animals. In comparison to the EU (Restriction of Hazardous Substances Directive)<sup>100</sup>, the legal restrictions for chromates are less strict in other parts of the world, e.g. in the USA, where it was found recently that chromates in tap water exceeded the recommended values in several cities<sup>101</sup>, or the far east, where the overall use of chromates is actually increasing<sup>99</sup>. Among many other inorganic inhibitors, phosphate metal salts gained importance as inhibitive pigments.<sup>102-104</sup> However, organic inhibitors in coatings are also considered as potential chromate replacements.<sup>105, 106</sup> For this class of inhibitors, it is useful to encapsulate them in suitable reservoirs which are dispersible homogeneously in the coating matrix. Recently it was reported that nano-sized reservoirs containing organic inhibitors are capable of self-healing damaged coatings by passivation of the metal.<sup>107-110</sup> The general physicochemical mechanism of inhibitors is the formation of complexes, formed by reactions with corrosion products (hydroxide ions, metal cations) and their precipitation as barriers on the corrosion sites, which lead to a passivation of the surface. Depending on whether the inhibitors passivate the anode or the cathode of a corrosion cell, they are classified as anodic or cathodic inhibitors. When a coating is permeated by water, the inhibitive molecules in pigments are dissolved and transferred to the metal surface and the aforementioned physicochemical processes can take place. This picture is mutually contradictory, because on one hand the coating should be highly impermeable for corrosion reactants (like water) and on the other hand it should allow the transport of the inhibitive molecules.<sup>99</sup>

In chapter 3.3 and 3.4 an approach for the encapsulation of organic corrosion inhibitors is introduced and the anticorrosive properties for the protection of the aluminium-copper alloy AA-2024 are studied. AA-2024 is mainly used in aerospace applications due to its low weight-to-strength ratio. However, copper inclusions make this alloy highly sensitive to corrosion<sup>106</sup>, especially in the presence of chloride ions which are capable of destructing the passivating oxide layer on the surface. The reduction of the corrosion potential can be accomplished by the

passivation of the cathodic copper sides by suitable corrosion-inhibitors. A potential cathodic corrosion inhibitor is 8-hydroxyquinoline (8-HQ), which forms water insoluble chelates with  $\text{Al}^{3+}$  ions at neutral pH.<sup>111-114</sup> The barrier coating matrix for the embedment of the 8-HQ filled reservoirs was chosen to be a commercial air-drying water-borne alkyd-resin. Alkyd-resins are polyesters, chemically modified with unsaturated fatty-acids. The oxygen-rich polyester backbone enables good adhesion to the aluminium-oxide layer on the substrate through hydrogen bonding. Under alkaline conditions, the alkyd-coating is susceptible to saponification and thereby degradation of the coating.<sup>99</sup> The alkyd-resin is in the form of colloidal emulsion droplets in water. By the addition of siccatives or oil drying agents the drying and cross-linking of the resin can be accelerated. Such siccatives are salts of bivalent metals with organic acids ( $8 < n_C < 11$ ) and act as catalysts for the formation of  $\text{RO}\cdot$  and  $\text{ROO}\cdot$  radicals, which act as cross-linkers for the unsaturated bonds of the fatty-acid constituents in the presence of oxygen. Other additives can be volatile ligands, which deactivate the siccatives to prevent the curing of the alkyd-resin before application. The film-formation on the substrate for an alkyd-coating with such additives consists then of the following steps: evaporation of the siccativ-ligands and water, diffusion of oxygen from the air, coalescence of the alkyd-resin droplets, siccativ catalyzed cross-linking of the fatty acids.

## 2 Experimental methods

### 2.1 Materials

Diethylphthalate (99.5%), 8-hydroxyquinoline (99%), hexadecane ( $\geq 98\%$ ) were purchased from Sigma-Aldrich and used without further purification. Dodecane and hexane (99.9%, Sigma Aldrich) were purified from polar impurities by mixing twice with activated basic alumina (5016 Brockmann 1 stand grade), and removal of solid was done with a folded filter. Diluted sodium hydroxide and hydrochloric acid (1M Titripur from Merck) were used to adjust the pH. Water was purified before use in a three-stage Millipore Milli-Q Plus 185 purification system and had a conductivity lower than  $18.2\text{ M}\Omega\cdot\text{cm}^{-1}$ . Styrene ( $\geq 99\%$ , 10-15 ppm 4-*tert*-butylcatechol as inhibitor) was distilled under reduced pressure at  $50^\circ\text{C}$ . 4-vinylpyridine (95 %, 100 ppm hydroquinone as inhibitor) was purified by passing twice through an activated alumina (5016 Brockmann 1 stand grade) filled column.

Ludox TMA suspension (average particle diameter: from BET sorption data ( $134\text{ m}^2/\text{g}$ ,  $2.34\text{ g/mL}$ ) 19.1 nm, obtained by DLS measurements 16 nm), alumina nanoparticles suspension (particle diameter: from BET sorption data ( $396\text{ m}^2/\text{g}$ ,  $3.94\text{ g/mL}$ ) 4 nm, obtained by DLS measurements 16 nm), poly(allylamine hydrochloride) (PAH, average MW  $\approx 17\,000\text{ g/mol}$ ), poly(methacrylic acid, sodium salt) solution (PMAA, average MW by GPC  $\approx 9500\text{ g/mol}$ ) were purchased from Sigma-Aldrich. Butyl- ( $\geq 98\%$ , AK Scientific, USA), hexyl-, octyl-, decyl- ( $\geq 98\%$ , Sigma-Aldrich), dodecyl-trimethylammonium bromide (for synthesis, Merck, Germany) were purchased and used without further purification.

Silicon wafers were purchased from Silchem HmbH (Freiberg, Germany, type n Antimon, resistivity  $16\text{ m}\Omega/\text{m}$ , crystal orientation 111, thickness  $381\mu\text{m}$ ). Polished alumina plates were purchased from MTI Corporation (size  $10\times 10\times 1\text{ mm}^3$ , crystal orientation 0001).

Worlée alkyd-resin emulsion in water (Worlée-Chemie GmbH, Hamburg - Germany) W'Sol E330W – a linseed oil, polyurethane modified alkyd resin without any additives.

### 2.2 Determination of the 8-hydroxyquinoline partitioning and adsorption

**Measurement of the Partition of 8-hydroxyquinoline (8-HQ) between Water and Diethylphthalate (DEP).** DEP containing 16.5 wt-% 8-HQ was added to an equal volume of water containing sufficient hydrochloric acid or sodium hydroxide to create a desired pH value in the

## 2. Experimental methods

equilibrium mixture. The emulsion was shaken in a vortex for 12 h and afterward centrifuged at 1000 min<sup>-1</sup> for 5 min to separate the phases. The pH value of the aqueous phase was determined by using a calibrated glass electrode (SenTix Mic, WTW InoLab). An accurately defined volume of the aqueous phase was then transferred to a volumetric flask containing 10 mM of aqueous HCl. The UV-vis spectra of the diluted solution were measured in a UV spectrophotometer (Agilent 8453) and compared with a previously prepared calibration function. The absorbance at the isosbestic point in the spectra at 334 nm was used for calibration and measurement.

**Determination of the Adsorption Isotherm of 8-HQ on Silica Particles.** Solid 8-HQ crystals were weighed in. The volumes of subsequently added water, Ludox TMA suspension, and diluted HCl were chosen to establish fixed concentrations of 8-HQ in water. In particular the volume of HCl was chosen to guarantee complete dissolution of 8-HQ. The amount of HCl was varied to obtain different pH values. The silica particle concentration was always 30 wt-% to provide a high surface area and measurable adsorbed amounts. The mixtures were then alternately treated in an ultrasonic bath containing water at 50 °C and shaken in a Vortex until complete dissolution of 8-HQ was obtained. After an equilibration time of 12 h under shaking (i) the pH value of the suspension was measured and (ii) the particles were centrifuged down at 20000 min<sup>-1</sup> for 3 h. The clear supernatant was diluted and measured in the UV spectrophotometer. The difference of the known initial concentration and the measured concentration was taken for the adsorbed 8-HQ amount. The determination of the adsorbed 8-HQ amount in the three component system (water, DEP and silica) can be calculated from the following mass-balance:

$$\begin{aligned} m_{8\text{HQ-total}} &= m_{8\text{HQ-DEP}}^{(1)} = m_{8\text{HQ-DEP}}^{(2)} + m_{8\text{HQ-water}}^{(2)} + m_{8\text{HQ-silica}}^{(2)} \\ m_{8\text{HQ-total}} &= c_{8\text{HQ-DEP}}^{(1)} V_{\text{DEP}} = c_{8\text{HQ-DEP}}^{(2)} V_{\text{DEP}} + c_{8\text{HQ-water}}^{(2)} V_{\text{water}} + A_{8\text{HQ-silica}}^{(2)} V_{\text{water}} c_{\text{silica}} \end{aligned} \quad (2.1)$$

With  $m_{8\text{HQ-total}}$  the total mass of 8-HQ,  $m_{8\text{HQ-DEP}}$  and  $m_{8\text{HQ-water}}$  the mass of 8-HQ dissolved in DEP and water,  $m_{8\text{HQ-silica}}$  the mass of 8-HQ adsorbed onto silica,  $c_{8\text{HQ-DEP}}$ ,  $c_{8\text{HQ-water}}$  and  $c_{\text{silica}}$  are the respective concentrations in g/ml,  $V_{\text{DEP}}$  and  $V_{\text{water}}$  the respective volumes and  $A_{8\text{HQ-silica}}$  the adsorbed amount of 8-HQ in g<sub>8HQ</sub>/g<sub>silica</sub>. The indices (1) and (2) denote the state before and after all compounds were mixed. By measuring  $c_{8\text{HQ-DEP}}^{(2)}$  and  $c_{8\text{HQ-water}}^{(2)}$  with the spectrophotometer,  $A_{8\text{HQ-silica}}^{(2)}$  can be calculated. After mixing all components (HCl used for pH adjustment), an equilibration time follows. It is important to select appropriate DEP-volumes (with 16.5 wt-% HQ) and high silica concentrations (40 wt-%) to obtain (i) measurable concentration decreases of 8-HQ in DEP (low aqueous solubility and adsorption of 8-HQ compared to the initial 8-HQ mass in DEP)

and (ii) still provide excess 8-HQ in DEP. The liquid phases must then be separated from the silica, which requires high rotation frequencies of the centrifuge ( $30000 \text{ min}^{-1}$ ) to squeeze out the oil from the particle stabilized emulsion and to separate the water from excess nanoparticles. Furthermore the dissolved water in the DEP phase must be removed under reduced pressure to obtain higher accuracy. To measure the concentration of 8-HQ in DEP a linear calibration function was established with samples of known concentrations.

### 2.3 Cryogenic SEM

The morphology of particle stabilized emulsions was examined by high-resolution cryo-scanning electron microscopy (Cryo-SEM). A sample ( $10 \mu\text{l}$ ) of the emulsion was frozen by immersing it into liquid nitrogen at atmospheric pressure. The sample was then transferred into a GATAN Alto 2500 Cryo preparation chamber. The frozen water containing the solidified oil droplets was then freeze-fractured at  $-150^\circ\text{C}$  under vacuum. By increasing the temperature for 60 sec up to  $-98^\circ\text{C}$ , a thin ice film on the fractured surface sublimates (a few hundred nanometers) and the solid emulsion droplets become partly uncovered. To prevent charging of the surface during the electron microscopic investigation, sputtering with platinum was done afterwards. The sample was then transferred into the cryo-SEM chamber.

### 2.4 Dynamic light scattering and $\zeta$ -potential

For all dynamic light scattering results within this work, only measurements with consistent correlation functions and polydispersity indices (PDI)  $< 0.4$  have been considered. For the optical parameters (real and imaginary part of the refractive index) the respective values of the bulk materials were used, for the silica-polystyrene composite particles (chapter 3.4) the core shell model included in the Malvern software (considering two refractive indices) was used. Before the measurement, all samples were appropriately diluted to obtain slightly turbid dispersions. Measurements were done in backscattering mode at a detector position of  $173^\circ$ . At least three measurements of each 15 runs were averaged. The scattering data analysis was done with the CONTIN algorithm.

The measurement of the electrophoretic mobility for polyelectrolyte coated colloidal particles (alumina-, silica-nanoparticles or particle stabilized emulsion droplets) was always performed after three consecutive washing steps. This procedure is required to measure only the  $\zeta$ -potential of the

polyelectrolyte coated particles and not that of dissolved excess polyelectrolyte molecules. By addition of diluted NaOH or HCl the pH values were adjusted. All  $\zeta$ -potentials were measured by applying the Smoluchowski model.

To characterize the charging of silica nanoparticles in 8-HQ saturated aqueous solutions with different pH values, the  $\zeta$ -potential of excess particles of an emulsion was measured. The pH value was adjusted with diluted HCl, the emulsion equilibrated for 1 hour by shaking and the particles were separated by centrifugation. The high ionic strengths at low pH values damage the electrodes due to electrochemical degradation. Therefore all measurements were done at the comparably low voltage of 10V, also to guarantee comparability at different pH values.

All measurements of the electrophoretic mobility and the dynamic light scattering were done in a DTS 1060C cell with a Malvern ZetaSizer Nano ZS, equipped with a laser operating at 533 nm.

### 2.5 Contact angle measurements

Silicon-wafer plates were cleaned in hot “Piranha solution” (3:1, 98% H<sub>2</sub>SO<sub>4</sub> to 30% H<sub>2</sub>O<sub>2</sub>) prior to all measurements. Afterwards the wafers were extensively rinsed with deionised water, dried under a nitrogen flow and immediately transferred to specially designed glass sample containers, which were then filled with aqueous buffer solutions of 1 mM alkylammonium bromides of varying chain-length. The “Piranha-treatment” of the wafer plates is required to (i) create a high density of silanol groups on the surface and (ii) decompose all organic carbon on the plates to CO<sub>2</sub>. Also the glass sample containers were cleaned with 98 % H<sub>2</sub>SO<sub>4</sub>, rinsed with water and dried in an oven at 100°C before use. Because the measurements were done above the natural pH value of water (pH 5.4), buffer solutions of NaH<sub>2</sub>PO<sub>4</sub> with Na<sub>2</sub>HPO<sub>4</sub> (5 < pH < 8) and NaHCO<sub>3</sub> with Na<sub>2</sub>CO<sub>3</sub> (8 < pH < 10) were prepared. The electrical double layer above the silanol surface of the wafer plates is made up by the positively charged hydronium-counterions and the sodium ions from the buffer components. To maintain a constant concentration of positively charged sodium ions, the concentration of the sodium was fixed to 1mM, irrespective of the ratio of the two buffer components. Thereby different buffer-capacities have been employed, but it was proofed that those were sufficient to compensate for the CO<sub>2</sub> diffusion from air during the experimental period. After equilibration of the plates in the buffered alkyl-ammonium bromide solutions for two hours, the plates were dried under a nitrogen flow and transferred to a quartz cuvette (cleaned in conc. H<sub>2</sub>SO<sub>4</sub>) filled with hexane. Drops of the corresponding buffered alkylammonium bromide solution ( $\approx 2 \mu\text{l}$ ) were deposited on the wafer plate with a microsyringe and their advancing  $\theta$  were measured on a Kruss contact angle

goniometer G10, equipped with a CCD video camera (Zoom 1:6.5). At least 10 drops per sample were measured for statistical reasons. The contact angles were evaluated with the Kruss software and for very low  $\theta$  ( $<20^\circ$ ) with the imageJ plugin LB-ADSA (Ecole Polytechnique Federale de Lausanne).

For PMAA coated alumina plates the procedure for the advancing contact angle measurements was similar to the above mentioned. The plates were coated with PMAA by dip-coating in a 2 wt-% aqueous solution at pH 4. Three consecutive washing steps, each one for 5 min in ultrapure water, followed. For the contact angle measurements, the plates were immersed in a 1 mM NaCl solution with a defined pH and after that dried in a nitrogen flow. Drops of the corresponding NaCl solution were deposited on the plates.

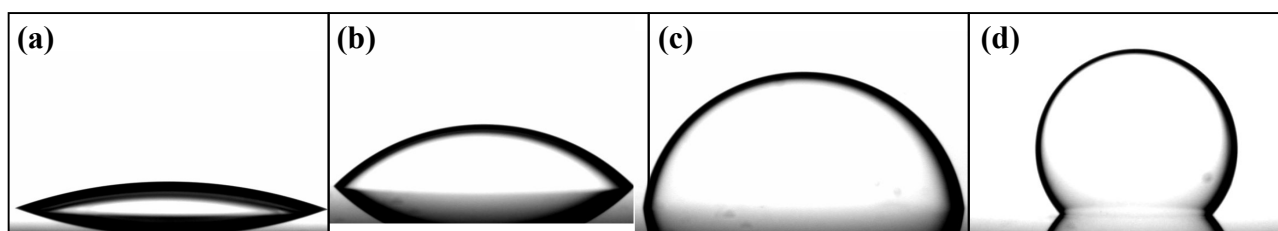


**Figure 5.** Example micrographs of sessile water droplets under hexane on a silicon-wafer plate with (a)  $20^\circ$ , (b)  $48^\circ$ , (c)  $84^\circ$  and (d)  $130^\circ$  contact angle

### 2.6 Droplet size measurements

A drop of the emulsion was added to a glass slide, covered with a coverslip, and investigated with an optical microscope (Olympus BH-2) operating in dark field mode at a magnification of  $100\times$  or  $400\times$ . In comparison with the regular transmission mode of the microscope, the dark field mode facilitated a much better processability of the images with the graphical software. In dark field microscopy only the light scattered by objects in the optical path is seen through the objective.

Ten micrographs per sample were taken by means of a camera (Olympus C-5050Zoom) with an optical zoom of  $5\times$ . The software imageJ was used for the image analysis of the micrographs. Figure 6 shows the individual steps of the image processing of the micrographs.

The function aggregate splitting recognizes spherical areas and separates droplet-flocs graphically into individual ones. After step (5) the cross-sectional areas of the droplets are obtained in square-pixels and by considering the information from (1) a conversion to  $\mu\text{m}^2$  is possible. By using the

## 2. Experimental methods

formula  $d = \sqrt{4/\pi \cdot A}$  the desired droplet-diameter is obtained. For each sample at least 3000 drops were counted.

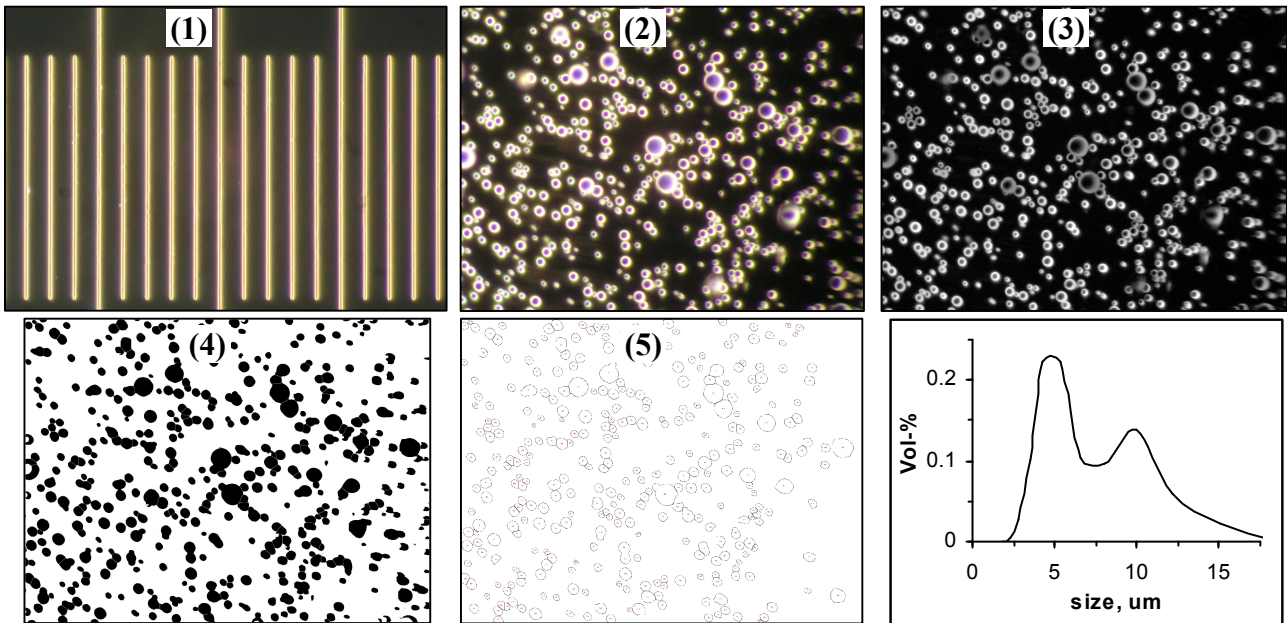


**Figure 6.** Dark-field micrographs of (1) the stage micrometer, (2) a polydisperse PSE, (3) after 8-bit reduction and contrasting, (4) after binarization and aggregate splitting and (5) evaluation of the circular areas

### 2.7 Particle attachment onto droplets

The separation of excess particles from the emulsion could easily be done by centrifugation at  $1000 \text{ min}^{-1}$  for 5 min for samples with a low degree of aggregation of the silica particles at pH values above 4.7. The aqueous supernatant of the sample containing excess particles was then transferred into a glass vessel and dried for 12 h at  $80 \text{ }^\circ\text{C}$ . The dried particles were subjected to a second heat treatment at  $500 \text{ }^\circ\text{C}$  for 6 h to remove all 8-HQ residues. With the initial particle concentration and the known volume of the sample suspension the consumption of particles per oil volume could be calculated.

### 2.8 Polyelectrolyte adsorption procedure

**Polyelectrolyte adsorption on alumina and silica nanoparticles.** A stock solution of 5 wt% PMAA-NaCl and 4 wt% PAH, respectively, was diluted in water with an appropriate volume of 1

## 2. Experimental methods

---

M HCl or NaOH, respectively, to obtain the desired pH value (PMAA-NaCl: pH 4, 5, 6, 7; PAH: pH 8, 8.5, 9.5). The same pH adjustment was done for 8 wt % alumina and 20 wt % Ludox TMA dispersion. The particle suspensions were added dropwise to the PE stock solutions with the same pH value under vigorous stirring. During this addition, the pH value was monitored continuously with a calibrated pH electrode (WTW SenTixMic) and maintained by the addition of either 1 M HCl (alumina-PMAA) or 1M NaOH (silica-PAH) with a maximum deviation of 0.1 pH units from the desired pH value. This pH value, where the coating occurs, is abbreviated as  $\text{pH}_c$ , where C in the index stands for PE-coating. This  $\text{pH}_c$  value is to be distinguished from the pH value during emulsification. The addition of the particle suspension was finished when the particle mass-fraction reached 5 wt% (alumina-PMAA) or 10 wt% (silica-PAH), respectively. All suspensions were gelated during this treatment and were sonicated in an ultrasonic bath for 20min afterward. The suspensions were subsequently ultracentrifuged for 1 h at 30 000 rpm (RCF 82700) in an ultracentrifuge (Beckmann L70 ultracentrifuge). The clear supernatant was removed, and the sediment was redispersed in ultrapure water via sonication (Ultrasonic Processor VCX 505, Sonics & Materials, Inc., USA, 20kHz, 500W, 10 mm tip diameter). Two more centrifugations at 30 000 rpm followed each one for 3 h. The suspension of redispersed nanoparticles became less turbid with each washing cycle, and optically clear suspensions were obtained (representing a low degree of nanoparticle aggregation) after the third redispersion. The excessive washing procedure here was mainly applied to show later in this work that emulsification occurs only because of PE-modified particles and not because of free polymer in solution.

**Polyelectrolyte multilayer deposition on silica nanoparticle stabilized DEP-8HQ emulsion droplets.** All layers were deposited in 0.5 M NaCl, in the pH range 4 – 5 and 8-HQ saturated solutions. The pH range is important to maintain the hydrophobicity of the 8-HQ modified silica particles and thereby maintain the stability of the emulsion. The first layer was PAH (56kDa). During the centrifugation the emulsion droplets sediment because of the higher density of DEP (1.1 g/ml) compared to water. The supernatant containing the excess polyelectrolytes can then be decanted and 8HQ saturated water at pH 5 is added for washing. The centrifugation/washing cycle was repeated two more times. The same procedure followed for the next layer of PAA (70kDa) and for the 4 subsequent alternating layers of PAH and PAA

### 2.9 Preparation of particle stabilized emulsions, core-polymerization and transfer to the waterborne alkyd-resin

**Weak polyelectrolyte coated particles as emulsifiers.** Emulsions were always prepared with 2 wt-% of particles dispersed in water at the desired pH value and 25 vol-% of the oil-phase. Emulsification was done by ultrasonication with an ultrasonic processor (Sonopuls HD200, Bandel-Germany, 20kHz, 200W, 2 mm tip-diameter) for 4 min under cooling in a stirred ice-bath. Samples were characterized 12 h after preparation. Each emulsification was performed at the same ultrasonic intensity, emulsification time, emulsion volume, dipping depth of the sonotrode, and cooling rate.

**8-HQ modified silica particles as emulsifiers.** Emulsions were always prepared with 2.5 wt-% Ludox TMA particles dispersed in water and 25 vol-% of DEP (16.5 wt-% 8-HQ), after mixing the pH was adjusted by the addition of diluted HCl. Emulsification was done by ultrasonication with an ultrasonic processor (VCX 505, Sonics & Materials Inc. Newtown, U.S.A., 20 kHz, 40 W, 10 mm tip-diameter) for 2 min under cooling in a stirred ice-bath. Flocculated emulsions could be dispersed by stirring.

**Miniemulsions with silica particles.** Emulsions were always prepared with Ludox TMA particles and 13.5 wt-% of the monomer mixtures. The following listing gives the mass fractions of the components for the styrene polymer: 0.771 styrene, 0.18 8-HQ, 0.041 HD, 0.008 AIBN and for the styrene-4VP copolymer: 0.514 styrene, 0.257 4-VP, 0.18 MBTA, 0.041 HD, 0.008 AIBN. A nitrogen flow was passed through the monomer mixtures and the aqueous particle suspension for 5 min to remove dissolved oxygen. The aqueous suspension contained sufficient NaOH or HCl to adjust the pH value for the styrene-4VP-MBTA emulsion to pH 8 and for the styrene-8HQ emulsion to pH 4.8. The emulsification was done as described in the previous passage, but during emulsification nitrogen gas was passed through the emulsion. Polymerization of the emulsions took place in closed glass containers and was done in a stirred polyethylene glycol bath (600 Da) at 70°C for 24 hrs. After that the polymerized miniemulsions were centrifuged down at 70°C. The temperature maintenance during the centrifugation is required due to the problem that at 70°C more 8-HQ or MBTA is dissolved in water, and cooling down the aqueous phase to room temperature leads to the precipitation of this material and thereby contamination of the polymer-capsules. The sediment was directly added to the water-borne alkyd resin and dispersed with an ultra-turrax mixer at 10000 min<sup>-1</sup> for several minutes. The viscous dispersion was allowed to stand for 12 hrs so that air bubbles (introduced during dispersing) could ascend. Aluminium plates were then dip-coated and allowed to dry afterwards for 2 days before anticorrosive tests took place.

### 2.10 Aluminium plates pre-treatment and dip-coating

For cleaning and generating a homogeneous oxide layer aluminium plates were subjected to the following procedure. (i) Immersion into hot (60°C) 1 M NaOH solution for 15 minutes, (ii) rinsing with water, (iii) immersion into (room-temperature) 15 wt-% HNO<sub>3</sub>, (iv) rinsing with deionized water and (v) drying with a nitrogen flow.

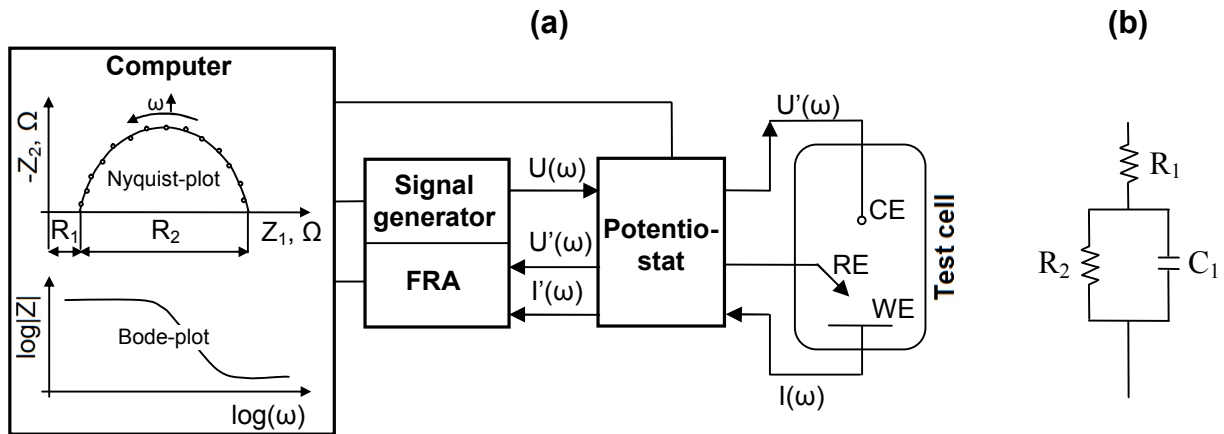
Dry silica/polymer composite particles were transferred to the coating resin and dispersed with an ultra-turrax for several minutes. The dispersion was stored for 12 hrs to allow for air-bubbles (introduced during the dispersion step) to ascend. For coating the plates with a water-based resin a dip-coating apparatus (Siemens LOGO, 12/24RC) was used. Plates were immersed vertically into the resin for 60 seconds. Film formation was performed at a pull-out speed of 0.3 mm/s. The plates were then dried for 4 days in a horizontal alignment.

### 2.11 Electrochemical impedance spectroscopy

During an electrochemical impedance spectroscopy (EIS) measurement the sample (e.g. an aluminium plate with an overlying polymer-film) is subjected to a sinusoidal voltage signal ( $U = U_0 \sin(\omega t)$ ). The system answer is a phase shifted oscillating current signal ( $I = I_0 \sin(\omega t + \phi)$ ). Both  $V$  and  $I$  can be represented vectorially and by dividing the absolute values of these vectors the systems impedance is obtained.

$$|\vec{Z}| = |\vec{U}| / |\vec{I}| \quad (2.2)$$

The representation of the impedance by complex numbers combines the ratio of the voltage and current amplitudes  $U_0/I_0$  with the phase shift  $\phi$  in one mathematical expression. In its Cartesian form the complex impedance writes  $Z = Z_1 + jZ_2$ . An EIS test is performed for a set of different frequencies of the sinusoidal voltage signal (usually in the range  $10^{-4} - 10^5$  Hz). The measurements in the frequency domain are performed with a frequency response analyzer (FRA). A typical experimental setup is shown in Scheme 4(a).



**Scheme 4.** (a) Impedance setup using a frequency response analyzer (FRA). CE calomel electrode, RE reference electrode, WE working electrode. (b) electrical circuit of a resistor ( $R_1$ ) in a series with a parallel circuit of another resistor ( $R_2$ ) and a capacitor ( $C_1$ ).

In the signal generator the sinusoidal voltage  $U(\omega)$  is generated and transmitted via the potentiostat through the calomel electrode to the test cell. The test cell is filled with an electrolyte solution and contains the immersed sample to investigate. The sample is connected to the working electrode (WE). Measurement of the electrical current  $I(\omega)$  takes place in the potentiostat, which also transfers the in- ( $U'(\omega)$ ) and output ( $I'(\omega)$ ) signal to the FRA. In the FRA the impedance  $Z(\omega) = U'(\omega)/I'(\omega)$  is calculated and transferred to a computer for data-processing. The real and imaginary parts of the impedance for each frequency can then be plotted in a Nyquist- or Bode- plot. Depending on the shape of the data representation in these plots different physical models can be used for the analytical representation of the data. The models can be obtained by fitting the data numerically to an equivalent electrical circuit, which consists of parallel- or series circuits of elementary electrical modules (resistor, capacitor, inductor). The appearance of the impedance data in the Nyquist- or Bode- plot allows for the selection of an appropriate electrical circuit. In Scheme 4(a) an example of this appearance is shown, which corresponds to a series circuit of a resistor with a parallel circuit of a second resistor and a capacitor  $R_1(R_2/C_1)$  as depicted in Scheme 4(b). Herein  $R_1$  can be physically interpreted as the resistance of the electrolyte solution. For a sample consisting of e.g. a blank aluminium plate  $C_1$  can be interpreted as the electrical double layer capacitance and  $R_2$  as the resistance of the oxide layer on the surface. For the case of a polymer-film on the aluminium substrate  $C_1$  and  $R_2$  can be assigned to the properties of this polymer-film. The analytical expression of the complex impedance for this circuit is given in equation (2.3)

$$Z = R_1 + \frac{R_2}{1 + \omega^2 C_1^2 R_2^2} - j \frac{\omega R_2^2}{1 + \omega^2 C_1^2 R_2^2} \quad (2.3)$$

In chapter 3.4.6 this model is applied to measured EIS data by numerically fitting the data with equation (2.3) by means of the software IviumSoft (1.611). All measurements were performed at a constant voltage amplitude of 10mV in a frequency range of  $65 \cdot 10^3 - 10^{-2}$  Hz (5 frequencies per decade). Before the measurement the open cell potential was detected, and measured impedances were corrected by the obtained value. The potentiostat-microprocessor combination used for the measurements was a CompactStat instrument from Ivium Technologies.

## 2.12 Scanning vibrational electrode technique

EIS measurements give integral information about electrochemical processes occurring on a given surface area. The Scanning Vibrational Electrode Technique (SVET) allows studying locally the electrochemical processes occurring on the surface. Electrochemical corrosion of metallic samples is always accompanied by oxidative and reductive reactions on the surface.<sup>115</sup> This again results in an ionic flow along potential gradients from the anodic to the cathodic areas in the electrolyte solution. The spatial distribution of these potential gradients can be measured with a vibrating microelectrode by scanning horizontally some hundred micrometers over the surface. The vibration plane is perpendicular to the sample surface and its amplitude is in the order of tens of micrometers. The vibration in the electric field causes an alternating current in the electrode, which is analyzed in a phase sensitive detector and amplifier. A high sensitivity of the measuring electrode is given for a high surface area of the tip, which can e.g. be achieved by the electrochemical deposition of a porous platinum surface coating. For calibration a second microelectrode is placed at a defined separation distance from the measuring electrode and a known direct current is transmitted. The measurements can then be expressed as current densities. Figure 7 shows the results of a SVET measurement in an area of  $3 \times 3 \text{ mm}^2$  above a scratched polymer film on a corroding aluminium substrate.

The maximum in Figure 7(a) and (b) grows with time and reaches normally a plateau value after some hours. It represents quantitatively the localized anodic reaction rate on the surface, while the cathodic reaction is normally delocalized as can be seen by the blue minima areas in Figure 7(a) and (b). In chapter 3.4.7 the maximum of the spatial current density distribution will be investigated to evaluate the efficiency of inhibitive pigments in a fractured polymer-film on aluminium.

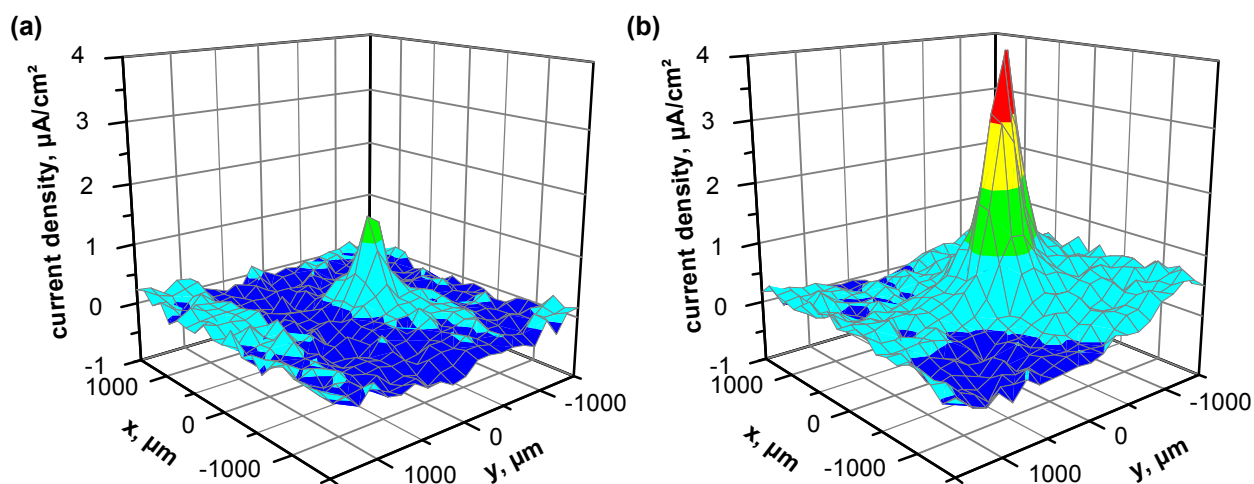


**Figure 7.** Graphical representation of the current density distribution measured 300  $\mu\text{m}$  above a scratched polymer-film on an aluminium substrate in a 0.1 M NaCl solution. **(a)** after 30 min and **(b)** after 8 hrs.

Measuring parameters: Tip vibration frequency 840 Hz, diameter 20  $\mu\text{m}$  Pt-Tip with a capacitance of 6.6 nF, vibration amplitude 60  $\mu\text{m}$ , tip position 300  $\mu\text{m}$  above surface, current density detection with a scanning resolution of 150  $\mu\text{m}$ , scanned area 3x3  $\text{mm}^2$ , periodical scanning each 15 min.

### 2.13 Confocal laser scanning microscopy

In chapter 3.4.4 the distribution of particles inside a polymer-film is discussed. To visualize the three-dimensional distribution of particles in such a film a conventional microscope cannot be used, since one picture contains optical information about many different depth-levels of the sample at once. In a confocal laser scanning microscope (CLSM) a pinhole blocks the light coming from out of the focal plane, and only scattered, reflected or fluorescent light from the focal plane is detected. A picture is obtained by scanning point-by-point over the sample and each illuminated point is then electronically transformed to a pixel with a defined intensity. Reconstruction of the complete picture is then done by means of a computer. Raising or lowering the microscope's stage changes the focal plane. The combination of several so obtained pictures from different depth levels allows for a 3-dimensional reconstruction of the investigated sample by means of a suitable software. Objects to be investigated can be marked by fluorescent dyes, which allow for distinguishing the

objects from others. More detailed technical information about the CLSM can be found elsewhere.<sup>116</sup>

In the present work the fluorescence dye Nil red was dissolved in styrene (1 wt-% Nil red, 20 wt-% 8-HQ) and subsequent emulsification and polymerization (see chapter 2.9 last paragraph) yielded fluorescent dye filled polymer-spheres. These particles were dispersed in a water-based alkyd-emulsion and one side of a microscopic glass slide was coated with the dispersion by dip-coating. CLSM was performed with a Leica TCS SP2 microscope. For the fluorescence excitation a laser with a wavelength of 488 nm was used, while the fluorescence light was observed in the wavelength interval 550 – 650 nm. The used objective had magnification of 100x and a numerical aperture of 1.4. For the vertical scan through the polymer film a step size per image acquisition of 0.1  $\mu\text{m}$  was used.

### **2.14 Du Noüy ring tensiometry**

For the interfacial tension measurements all glass-ware was cleaned with 98 % sulphuric acid. The shape of the platinum ring was directed and organic contaminations were burned in an ethanol flame before measurement. Aqueous solutions of 1 mM alkylammonium bromides and hexane were equilibrated against each other in a closed bottle over 36 hrs. Measurements of the interfacial tension were performed in this bottle on the equilibrated interface. For the measurements a ring tensiometer (Lauda, force sensor Q11 HBM) with a ring radius 9.55mm, a wire radius 0.18 mm and a lifting speed of 0.3 mm/s was used. Results were evaluated with the software TE-2 1.03.06.

## 3 Results and discussion

### 3.1 Short Amphiphiles

The adsorption of short chain amphiphiles can change the wetting characteristics of inorganic surfaces as discussed before.<sup>78-80</sup> Here, the wettability changes of silica, modified with alkyltrimethylammonium bromides (ATMAB) of varying alkyl chain length are studied. The quaternary ammonium head group has practically a pH independent dissociation, but the silica surface itself changes its charge density upon pH changes. Basing on contact angle and interfacial tension measurements a calculation of the interfacial energy of the solid surface is performed.

#### 3.1.1 Contact angle measurements

For the contact angle measurements silicon-wafer plates were used. The pre-treatment of the plates in a mixture of 1 part 30 % hydrogen peroxide and 3 parts 98 % sulphuric acid (Piranha solution) results in a silanol-group saturated surface. The surface therefore is chemically similar to a silica surface and can be regarded as a flat analogue of the curved surface of a silica particle. A silanol surface group acts as an acid/base group by dissociation and release of a proton to the aqueous solution. Similar to a dissolved acid molecule the degree of dissociation of a silanol surface group depends on the pH value. However the electrostatic interaction with neighbouring silanol groups suppresses the dissociation and the charge density of the surface can not be described with the simple Henderson-Hasselbalch equation. The surface charge density of silica powders has been evaluated in several classical works<sup>117-119</sup>. It grows exponentially above pH 6 and the silica surface exposes thereby an increasing amount of negatively charged dissociated silanol groups towards the aqueous solution. For cationic ATMAB with increasing pH the electrostatic attraction rises and a higher adsorption density can be found at the same aqueous concentrations<sup>120</sup>. For high adsorption densities and long alkyl chain lengths the lateral hydrophobic interactions enable also the formation of bi-layers on the surface. However, for the low ATMAB concentration and short chain lengths in this work, this effect should be negligible and only monolayer adsorption can be assumed. Figure 8(a) shows the pH dependence of the  $\theta$  of droplets of aqueous solutions containing 1 mM ATMAB with different alkyl chain lengths on silica surfaces under hexane and in Figure 8(b) under air.

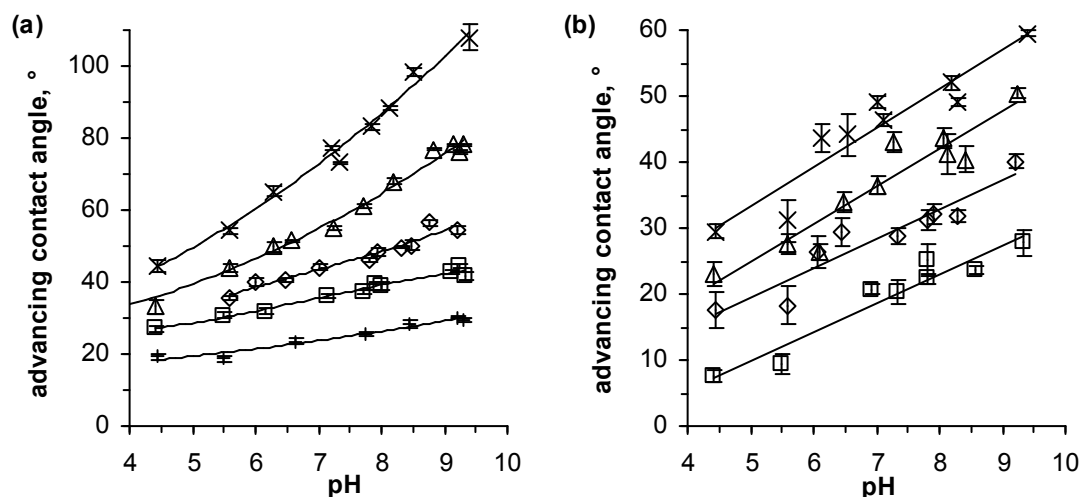


**Figure 8.** Advancing contact angles for droplets of aqueous solutions of 1 mM ATMAB on silicon-wafers (enriched with silanol surface groups) under (a) hexane and (b) air in dependence of the pH value. + butyl-, □ hexyl-, ◇ octyl-, △ decyl- and × dodecyltrimethylammoniumbromide. Lines are drawn to guide the eye.

For a given alkyl chain length the  $\theta$  increases with the pH under hexane and air. The increase of the pH is accompanied by an increase of the silica charge density, which in principle increases the hydrophilic character of the surface. The  $\theta$  is a function of the surface energies involved at the three-phase contact line. These surface energies in turn depend on the concentration of surface active molecules at these interfaces. By increasing the surface charge, the adsorbed amount of positively charged ATMAB molecules increases, accompanied by an increase of the  $\theta$  for a water droplet.

Droplets under hexane show higher  $\theta$  than droplets in air, which is related to the combination of the interfacial tensions acting at the three phase contact line as shown later. From the curves in Figure 8 the  $\theta$  for constant silica charge densities (pH values), but different ATMAB chain lengths can be obtained. This alkylchain-length dependence of the  $\theta$  for constant pH values is shown in Figure 9.

At low silica charge densities (pH 5) the advancing  $\theta$  of water droplets under hexane increases almost linearly with the alkyl chain length. But by increasing the surface charge density the dependence of the  $\theta$  on the chain length gets more nonlinear (pH 7 and pH 9). This indicates an increased lateral hydrophobic interaction between the alkyl chains, which becomes pronounced when the distance between the negatively charged adsorption sites is reduced. This interaction becomes more strong at longer alkyl chain lengths and is capable of increasing the adsorption density.<sup>121</sup> For water droplets under air the  $\theta$  dependence on the alkyl chain length appears linear for

all pH values. With the  $\theta$  data under hexane and air a surface energy analysis can be done, which additionally requires the fluid/fluid interfacial tensions.

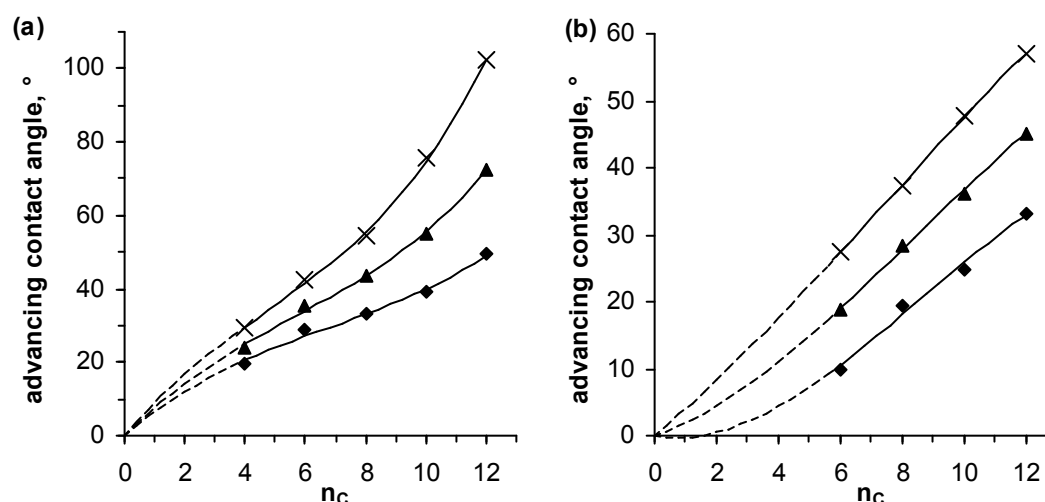


**Figure 9.** Representation of the advancing contact angles for droplets of aqueous solutions of 1 mM ATMAB vs. the number of carbon atoms of the alkyl chain under (a) hexane and (b) air. ◆ pH 5, ▲ pH 7 and × pH 9. Lines are drawn to guide the eye.

### 3.1.2 Results of fluid-fluid interfacial tension measurements

Figure 10 shows the air/water and hexane/water interfacial tensions of 1 mM aqueous ATMAB solutions of different alkyl chain lengths. For the interfacial tension between water and hexane both phases are saturated against each other. The interfacial tension is assumed to be in its equilibrium state after 14 hrs of equilibration.

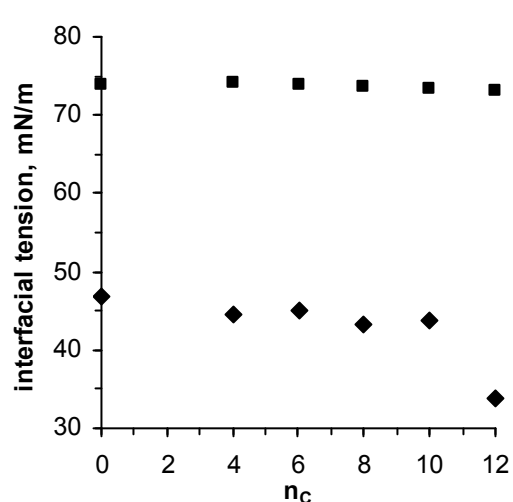


**Figure 10.** Interfacial tension of aqueous solutions of 1 mM ATMAB at the interface to ■ air and ◆ hexane vs. the number of carbon atoms of the alkylchain.

The interfacial tension against air does not change remarkably for all ATMAB investigated here. Up to decyltrimethylammonium bromide also the interfacial tension against hexane decreases only slightly. It follows that except for 1 mM aqueous

dodecyltrimethylammonium bromide solution the interfacial activity of the short ATMAB at this concentration is very low and the water/air or water/hexane interface contains only negligible amounts of the short amphiphiles. For concentrations of 1 mM the short alkyl chains do neither for air nor for hexane provide sufficient hydrophobic interaction with the nonpolar phase to compensate for the attraction to the aqueous phase due to the high polarity and repulsive character of the quaternary ammonium group.

#### 3.1.3 Calculation of the surface energy of the solid

The surface tension of the solid cannot be measured directly but can be calculated with the contact angles under hexane and air from section 3.1.1 and the fluid-fluid interfacial tensions from section 3.1.2. The calculation bases on the assumption that any interfacial tension against a gas (here air) equals the sum of the dispersive ( $\gamma^d$ ) and polar ( $\gamma^p$ ) components of the respective surface tensions:<sup>122</sup>

$$\gamma_{xa} = \gamma^d + \gamma^p \quad (3.1)$$

To estimate the interfacial tensions between two liquids or a solid and a liquid so called combining rules of the polar and dispersive components of the two involved materials are required. One established method to do so is to estimate the contribution of the dispersive<sup>122</sup> and the polar<sup>123</sup> interactions by their geometric mean values

$$\gamma_{\alpha\beta} = \gamma_\alpha + \gamma_\beta - 2\sqrt{\gamma_\alpha^d \gamma_\beta^d} - 2\sqrt{\gamma_\alpha^p \gamma_\beta^p} \quad (3.2)$$

for the two phases  $\alpha$  and  $\beta$ . A method to use this expression for the calculation of the solid surface tension on the basis of  $\theta$  measurements of water-droplets under two nonpolar liquids was introduced by Tamai et al.<sup>124</sup>. Here a modification of their two liquids method is applied, which uses the  $\theta$  under a nonpolar liquid and air.<sup>125</sup>

#### 1. Calculation of the polar and dispersive component of the water/air interfacial tension

With the indices a = air, h = hexane, w = water the following definitions can be done:

$$\gamma_a^p = \gamma_a^d = 0 \quad (3.3)$$

$$\gamma_h^p = 0 \quad (3.4)$$

$$\gamma_{wa} = \gamma_w^p + \gamma_w^d \quad (3.5)$$

$$\gamma_{ha} = \gamma_h^d \quad (3.6)$$

With equation (3.2) the water-hexane interfacial tension can be expressed. By considering equations (3.4), (3.6) and after some rearrangements the dispersive component of the interfacial tension of water can be written as

$$\gamma_w^d = \frac{1}{\gamma_{ha}} \left( \frac{\gamma_{wa} + \gamma_{ha} - \gamma_{hw}}{2} \right)^2 \quad (3.7)$$

Equation (3.5) yields then the polar component of the interfacial tension of water.

$$\gamma_w^p = \gamma_{wa} - \gamma_w^d \quad (3.8)$$

The calculation with the measured fluid-fluid interfacial tensions yields  $\gamma_w^p = 46$  mN/m and  $\gamma_w^d = 28$  mN/m which is in acceptable agreement with the literature values ( $\gamma_w^p = 50.4$  mN/m and  $\gamma_w^d = 21.5$  mN/m)<sup>126</sup>. Differences result from the inaccuracy of the liquid-liquid interfacial tensions during the measurements here. For the following calculations  $\gamma_w^p$  and  $\gamma_w^d$  obtained in this work will be used.

## 2. Calculation of the polar and dispersive components of the solid/air interfacial tension

In the following, it is assumed that the adsorbed amount of ATMA B is equal on the solid-oil, solid-air and solid-water interface. This assumption is reasonable, since the silicon wafer plates were equilibrated in an aqueous solution of the ATMA B. After taking out the plates from the solution, residual water on the surface was blown away by a nitrogen stream. Visually the surface showed no inhomogeneities afterwards and it was homogeneously reflecting light. The adsorbed amount of the ATMA B should not have changed significantly upon water removal, since the ATMA B are still held at the surface due to the strong electrostatic attraction of the oppositely charged silica surface groups. The same should hold true when the plates are immersed into hexane, since the strongly charged amphiphiles experience almost no solubility in this nonpolar liquid. After adding water-droplets containing 1 mM ATMA B onto the plates under hexane, the  $\theta$  did not change with time, indicating that no redistributions of the ATMA B on the surfaces took place. However, this holds not true for droplets under air, but here it is the evaporation of the water droplet, which decreases  $\theta$  with time (the receding  $\theta$  is then observed).

For a sessile water-droplet under air and another one under hexane two Young equations can be set up:

$$\cos\theta_{aw} = \frac{\gamma_{sa} - \gamma_{sw}}{\gamma_{aw}} \quad (3.9)$$

### 3.1 Results and discussion: Short Amphiphiles

$$\cos \theta_{hw} = \frac{\gamma_{sh} - \gamma_{sw}}{\gamma_{hw}} \quad (3.10)$$

For the interfacial tension between a solid and water the complete equation (3.2) must be taken into account while for the system solid-hexane the square-root of the polar components of the interfacial tension can be neglected due to equation (3.4).

$$\gamma_{sw} = \gamma_{sa} + \gamma_{wa} - 2\sqrt{\gamma_s^d \gamma_w^d} - 2\sqrt{\gamma_s^p \gamma_w^p} \quad (3.11)$$

$$\gamma_{sh} = \gamma_{sa} + \gamma_{ha} - 2\sqrt{\gamma_s^d \gamma_h^d} \quad (3.12)$$

Combining equation (3.9) with (3.11) and (3.10) with (3.12) and considering equation (3.6) yields

$$\cos \theta_{aw} = \frac{2\sqrt{\gamma_s^d \gamma_w^d} + 2\sqrt{\gamma_s^p \gamma_w^p} - \gamma_{aw}}{\gamma_{aw}} \quad (3.13)$$

$$\cos \theta_{hw} = \frac{\gamma_{ha} - \gamma_{wa} - 2\sqrt{\gamma_s^d \gamma_{ha}^d} + 2\sqrt{\gamma_s^d \gamma_w^d} + 2\sqrt{\gamma_s^p \gamma_w^p}}{\gamma_{hw}} \quad (3.14)$$

The combination of equation (3.13) with (3.14) gives an equation for the dispersive component of the interfacial tension of the solid with only measurable quantities

$$\gamma_s^d = \frac{1}{4\gamma_{ha}} (\gamma_{ha} + \gamma_{aw} \cos \theta_{aw} - \gamma_{hw} \cos \theta_{hw})^2 \quad (3.15)$$

The polar component can then easily be obtained by rearranging equation (3.13)

$$\gamma_s^p = \frac{1}{\gamma_w^p} \left( \frac{\gamma_{aw} + \gamma_{aw} \cos \theta_{aw} - 2\sqrt{\gamma_s^d \gamma_w^d}}{2} \right)^2 \quad (3.16)$$

For the measured contact angles  $\theta_{aw}$ ,  $\theta_{hw}$ , interfacial tensions  $\gamma_{aw}$ ,  $\gamma_{hw}$ ,  $\gamma_{ha}$  and the calculated polar and dispersive components of the interfacial tension of water  $\gamma_w^p$ ,  $\gamma_w^d$  the polar and dispersive components of the solid surface tension  $\gamma_s^p$ ,  $\gamma_s^d$  can now be calculated. The results for the silica surface with adsorbed ATMBAB of different chain-lengths are shown in Figure 11(a) and (b).

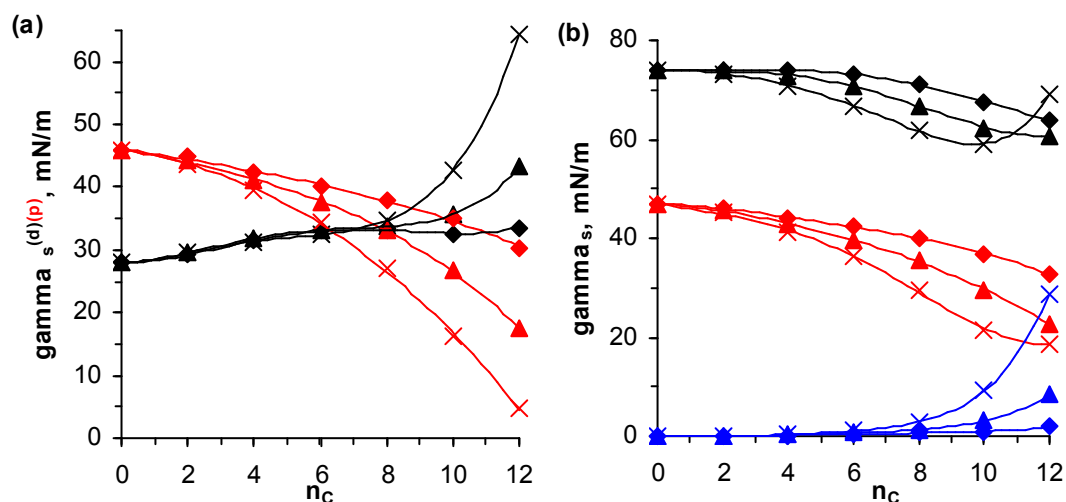


**Figure 11.** Surface tensions of the silica surface with adsorbed alkyltrimethylammonium bromides **(a)** dispersive and polar components of the surface tension, **(b)** surface tension against air (black), against hexane (red) and water (blue) for different pH values in dependence of the number of carbon atoms in the alkyl chain.  $\blacklozenge$  pH 5,  $\blacktriangle$  pH 7 and  $\times$  pH 9. Lines are drawn to guide the eye.

The dispersive component of the solid interfacial tension increases, while the polar component decreases with increasing alkyl chain length. For  $\gamma_s^p$  the decrease is always bigger with higher pH values, while for  $\gamma_s^d$  the increase becomes bigger for alkyl chain lengths above  $n_c = 8$  with higher pH values. This results from the higher lateral hydrophobic interactions of the longer alkyl chains at high adsorption densities, as recognized also in the tilt of the curves in Figure 9(a). The drop of  $\gamma_s^p$  can be understood by considering the adsorbed ATMAAB layer as a shielding film above the polar silica surface.

In comparison to the work of Meglias-Alguacil et. al.<sup>80</sup> the low amphiphile concentration studied here allows for neglecting effects on the  $\theta$  arising from changes of the fluid-fluid interfaces (except for  $n_c \geq 12$ ). Thus, only the changes of the solid surface energies can be considered to influence the  $\theta$ . Figure 11 (b) shows the solid surface tensions in dependence of the alkyl chain length. While below  $n_c = 8$  the interfacial tension of the solid against water increases only slightly, the interfacial tension against air and especially hexane decreases already remarkably (especially for higher pH values). Therefore the improvement of the wettability of the nonpolar phase can be considered as the main influence governing the increase of  $\theta$ . Thus, the terminology of an increase of the “hydrophobicity” conventionally used in the field of particle stabilized oil/water emulsions should here be replaced by an increase of the “lipophilicity”. However, the situation changes for  $n_c > 12$  at

pH 9. Here, beside the change of the hexane-water interfacial tension, in fact the increased hydrophobicity dominates the  $\theta$ , as  $\gamma_{sw}$  becomes bigger than  $\gamma_{sh}$ .

Since the interfacial tension of the solid against air is composed only of the sum  $\gamma_{sa} = \gamma_s^p + \gamma_s^d$ , the minimum of  $\gamma_{sa}$  at  $n_C = 10$  for pH 9 results from the strong increase of  $\gamma_s^d$  in this region. However, for  $\gamma_{sh}$  the consideration of the geometric means of the polar and dispersive components in equation (3.2) shifts this minimum to a higher  $n_C$ .

To an aqueous solution of 1 mM dodecyltrimethylammonium bromide with a pH value of 9, silica nanoparticles (LudoxTMA) and hexane were added. The mixture was shaken. In contrary to the expectation basing on the  $\theta$  measurements ( $\theta > 90^\circ$ ) the formation of an oil-in-water emulsion was observed. This might have several reasons: (i) the line tension effect described by Aveyard<sup>31</sup> might be responsible for a significant decrease of  $\theta$  below  $90^\circ$ , (ii) the charge density of the silica nanoparticle surface might be lower, thereby reducing the amount of adsorbed ATMA molecules in comparison with the silanol group enriched silicon surface. Also contact angle hysteresis might play a role. As discussed in the introduction, a phase inversion from o/w to w/o by the modification of hydrophilic particles with charged single-chain-surfactants is usually only observed, when two amphiphiles per surface group adsorb and very high surface coverage is obtained.<sup>7, 74, 76</sup>

Therefore it can be concluded, that the  $\theta$  measurements here cannot be quantitatively assigned to silica nanoparticles, but can be considered to show qualitatively the trend of the wettability also of nanoparticles for hexane, air or water in the presence of ATMA.

## 3.2 Weak Polyelectrolytes

The affinity of weak polyelectrolyte coated oxide particles to the oil-water interface can be controlled by the degree of dissociation and the thickness of the weak polyelectrolyte layer. Thereby the oil-in-water (o/w) emulsification ability of the particles can be enabled. The weak polyacid poly(methacrylic acid sodium salt) (PMAA) and the weak polybase poly(allylamine hydrochloride) (PAH) were selected for the surface modification of oppositely charged alumina and silica colloids to demonstrate this effect in the following section.

### 3.2.1 Characterization of weak polyelectrolyte coated nanoparticles

#### 3.2.1.1 Size distribution measured by dynamic light scattering

After the adsorption of PMAA on alumina particles at different pH values ( $\text{pH}_C$  values, see experimental chapter, section 2.8) and subsequent removal of the excess polyelectrolytes the size distributions of the particles were measured and the results are shown in Figure 12.

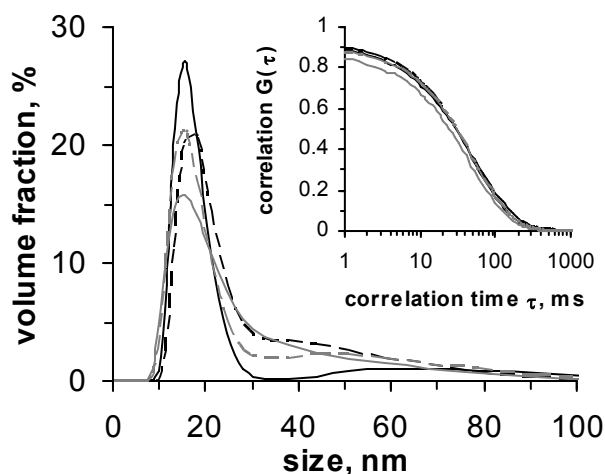


**Figure 12.** Measured correlation functions and calculated volumetric size distributions for PMAA coated alumina particles. Key to the lines for both diagrams: black dashed  $\text{pH}_C$  6, grey continuous  $\text{pH}_C$  5, black continuous  $\text{pH}_C$  4, grey dashed uncoated alumina particles at pH 4. The suspension pH value of all PMAA coated particles lies between pH 6 and 7. For all measurements the refractive index of alumina of 1.776 was used.

The main maximum of the distributions can be found for all particles at approximately 16 nm. A coexisting small fraction of bigger particles can be found for coated and uncoated particles at bigger sizes below 100 nm. Considering the data obtained from DLS measurements and the translucency of the suspensions it can be concluded, that the initial particle size-distribution of the particles can be preserved.

3.2.1.2 pH and polyelectrolyte layer thickness dependent  $\zeta$ -potential measurements

Cesarano et al.<sup>21</sup> studied the adsorption of PMAA (15000 g/mol) onto alumina and found the adsorbed amount to depend strongly on the pH value during the adsorption step. With a decreasing pH value the adsorbed PMAA amount increases greatly, in particular in the pH region in which the degree of dissociation ( $\alpha$ ) of the PMAA acid groups changes dramatically (pH 3 - 6). This concept can be generalized to the adsorption behaviour of PAH on silica. The only differences are the different pH range and the reverse pH direction for a decreasing charge (see section 1.2).

BET measurements of the alumina nanoparticles used in this work gave a specific surface area of 396 m<sup>2</sup>/g. With this surface area and the adsorbed amount measured by Cesarano et al.<sup>21</sup> one can calculate the adsorption for alumina nanoparticles used in this work to be approximately 0.55 g<sub>PMAA</sub>/g<sub>alumina</sub> maximum. To guarantee the adsorbed amount of PMAA to be as high as possible for each pH<sub>C</sub> the PMAA/particle ratio was selected to be 0.58 g<sub>PMAA</sub>/g<sub>alumina</sub> (4 mmol PMAA-monomer/g<sub>alumina</sub>) to provide excess polyelectrolytes (PEs) in the solution. For the system PAH-silica the same ratio of PE monomer moles per particle mass was used. The adsorbed amount of PAH on silica is expected to be lower due to the smaller surface area. This rough assumption was done because no quantitative information about the adsorbed amount of PAH onto silica could be found in literature.

After washing, the measured  $\zeta$ -potential of the PE-modified particles should be influenced only by the contribution of the pH dependent dissociation of the adsorbed PE, the underlying oxide particle surface, and the ionic strength. The results of  $\zeta$ -potential measurements are shown in Figure 13(a) for PMAA-coated alumina and in Figure 13(b) for PAH-coated silica particles.

Alumina particles themselves have an isoelectric point (IEP) at pH  $\approx$  9 and are positively charged in the range of the pH values displayed in Figure 13(a), whereas the IEP of silica particles can be found at pH  $\approx$  2, and their surface is negatively charged at the pH values displayed in Figure 13(b). With the PEs on the surface, the  $\zeta$ -potential sign of the particles is reversed. By changing the pH value to decrease  $\alpha$  of the adsorbed PEs, the  $\zeta$ -potential in absolute value decreases. The sign is reversed to the charge corresponding to the bare particle surface at the IEP of the PE/particle composite.

From Figure 13, three main conclusions, valid for both PE particle combinations, can be drawn: With decreasing  $\alpha$  of the PE (increasing pH<sub>C</sub> for PAH, decreasing pH<sub>C</sub> for PMAA) during the adsorption step, (i) the IEP shifts toward pH values corresponding to lower  $\alpha$ , (ii) the absolute value of the  $\zeta$ -potential of the particles with a charged PE layer is higher for the same pH value, and (iii) particle flocculation in the suspension occurs at pH values with a lower corresponding  $\alpha$ .

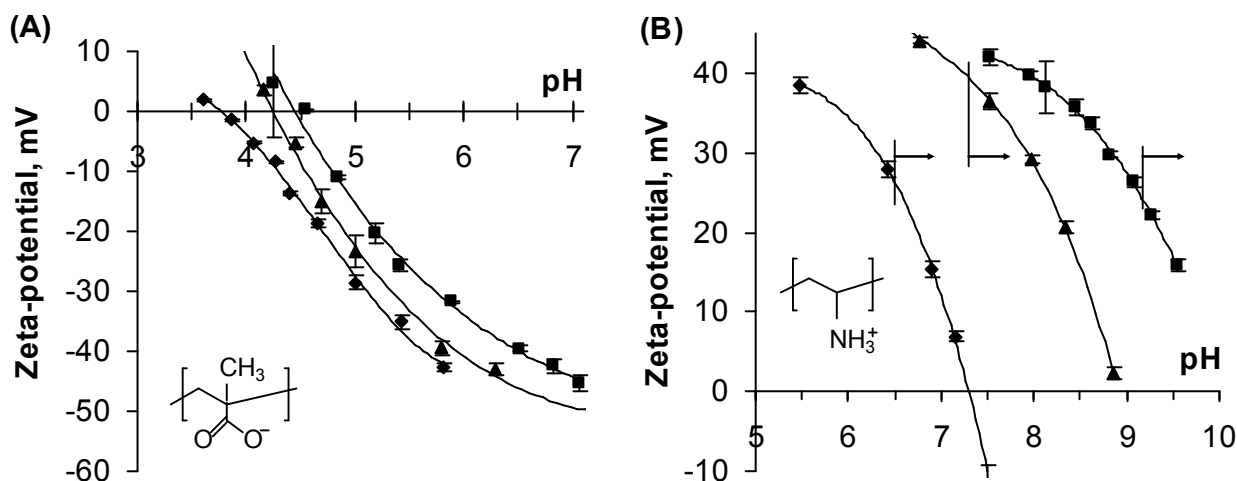
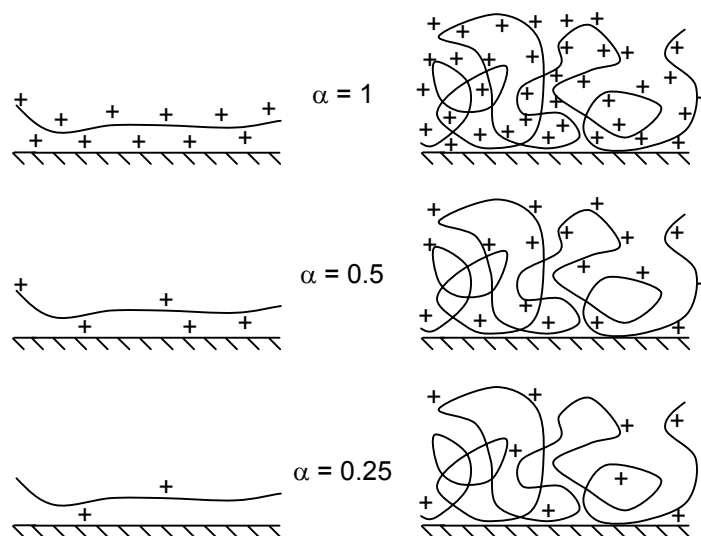


**Figure 13.** pH dependence of the  $\zeta$ -potential for PE coated nanoparticles with different pH values of PE-coating ( $\text{pH}_C$ ): (A) PMAA coated Alumina: ■ -  $\text{pH}_C = 7.0$  ; ▲  $\text{pH}_C = 6.0$  ; ◆  $\text{pH}_C = 4.0$  ( $\text{pH}_C = 5$  excluded to prevent overcrowding) (B) PAH coated Silica: ■ -  $\text{pH}_C = 9.5$  ; ▲  $\text{pH}_C = 8.0$  ; ◆  $\text{pH}_C = 7.0$ . Vertical lines with arrows show the pH value where the occurrence of turbidity was observed. Error bars give standard deviation of 5 measurements. For alumina-PMAA turbidity occurs for  $\text{pH}_C = 7, 6, 5, 4$  at pH 5.6, 5.3, 4.5 and 4.0 respectively.

These conclusions can be explained by the  $\text{pH}_C$ -dependent amount of adsorbed PE on the surface, as described at the beginning of this section. With lower  $\alpha$  during the PE adsorption step, a larger amount of the PE per surface area is adsorbed (thicker PE layer). It can be concluded therefore that thicker PE layers provide more charges per surface area at a given pH value. This explains the higher absolute  $\zeta$ -potentials for thicker layers at similar pH values. For thick layers, even at low values of  $\alpha$ , there is still sufficient total charge to compensate for the counteracting charge of the bare particle surface. Because of that, the IEP of the particles is shifted. Scheme 5 illustrates this argumentation.

The pH value for the occurrence of turbidity in the suspension is denoted as the critical flocculation pH (c.f.pH), and a broader pH-dependent stability window is observed for thicker layers. For many electrostatically stabilized particles, an absolute  $\zeta$ -potential above 30-35 mV provides good stability. For  $\text{pH}_C$  values of the systems, alumina-PMAA above  $\text{pH}_C = 6$  and silica-PAH below  $\text{pH}_C = 8$ , this is the case, but for PE layers deposited at very low values of  $\alpha$ , colloidal stability is also achieved at absolute values of the  $\zeta$ -potential below 30 mV and for alumina-PMAA of  $\text{pH}_C = 4$  even at an absolute  $\zeta$ -potential below 10 mV. A possible explanation could still be the electrostatic repulsion of two overlapping thick PE layers of two particles. Even if  $\alpha$  is too low that loops and tails of the adsorbed PE can contribute strongly to the electrophoretic mobility, charges inside the

thick PE layer can provide repulsive interaction of two overlapping layers. This repulsive effect may also be enhanced by steric stabilization due to a contribution of an osmotic pressure for water. The penetration of water molecules into the PE layer moves the overlapping PE layers apart.



**Scheme 5.** Comparison of a thick vs. a thin adsorbed weak polyelectrolyte film at different degrees of dissociation  $\alpha$

For uncharged PEs at pH values away from the IEP of the PE modified particles, the charge of the oxide particle surface dominates the  $\zeta$ -potential. One might expect that the PEs desorb from the surface, but by titrating the supernatant of centrifuged suspensions of alumina-PMAA suspensions exposed for several hours to pH values below 4, no titrable polyelectrolytes could be determined (for particles of any  $\text{pH}_C$  value). Furthermore the ability of the particles to emulsify oils in this pH range (see section 3.2.3) confirms the maintenance of the adsorbed state here. The particles alone, at such pH values, could not achieve this, supporting the assumption that PEs remain adsorbed. Van der Waals interactions, hydrogen bonding, or both are likely responsible for the maintenance of this adsorbed state. Desorption might also be unfavorable because of the low solubility of the uncharged PE in water. However, desorption of PMAA might take place for alkaline pH values, when the alumina surface becomes negatively charged ( $\text{pH} > 9$ ) and the PMAA is also fully negatively charged.

## 3.2.2 Contact angle measurements on PMAA coated alumina plates

Contact angle measurements of water droplets (1 mM NaCl, varying pH) under dodecane on a polished alumina plate were carried out to demonstrate the effect of the charge density of the PE layer on the wettability of the particle surface. Figure 14 shows the pH dependency of the  $\theta$  on a PMAA-coated alumina plate ( $\text{pH}_C$  4).

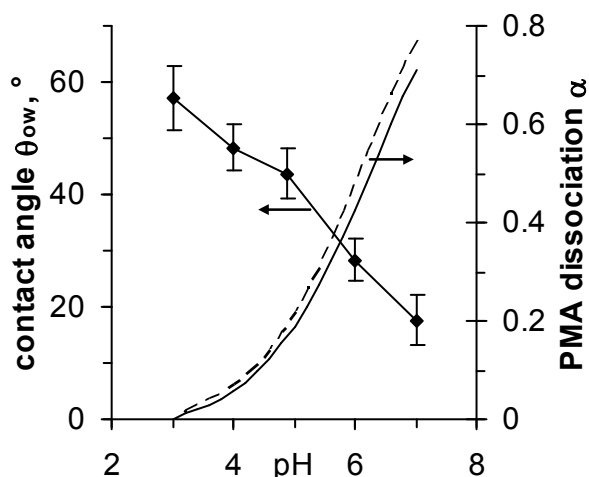


**Figure 14.** Advancing contact angles (left axis) of water droplets of different pH values under dodecane on a PMAA coated ( $\text{pH}_C$  4) alumina plate. Error bars correspond to the standard deviation calculated from at least 5 measurements. Degree of dissociation of dissolved (non-adsorbed) PMAA (right axis) in (i) 1 mM (continuous line) and (ii) 10 mM (dashed line) NaCl.

A comparison of the pH dependency of the  $\theta$  with the degree of dissociation of the free PMAA<sup>22</sup> can be used to assist the interpretation (Figure 14). However, when doing this comparison, it is important to recognize that the pH dependence of the PMAA dissociation in the adsorbed state might differ slightly from that of the dissolved nonadsorbed PMAA due to the contact with the substrate. The increase in  $\theta$  with decreasing pH comes along with a decrease in the charge density of the PMAA layer. For pH 5 - 7, the slope of the  $\theta$  dependence versus pH is higher than that for pH 3 - 5. A similar observation can be made for the slope of the  $\alpha$ -curve of free PMAA in this pH ranges. Therefore, it can be concluded that the wettability of the surface for water or oil respectively, correlates with the degree of dissociation of the PE layer.

Contact angle measurements were also performed for the uncoated alumina plate. A  $\theta$  of  $\approx 60^\circ$  was found, irrespective of the pH value. This surprisingly high  $\theta$  can be explained by surface active contaminations in, for example, dodecane. Alumina is a typical example of a high energy surface that is sensitive to contamination. The same is the case for PMAA-coated alumina with  $\text{pH}_C$  6. Here the adsorbed amount of PMAA is not seen to provide sufficient compensation of the high-energy properties of the underlying alumina surface. This is contrary to the  $\zeta$ -potential measurements, in which the surface charge is observed to be governed by the adsorbed PMAA layer. It can be

concluded that there is a transition from a high to a low energy surface with increasing PE thickness.

### 3.2.3 Characterization of nanoparticle stabilized emulsions

#### 3.2.3.1 Creaming behaviour of emulsions

To prepare the emulsion samples, first the aqueous components were mixed, and depending on the pH, colloidal or gelled suspensions of nanoparticles in water were obtained. Figure 15 shows photographs of dodecane in water emulsions prepared with alumina-PMAA of different  $\text{pH}_C$  values (PE coating thickness increases with decreasing  $\text{pH}_C$ ) after emulsification by sonication at different emulsification pH values.

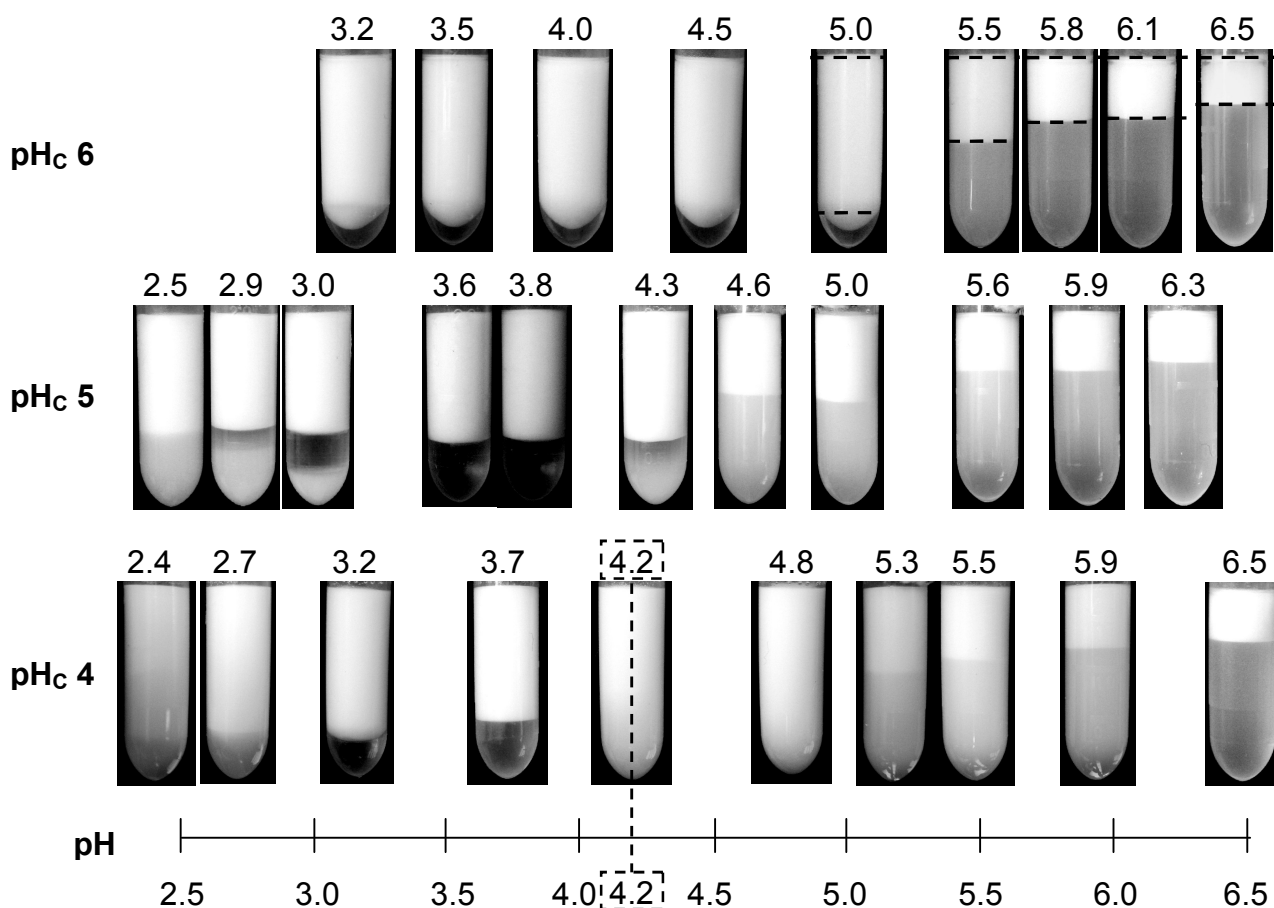


**Figure 15.** Photographs of 25 vol-% dodecane/water emulsions stabilized with 2 wt-% PMAA coated alumina nanoparticles with different PE-coating pH values ( $\text{pH}_C$  values) after 12 h of storage (all emulsions prepared below pH 6.2 do not release oil after 3 months). Vertical axis of the sample

tube images corresponds to pH axis on the bottom of the figure as indicated for sample with pH 4.2 at  $pH_C$  4, precise pH values of samples

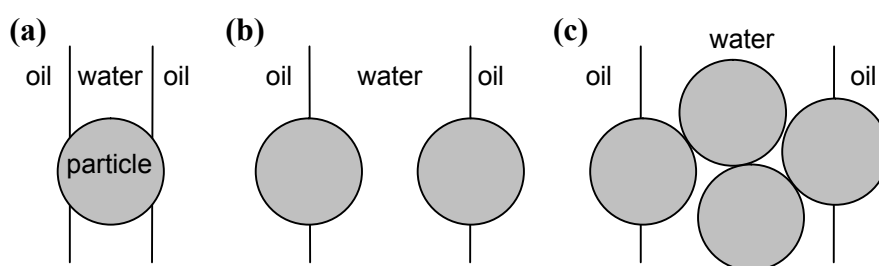
For the three different PE coating thicknesses ( $pH_C$  values), stable emulsions could be obtained below a pH value of  $\approx 6.7$  with a corresponding  $\alpha^{21}$  of 0.7 (no salt) or 0.84 (10 mM NaCl). Samples emulsified above this pH value coalesce rapidly and create two separated liquid phases in  $< 5$  min, probably because of the predominantly hydrophilic character of the PMAA layer with  $\alpha > 0.8$ . By decreasing the pH value below 6,  $\alpha$  falls below 0.5, and the hydrophobic character of PMAA increases. Alumina particles themselves are not capable of stabilizing dodecane in water emulsions at any of the shown pH values. The height of the creamed emulsion phase for particles of any  $pH_C$  value increases gradually with decreasing pH value after 12 h of storage until a maximum is reached. For samples with pH values above this maximum, further creaming after 12 h leads to a creaming layer occupying about 1/4 of the vials. The different creaming rates here can be explained with different droplet sizes and extents of droplet flocculation. (See Figure 16 and Figure 17) It can also be seen that the turbidity of the aqueous phase below the creamed layer has increased in comparison with the initial suspension of the alumina-PMAA particles. Cryo SEM measurements (see section 3.2.3.3) confirm, in particular for  $pH_C$  5 and 4, that the particles are aggregated. The initial PMAA-coated particles are not aggregated (Figure 12), so it can be concluded that aggregation takes place during emulsification.

At a certain pH (depending on the PE coating thickness), a maximum creaming layer height is achieved. The aqueous phase for this state is not turbid (also no Rayleigh scattering) and therefore does not contain particles. The comparison of this pH value with the critical flocculation pH (c.f.pH) in the caption of Figure 13 shows a correlation. Horozov and Binks<sup>55</sup> observed a similar effect but used hydrophobized silica nanoparticles at a certain ionic strength that corresponded to the critical flocculation concentration (cfc). Measurements of the resolved water fraction and the rheological properties of the emulsion led to the conclusion that above the cfc a “*viscoelastic 3D network of interconnected particles and emulsion droplets*”<sup>55</sup> develops, which abruptly increases the stability against further creaming. Here a similar phenomenon is observed but by studying the PE-covered particles at their c.f.pH. As already shown in the caption of Figure 13, with increasing PE coating thickness (decreasing  $pH_C$ ), the c.f.pH shifts to lower values. This is also the case for the pH value where the formation of the particle-droplet network occurs. Such analogous behaviour can be found for the dodecane in water emulsion stabilized with silica-PAH particles, only in the more alkaline region above pH 6.5 corresponding to the c.f.pH marked in Figure 13(b). For the samples

with intermediate PE coating thickness ( $pH_C$  5) at  $pH < 3$ , a whitish sediment of aggregated particles at the tube bottom can be observed. However, a further decrease in pH value leads again to the formation of a stable turbid aqueous phase. In the case of samples with the thickest PE coating ( $pH_C$  4), only a stable turbidity without sediment is observed. In both cases, the increasing positive  $\zeta$ -potential provides electrostatic restabilization of the excess particles. In all cases, the emulsions are stable, indicating that the PEs are still adsorbed to the particle surface. The oil wetting ability of the bare alumina surface is poor in this pH range due to the strong surface charge but the uncharged PE layer provides sufficient hydrophobicity to stabilize the emulsions. A separation of a distinguishable upper cream layer did not occur after 12 h of storage for emulsions stabilized with particles carrying the thickest PE coating ( $pH_C$  4) in the range of  $4.2 < pH < 5$ . This is due to the formation of unflocculated small droplets, which have a slower rate of creaming (see Figure 16).

For emulsions stabilized with particles of  $pH_C$  4, between pH 4.5 and 5.5 the extent of flocculation is low. This is also one of the reasons for the reduced rate of creaming for these emulsions shown in Figure 15. Thus, the emulsion cream occupies more than  $\frac{1}{4}$  of the vials after 12 hrs. With further ongoing time the creams become denser and their volumes approach  $\frac{1}{4}$  of the vial.

The flocculation behaviour of the droplets can be understood by considering three different cases: For emulsions stabilized with particles of  $pH_C$  4 above pH values of 6 huge parts of the droplets are found to be flocculated (see also Figure 16(d, e)). In this pH range, the particles are not aggregated but their hydrophobic character is not that pronounced because of the relatively high degree of dissociation (above 50 %) of the PMAA layer. The  $\theta$  of the particles should therefore be comparably small and this gives rise to particle bridging between droplets<sup>35, 39</sup> as illustrated in Scheme 6(a).



**Scheme 6.** (a). A particle with a low contact angle can cause flocculation of two droplets by forming a particle-bridge. (b) A particle with an intermediate or a contact angle close to  $90^\circ$  acts preferably as a stabilizer for one droplet. (c) Particles with good oil wettability but poor colloidal stability lead to flocculation due to aggregation of droplet shells.

For pH values between 4.2 and 5.5 the degree of flocculation of droplets is very low. Although in Figure 16(f) some droplets seem to be attached with each other, the view on the moving sample through the microscopic objective reveals exclusively the independent movement of individual drops. The low degree of flocculation with the decrease of PMAA dissociation is explained with the increase of the particles  $\theta$  and the thereby resulting preference of the particles to immerse only in one droplet, as illustrated in Scheme 6(b).

For pH values close to the c.f.pH particle aggregation takes place. Thereby also the particle shells of droplets can aggregate and droplet flocculation occurs as illustrated in Scheme 6(c).

#### 3.2.3.2 Droplet-size distributions and flocculation-behaviour

The droplet size distribution for each sample was measured, and the obtained size distributions for alumina-PMAA are shown in Figure 16 for different  $\text{pH}_C$  and emulsification pH values.

All obtained droplet size distributions are monomodal when plotted as volume fraction. The droplet size distribution did not change after emulsification times  $> 4$  min. During emulsification, the interplay between the stabilization of newly generated droplets and their coalescence determines the droplet size distribution. Depending on which process is dominant, the droplet size distribution shifts to smaller or bigger sizes.

Because emulsification is performed with high-intensity ultrasound, the break-up of droplets occurs because of the disruptive mechanical effects of acoustic cavitation. Droplet break-up goes along with increasing interfacial area. Because this is energetically unfavorable, the emulsion attempts to reduce the interfacial area again by coalescence of droplets. The higher the interfacial tension between water and oil, the faster the coalescence will proceed at a constant viscosity. However, in the presence of interfacially active particles, coalescence can be suppressed because of the formation of an attached particle barrier on the newly generated oil-water interface. The magnitude of this droplet stabilization depends on the availability of particles, their rate of deposition on the interface and on the packing density of the particles on the oil-water interface. The availability is proportional to the particle concentration, and it has been found that the obtainable droplet size depends on this parameter<sup>127-130</sup>. Because of decreasing droplet sizes, the overall droplet surface area increases, and so does the required quantity of particles for coverage. However, for the case of a particle excess during emulsification (as it is the case for the present experiments), their concentration determines the amount of particles and their average distance to uncovered droplet interfaces. The rate of deposition of the particles on the interface is determined by (i) their affinity

to the interface and (ii) their size. Both parameters affect the time required to cover uncovered oil-water interfaces. Because emulsification was always performed under the same conditions (ultrasonic intensity, emulsification time, emulsion volume, dipping depth of the sonotrode, cooling rate, oil volume content, and particle concentration), the droplet size distributions here are determined only by the properties of the particles and the oil phase. For PMAA-coated alumina particles of all PE coating thicknesses ( $\text{pH}_C$  values), the droplet size first decreases below  $\text{pH} 7$ . This observation is better illustrated in Figure 17(a), where the average volumetrically weighted diameter of the droplets is plotted versus the  $\text{pH}$  value of the emulsions.

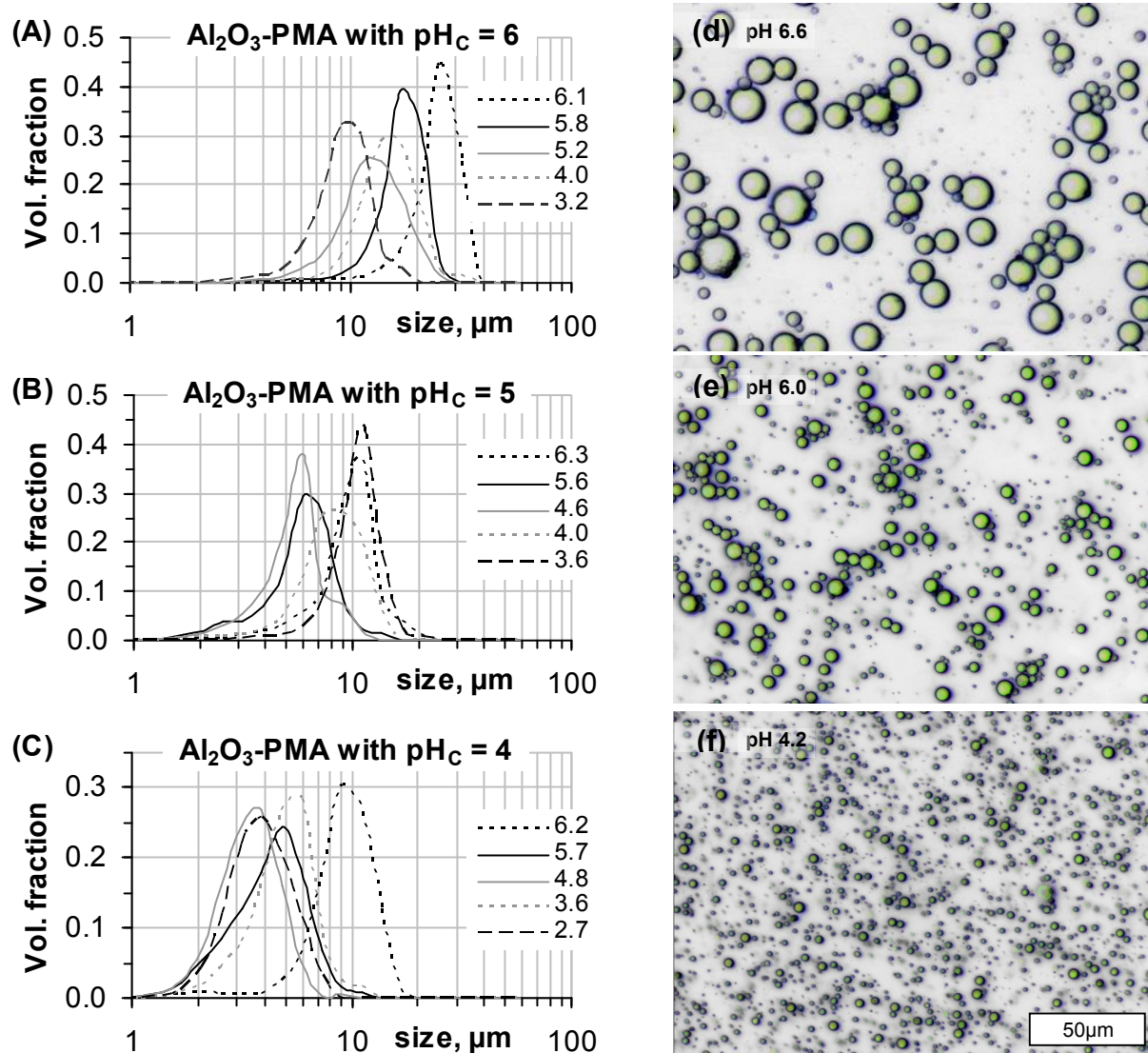


**Figure 16.** Size distributions of dodecane/water emulsion droplets stabilized by PMAA coated alumina nanoparticles with different PMAA-coating  $\text{pH}_C$ : (A)  $\text{pH}_C = 6$ ; (B)  $\text{pH}_C = 5$ ; (C)  $\text{pH}_C = 4$  and for different emulsification  $\text{pH}$  values (designated by line pattern)

The decreasing pH causes a decreasing  $\alpha$  in the adsorbed PMAA coating.  $\alpha$  of PMAA can be linked to the  $\theta$ , as shown in Figure 14. Because for decreasing  $\alpha$  a decreasing average droplet size is observed, the parameter  $\theta$  is proposed to influence the droplet size distributions obtained here. Particles with a high  $\theta$  are capable of forming more closely packed particle layers on the oil-water interface. Coalescence is thereby suppressed more effectively.

By comparing size distributions of different PE coating thicknesses ( $\text{pH}_C$  values) but the same emulsion pH values between pH 3.5 and 6, less broad droplet size distributions with a smaller average droplet size can be obtained with thicker PE coatings (smaller  $\text{pH}_C$  values). This can be explained by the increasing quantity of lipophilic moieties with thicker PE coatings and the more efficient screening of the hydrophilic surface of the bare alumina particles. Thus, the particles are capable to form a more closely-packed layer at a given pH value with thicker PE-layers on their surfaces.

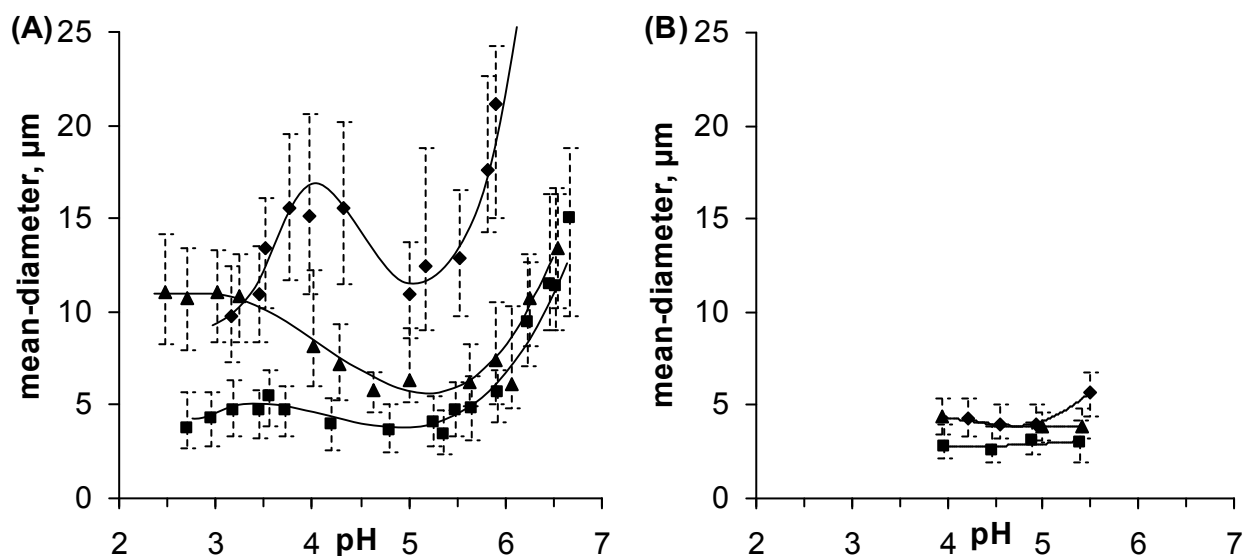


**Figure 17.** Mean volumetric diameter of emulsion droplets stabilized by PMAA coated alumina nanoparticles with different coating pH values  $\text{pH}_C$ :  $\blacklozenge$  -  $\text{pH}_C = 6.0$ ;  $\blacktriangle$   $\text{pH}_C = 5.0$ ;  $\blacksquare$   $\text{pH}_C = 4.0$ ; (A) dodecane as oil phase; (B) diethylphthalate as oil phase, lines are drawn to guide the eye, dashed bars give upper and lower diameter at 50 % height of the size distributions, not the error bars

The average droplet size reaches a minimum between pH 4.5 and 5.5 ( $0.15 < \alpha < 0.45$ ) for all  $\text{pH}_C$  values. For  $\text{pH}_C 6$ , particles are flocculated, but for  $\text{pH}_C 4$  and 5, particles are not flocculated at this minimum. Hence in the range of the minimum the particles provide the best properties to shift the competition between droplet stabilization and coalescence during emulsification toward stabilization. In the minimum for particles with the thickest PE coating ( $\text{pH}_C 4$ ,  $4.2 < \text{pH} < 5$ ), the

smallest average droplet diameter can be obtained for the system alumina-PMAA and dodecane. Here the well-balanced wetting properties provide high stability against coalescence due to the formation of a closely packed particle layer on the interface, and because of the low c.f.pH of 4.1 almost exclusively unflocculated individual droplets exist (see Figure 16(f)). The average droplet size for all PE coating thicknesses increases again beyond the minimum ( $\text{pH} < 5$ ). Strong particle aggregation, reducing the apparent nanoparticle number concentration, occurs over the pH range with increasing average droplet size.

As previously mentioned, in the pH range above the c.f.pH, particle aggregation takes place also during emulsification (for  $\text{pH}_C$  4 and 5, see Figure 20). The resulting aggregates are submicrometer-sized. (Figure 20). This decreases the rate of particle deposition on the interface as well as the apparent nanoparticle number concentration; however, compared to the strong aggregation at the c.f.pH this has a less pronounced effect on the droplet-size.

Thicker PE-coatings provide better colloidal stability of the particles and thereby reduce the c.f.pH and the extent of aggregation. As a result of this in Figure 17(a) it is recognizable that for thinner PE-coatings the approach towards the plateau of average droplet size is enhanced and thus it is achieved at a higher pH.

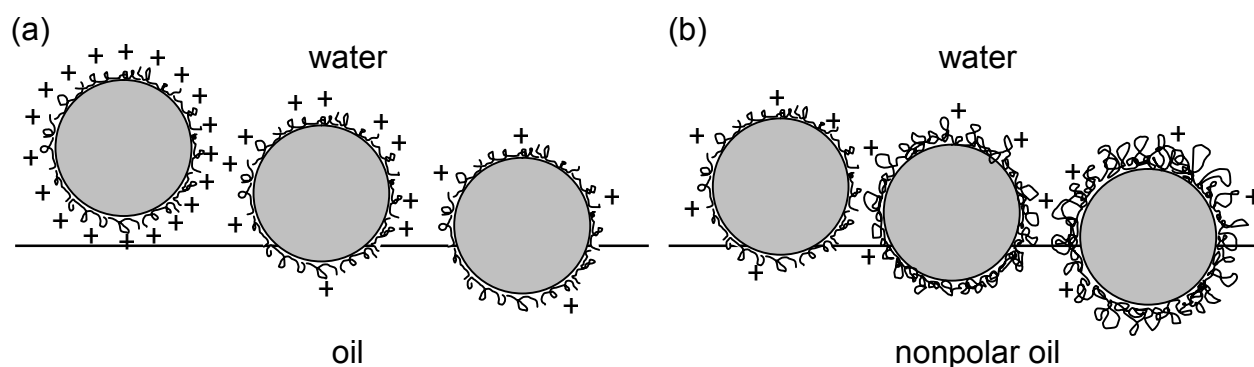
Instead of also forming a plateau, the average droplet size of emulsions stabilized by particles with the thinnest PE-coating ( $\text{pH}_C$  6) decreases beyond a maximum at pH 4. At this point it is important to take the ionic strength of the aqueous phase during the emulsification into account. For higher  $\text{pH}_C$  values, higher  $\alpha$  values existed in the adsorbed PE layer before the pH adjustment for emulsification was carried out. Therefore, more hydrochloric acid had to be added before emulsification to obtain a desired pH value. The conductivities of the emulsions at e.g. pH 3.5 for  $\text{pH}_C$  4, 5, 6 are 0.2, 0.5 and 1.5 mS/cm, respectively. The high ionic strength below pH 4 for particles of  $\text{pH}_C$  6 results from the high quantity of chloride ions, screening the positive alumina surface charges and thereby enabling the formation of closely packed particle layers on the oil-water interface.

Also for the alumina-PMAA particles of  $\text{pH}_C$  4, the average droplet size decreases again after a maximum at pH 3.5. As noticeable from Figure 15 and Figure 19(C1), the extent of particle aggregation decreases again, thereby increasing the effective nanoparticle number concentration for droplet stabilization.

To investigate the effect of the oil phase polarity, the experiments were repeated with the more polar oil diethylphthalate. The benzene and ester functionalities give this molecule a more polar character than the saturated alkane chain of dodecane. Only pH values at the minimum of the

average droplet size were investigated and it was found that the differences between the average droplet sizes for different  $\text{pH}_C$  values are much smaller (Figure 17(b)). Here even the relatively thin PE layer of  $\text{pH}_C$  6 provides sufficient affinity to the diethylphthalate-water interface to create highly stable emulsions with small droplet sizes. On one hand, this can be attributed to an increase in  $\theta$  due to the higher oil polarity (and thereby the formation of closely packed particle layers even for  $\text{pH}_C$  6); on the other hand, the interfacial tension between water and oil also might play a role, which implies a reduced rate of coalescence.

On the basis of the  $\theta$  measurements (Figure 14) and the observed correlation between the droplet-size and the oil wettability of the particles, Scheme 7 proposes the parameters influencing the oil-wettability of weak-PE coated nanoparticles.



**Scheme 7.** The oil-wettability on a nanoparticle carrying an adsorbed layer of a weak PE can be modified (a) for a given PE-layer thickness by the degree of dissociation of this weak PE-layer and (b) for a given degree of dissociation by the thickness of the adsorbed PE layer.

The emulsification ability of silica-PAH particles was investigated, and the average droplet sizes of dodecane/water emulsions in dependence of the emulsification pH value for two different  $\text{pH}_C$  values are shown in Figure 18.

Unlike the system alumina-PMAA, a higher  $\text{pH}_C$  value stands for a thicker PE layer for silica-PAH because  $\alpha$  of PAH decreases with increasing pH. The ability of silica-PAH particles to stabilize emulsions begins at a pH value of  $\approx 7.2$  with a corresponding  $\alpha^{131}$  of PAH of  $\approx 0.8$ , which is comparable to the system alumina-PMAA. Also, for emulsions prepared with silica-PAH, the average droplet size decreases with decrease in  $\alpha$ . Above pH 9 ( $\alpha < 0.45$ ) the average droplet size reaches a minimum. Less-pronounced but still significant is the fact that for the same emulsion pH, particles with thicker PE coatings (higher  $\text{pH}_C$  values) are capable of creating smaller droplets. Again, the same argument can be used that thicker PE layers provide more hydrophobic moieties to

screen the hydrophilic surface of the bare particles. Although emulsions obtained with silica-PAH are highly stable, the bigger average droplet size compared with that for alumina-PMAA indicates a less-pronounced lipophilicity of silica-PAH, even with the thickest PAH layer. Obviously, the methyl group in the PMAA monomer unit enables better emulsification by alumina-PMAA particles. An improvement of the emulsification ability of PAH-coated particles could be achieved when the PE coating step took place at a higher  $pH_C$  value. For the highest  $pH_C$  value of 9.5, the corresponding  $\alpha$  equals 0.34, whereby for alumina-PMAA at  $pH_C$  4, the corresponding  $\alpha$  is 0.08. To obtain this low value of  $\alpha$  and thereby a higher layer thickness, the PAH coating step would have to be done at  $pH_C$  10.6, which is not possible because of the solubility of silica under such alkaline conditions. The same limitation is given for the emulsification ability of silica-PAH particles above pH 10.

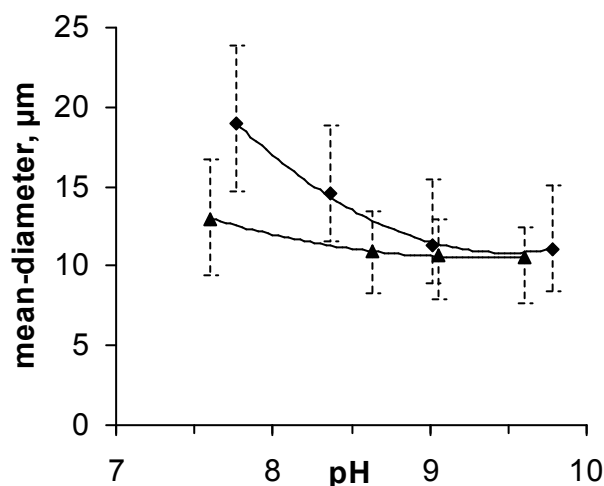


**Figure 18.** Average volumetric diameter of dodecane/water emulsion droplets stabilized by PAH coated Silica nanoparticles with different coating pH values  $pH_C$ : ◆ -  $pH_C = 8.5$ ; ▲ -  $pH_C = 9.5$ , lines are drawn to guide the eye, dashed bars give upper and lower diameter at 50 % height of the size distributions, not the error bars

### 3.2.3.3 Cryo-SEM characterization of the nanoparticle shell

The visualization of the droplet shell morphologies of dodecane droplets done by cryo-SEM measurements is shown in Figure 19 for different  $pH_C$  and emulsion pH values.

As can be seen in Figure 19 for emulsions prepared above the c.f.pH with particles of  $pH_C$  4 and 5, the droplet shell consists of partially aggregated alumina-PMAA particles forming a closely packed particle layer on the oil-water interface. Just below the c.f.pH, the droplet shell consists of highly aggregated particles, which create a disordered shell with varying thickness. Further below the c.f.pH, particularly for samples with  $pH_C$  4, aggregation is reversed, and the homogeneity of the droplet shell increases again. The dense packing of particles at the oil/water interface is suggested to be a reason for particle aggregation during emulsification. The close approach of particles here can

lead to aggregation due to van der Waals forces. The mechanical effects of the ultrasonic irradiation can remove aggregated domains from the interface back to the bulk suspension. Aggregated particles in the aqueous bulk phase can be seen in Figure 20.

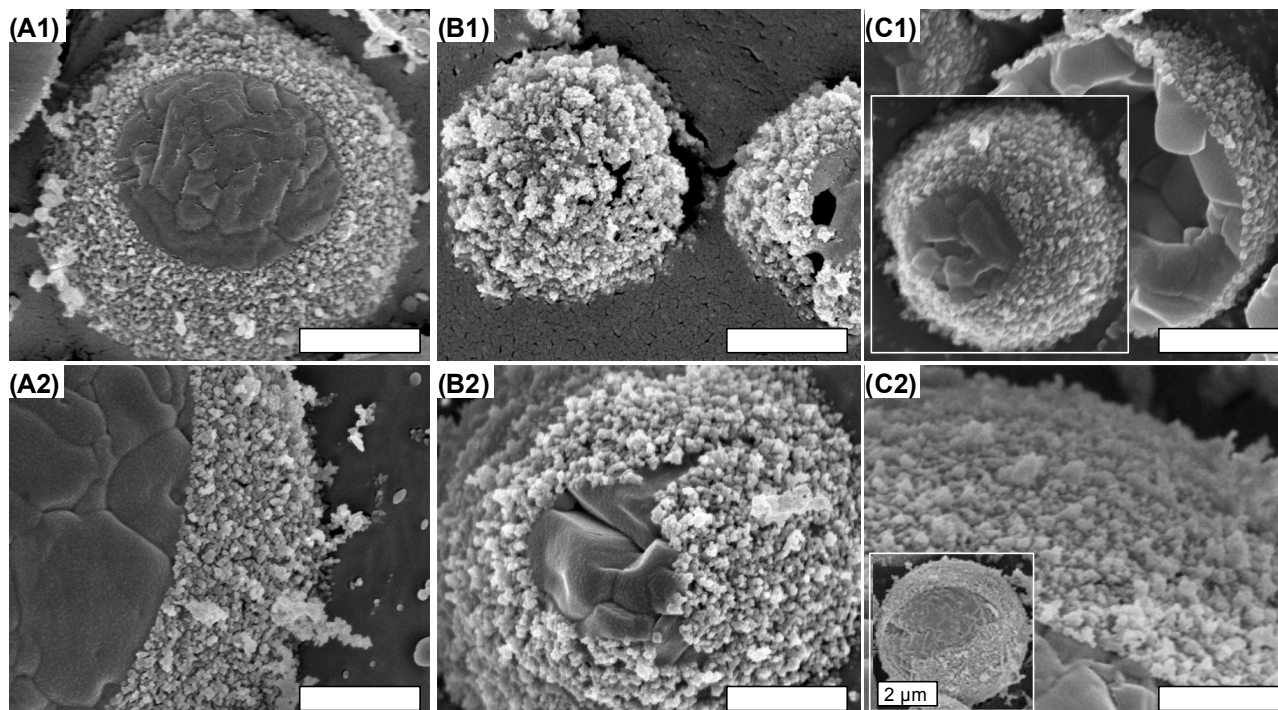


**Figure 19.** Cryo SEM images of dodecane droplets stabilized with alumina-PMAA particles (A1) – (C1)  $\text{pH}_C = 4$  and (A2) – (C2)  $\text{pH}_C = 5$ , corresponding pH values of emulsions are (A1) 4.8, (B1) 3.7, (C1) 2.4, (A2) 4.6, (B2) 4.3, (C2) 3.0. Cross sectional views of the droplets due to the sample preparation method. Length of unlabeled scale bars equals 500 nm.

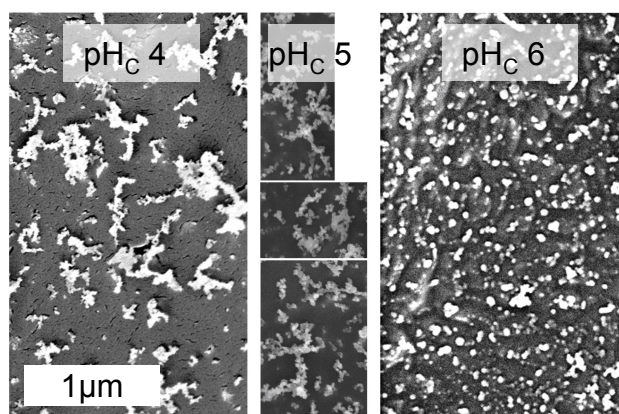


**Figure 20.** Cryo SEM image of excess alumina-PMA particles after emulsification at pH 5.5.

For the same emulsion pH value for particles with  $pH_C$  4 and  $pH_C$  5 aggregates can be found in the aqueous bulk phase after emulsification. However, for  $pH_C$  6 this is not the case, although the particles tend more to aggregate at this pH value in the bulk by colloidal destabilization. The reason for this is probably the formation of closely-packed particle layers on the oil-water interface for  $pH_C$  4 and  $pH_C$  5 and the resulting interfacial aggregation, while particles with  $pH_C$  4 do only form a loosely packed layer, which does not lead to interfacial aggregation.

The droplet shell morphology for silica-PAH stabilized dodecane droplets is shown in Figure 21 for different emulsion pH values.

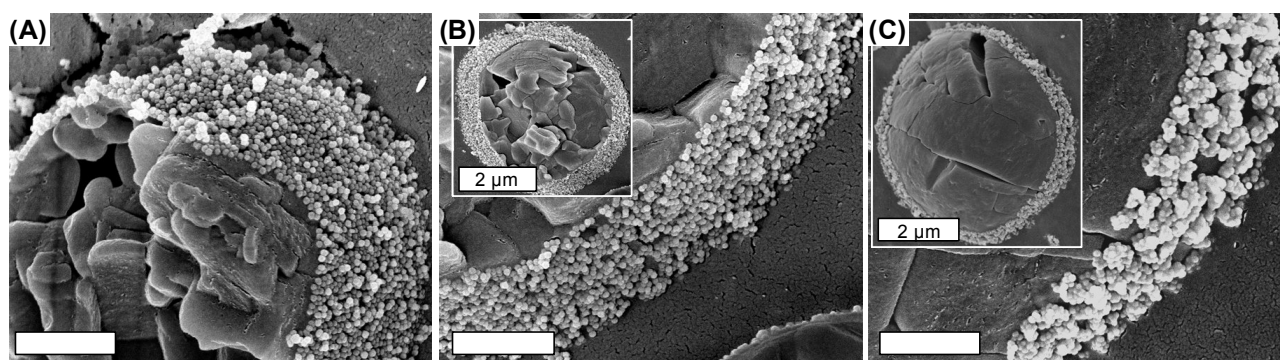


**Figure 21.** Cryo SEM images of dodecane droplets stabilized with silica-PAH particles of  $pH_C = 9.5$ , corresponding pH values of emulsions are (A) 8.5 (B) 9.1 (C) 9.8. Length of unlabeled scale bars equals 500 nm

Silica-PAH particles arrange in a monolayer, which partially consists of some aggregates below pH 9.2. The particle layers are not closely packed (compare Figure 32 in chapter 3.3.3) indicating a less pronounced dodecane-wettability. Above this pH value, flocculation of particles takes place and consequentially the droplet shell consists almost entirely of particle aggregates.

### 3.3 8-Hydroxyquinoline

The adsorption of charged organic molecules on oppositely charged surfaces has been shown to be an effective method to increase the wettability of solids for nonpolar fluids, as shown in chapter 3.1. In this chapter the same mechanism enables the oil-in-water emulsification ability of silica nanoparticles, but in contrary to chapter 3.1 here the charged organic molecule 8-hydroxyquinoline (8-HQ) shows a pH dependent dissociation. Furthermore 8-HQ is not initially dissolved in the aqueous phase, but in the oil phase and partitions between water and oil in dependence of the pH value.

#### 3.3.1 Physicochemical properties 8-hydroxyquinoline

##### 3.3.1.1 Dissociation behaviour of 8-hydroxyquinoline

The Lambert-Beer law can be applied for the analysis of the UV-spectra of 8-HQ. However, due to the amphoteric properties of 8-HQ, the dependence of the spectra on the concentration of hydronium and hydroxide ions in the solution needs to be considered. Spectra of 8-HQ in aqueous solutions of equal concentrations, but different pH values are shown in Figure 22(a).

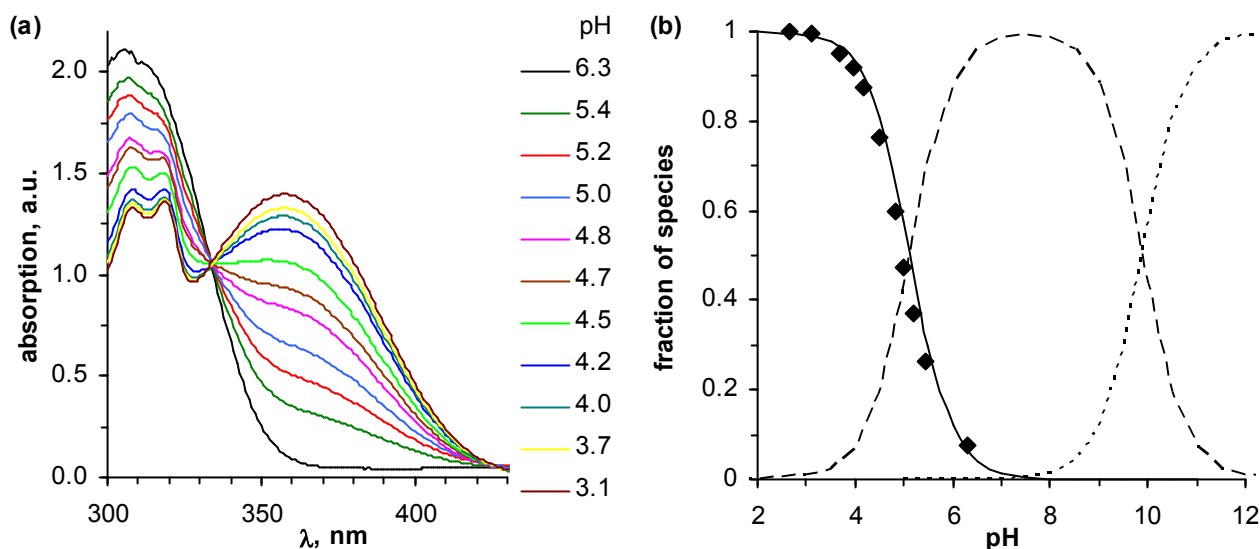


**Figure 22.** (a) UV-vis spectra of 0.5 mM 8-HQ in water for different pH-values. (b) calculated fraction of deprotonated (short dashed line), neutral (long dashed line) and protonated (continuous line) 8-HQ vs. pH value (obtained from evaluation of the Henderson-Hasselbalch equation with the  $pK_a$  values from the literature)<sup>132</sup>. Diamonds represent the fraction of protonated 8-HQ obtained from the evaluation of the peak height in the UV-vis spectra at 358 nm.

For acidic pH values ( $\text{pH} < 6$ ) the spectra exhibit a left and a right shoulder. A decrease in pH leads to an increase of the integral area below the right shoulder and a decrease below the left shoulder of the spectra. The variation of the spectra results from the change of the electronic structure in 8-HQ, induced by the protonation of the aromatic nitrogen atom with increasing concentration of hydronium ions in water. The increase of the peak height at 360 nm is characteristic for the protonation and increases linearly with the degree of dissociation ( $\alpha$ ) of 8-HQ. By assigning  $\alpha = 0$  to a peak height of zero and  $\alpha = 1$  to the maximum peak height, the intermediate values for  $\alpha$  can be obtained from the peak heights at the corresponding pH values by considering a linear dependence. In Figure 22(b) the points represent the degrees of dissociation obtained by this way and the lines the dependence of  $\alpha$  evaluated from the  $\text{pK}_a$  values of 8-HQ by the Henderson-Hasselbalch equation. At pH 7 almost all 8-HQ molecules are uncharged, while decreasing the pH below 7 leads to an increase of the protonated fraction, which reaches 100 % at  $\text{pH} = 3$ .

In the spectra of 8-HQ (Figure 22) there is an intersection point for all spectra at around 334 nm, which is the isosbestic point of the 8-HQ spectra. At this point the law of Lambert Beer can be applied to determine the total concentration of 8-HQ in water, irrespective of the pH value.

#### 3.3.1.2 Partitioning of 8-HQ between water and DEP

The partitioning of a substance between two immiscible phases is described by the Nernst partition law. Here water and diethylphthalate (DEP) are the two immiscible liquids in contact with another via their interfacial area and 8-HQ is the substance to be partitioned between them. 8-HQ exhibits a high solubility in DEP in its neutral form ( $\approx 18$  wt-%). In Figure 23 the concentration of 8-HQ in the aqueous phase after partitioning with DEP containing initially 16.5 wt-% 8-HQ is shown in dependence of the pH value.

The amphoteric character of 8-HQ determines also the concentration in the water phase in dependence of the pH value. The pH determines the degrees of protonation of the aromatic nitrogen atom ( $\text{pK}_a = 5.13$ ) and of deprotonation of the hydroxyl group ( $\text{pK}_a = 9.89$ ).<sup>132</sup> In the pH range between these two  $\text{pK}_a$  values the concentration of 8-HQ in water is below 10 mM. Albert and Hampton<sup>132</sup> relate this to the internal hydrogen bond between the nitrogen and oxygen atoms, which results in only one center for hydration of the molecule. Protonated or deprotonated 8-HQ molecules are much more soluble in water, since the internal hydrogen bond is disabled and the polarity of the molecule is increased. Thus, below pH 5 the solubility first increases by 3 orders of magnitude and reaches a plateau of 960 mM at pH 3. In the alkaline region the increase of solubility

with pH occurs less drastic, but it increases also by orders of magnitude. Important to recognize is the fact, that the initial concentration of 8-HQ in DEP influences the aqueous concentration of 8-HQ, since the Nernst law has to be fulfilled. It postulates that the ratio of the two concentrations of 8-HQ in the liquid phases is constant. Thus, by decreasing the initial 8-HQ concentration in DEP, also the concentration in water will be lower for a given pH value.

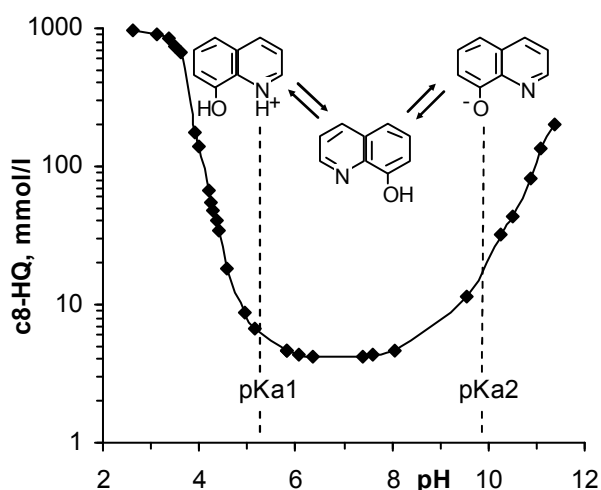


**Figure 23.** Dependence of 8-HQ concentration in the aqueous phase as a function of pH, DEP 50 vol-% with initially 16.5 wt-% 8-HQ, no silica particles. The inset graph shows the amphoteric dissociation behaviour of 8-HQ, and the two  $pK_a$  values are included by vertical dashed lines.

### 3.3.2 Properties of silica nanoparticles uncoated and modified with 8-HQ

#### 3.3.2.1 Bare silica particles

Ludox TMA particles appear almost monodisperse with diameters around 20 nm (Figure 24(a)). Results from dynamic light scattering displayed in Figure 24(b) agree reasonable with the SEM observation and give a narrow size distribution with a maximum at 14 nm and a PDI of 0.05. The calculation of the particle density follows from equation (3.17).

$$\rho_{silica} = \frac{w}{1/\rho_{H_2O} \cdot (w-1) + 1/\rho_{Ludox}} = 2.34 \text{ g/mL} \quad (3.17)$$

where  $\rho_{Ludox}$ ,  $\rho_{H_2O}$  and  $w$  are suspension density, water density, and silica mass fraction in the suspension and their values are 1.24 g/ml, 0.998 g/ml, and 0.34, respectively.

The specific surface area  $a = 134 \text{ m}^2/\text{g}$  obtained by BET measurements is in good agreement with the supplier value of  $140 \text{ m}^2/\text{g}$ . Assumption of spherical particles leads to equation (3.18) that allows the calculation of an average particle diameter  $d$  from BET measurements:

$$d = \frac{6}{a \cdot \rho_{\text{silica}}} = 19.1 \text{ nm} \quad (3.18)$$

This particle size was used in all further calculations.

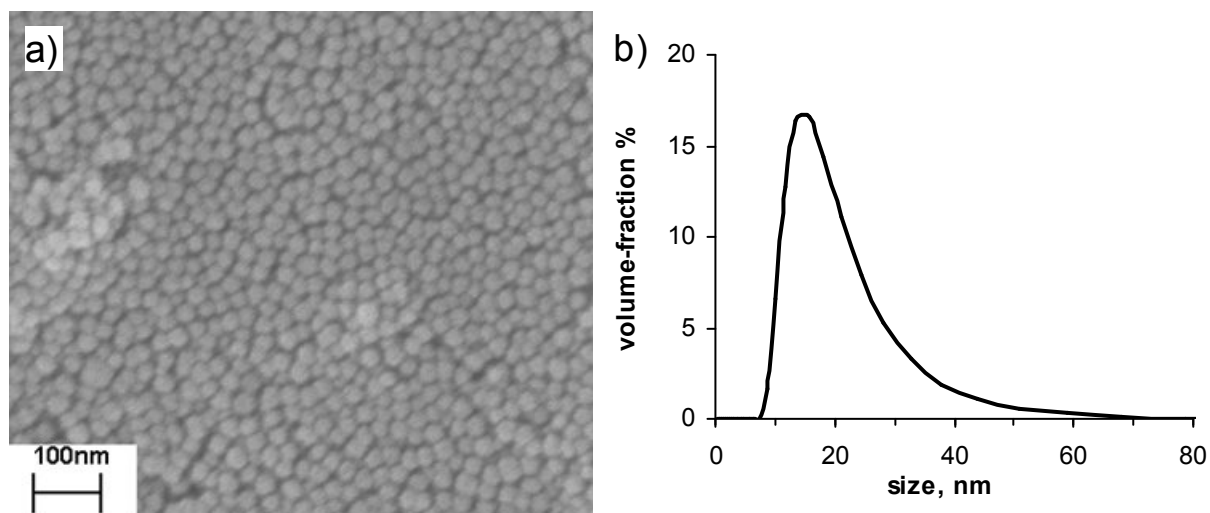


**Figure 24.** (a) SEM image and (b) DLS volumetric size distribution of Ludox TMA

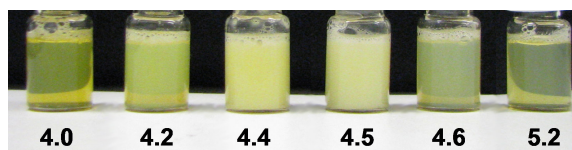
### 3.3.2.2 Particle dispersability in 8-HQ saturated solutions

Emulsions prepared in this work always consisted of 16.5 wt % 8-HQ in DEP, water containing the silica particles, and sufficient HCl to obtain the desired pH value. Before the emulsification was done, the two liquid phases were equilibrated by gentle stirring.

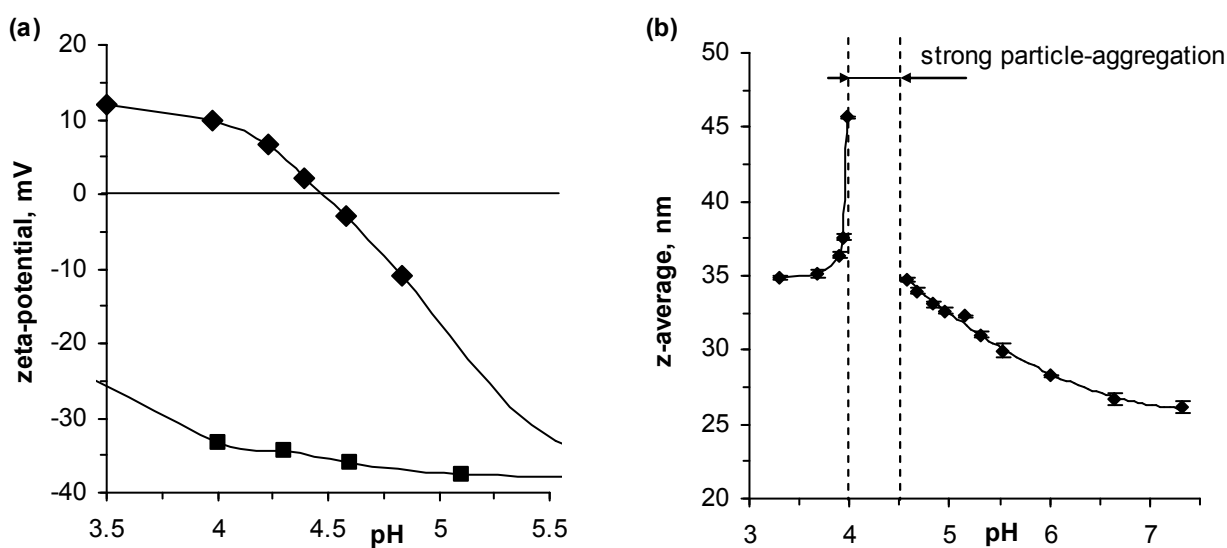
This equilibration can be considered as two simultaneously running processes: (i) partition of 8-HQ between both liquid phases and (ii) adsorption of 8-HQ onto silica nanoparticles from the aqueous phase. The final concentration of 8-HQ in the aqueous phase in each particular case is determined by its solubility limit at the corresponding pH as given in Figure 23. This concentration presents an equilibrium value of 8-HQ adsorbed on the silica surface, making also the adsorption-desorption equilibrium pH dependent.

Figure 25 shows a photograph of the silica suspensions with increasing pH value (from left to right) and 8-HQ individual concentrations corresponding to the solubility limit after 2 days (suspensions were shaken before photos were taken). Above pH 4.7 the suspensions are clear due to the low light scattering of the nonaggregated silica particles. Between pH 4.7 and 4.3 the suspensions become opaque as a result of aggregation of silica particles, and after several hours sedimentation takes

place. Surprisingly, clear suspensions and consequently nonaggregated particles can be observed again at  $\text{pH} < 4.1$ . For silica particles alone, clear suspensions were observed only in this pH range.



**Figure 25.** Stability of Ludox TMA with varying pH, concentration of 8-HQ always equals the solubility limit, for  $\text{pH} < 4.0$  and  $\text{pH} > 5.2$  the images correspond to those of the extremes

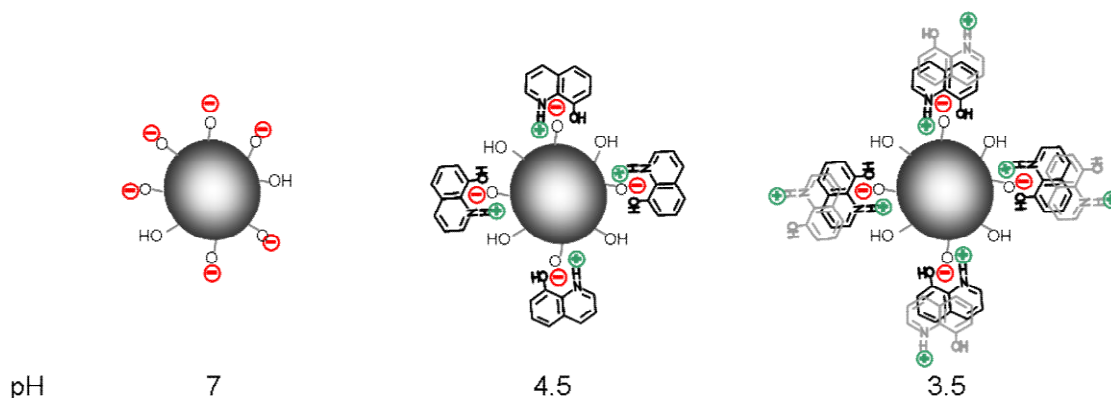


**Figure 26.** (a)  $\zeta$ -potential dependence of Ludox TMA silica nanoparticles on pH in water (■) and in aqueous 8-HQ solution corresponding to its solubility limit (◆). (b) average diameter of silica

To understand the reason for this “aggregation window”  $\zeta$ -potential measurements at different pH values were performed. The corresponding results are given in Figure 26(a). At pH 6, the  $\zeta$ -potential of bare silica with no 8-HQ present is around -36 mV due to the dissociated silanol groups on the surface. With decreasing pH, protonation of silanol groups takes place, resulting in the decay of the surface charge and consequently a decreasing absolute value of the  $\zeta$ -potential as shown in Figure 26(a). The decay of the absolute  $\zeta$ -potential is observed to begin at pH 4 and continues until the isoelectric point at a pH of approximately 2.

For the  $\zeta$ -potential of silica particles in aqueous phase equilibrated with DEP/8-HQ phase a completely different behavior is observed. The absolute value of the  $\zeta$ -potential already begins to fall at pH 5.5 and the isoelectric point is shifted to pH 4.5. Thus, the aggregation observed in the pH

range observed in Figure 25 can be explained in terms of electrostatic destabilization. The  $\zeta$ -potential can be affected by three processes induced by the gradual pH decrease. First, there is the increased protonation of silanol groups, which also takes place in 8-HQ aqueous solutions. Even stronger charge neutralization can be caused by the electrostatically driven adsorption of positively charged protonated 8-HQ molecules onto the particle surface. The significant increase of 8-HQ solubility, which is also directly related to its protonation as the pH decreases, is the third main factor influencing the  $\zeta$ -potential of the nanoparticles via an increase in ionic strength and an associated decrease of Debye length. The decreasing pH up to the isoelectric point is accompanied by an increase of the 8-HQ concentration to 20 mM and the conductivity reaches up to 2 mS/cm. Below pH 4.5 the  $\zeta$ -potential increases to +12 mV. The explanation for this effect could be the adsorption of 8-HQ in the form of molecular aggregates on the silica surface with the protonated and positively charged nitrogen atom in the aromatic ring of 8-HQ directed toward the solution as shown in Scheme 8.



**Scheme 8.** Model for the adsorption of 8-HQ onto silica particles for different pH values. At neutral pH only small fractions of 8-hydroxyquinoline (8-HQ) are dissolved and protonated leading to negligible adsorbed amount on the silica nanoparticle surface. Higher concentration and protonated fraction of 8-HQ at pH 4.5 result in the formation of an 8-HQ monolayer, whereas at pH 3.5 the very high 8-HQ concentration supports the adsorption of aggregated 8-HQ molecules onto the silica nanoparticle surface and a charge reversal.

Molecular aggregates of charged surfactants have been observed to adsorb on oppositely charged surfaces e.g. C<sub>14</sub>TAB on silica<sup>71</sup>. Hydrophobic interactions of alkyl chains enable the formation of such structures whereas here the interaction of the overlapping aromatic rings, e.g.  $\pi$ - $\pi$  stacking or van der Waals attraction, could be suggested as a driving force. This special configuration is possible for this small molecule as a consequence of the localization of polar groups on one side of

the molecule. However, because of the comparably weak strength of this interaction for only two aromatic rings, the concentration of 8-HQ needs to be sufficiently high to enable such structures. For adsorbed molecular aggregates with charged groups oriented to the solution one would expect a higher  $\zeta$ -potential. The relatively low  $\zeta$ -potential of +12 mV below pH 4 is explained with the high ionic strength of the solution (conductivity 7 mS/cm at pH 4).

### 3.3.2.3 Quantitative evaluation of the adsorption of 8-HQ

The adsorbed amount of 8-HQ on silica in the saturated aqueous solution and for fixed 8-HQ concentrations in water vs. the pH value is shown in Figure 27(a).

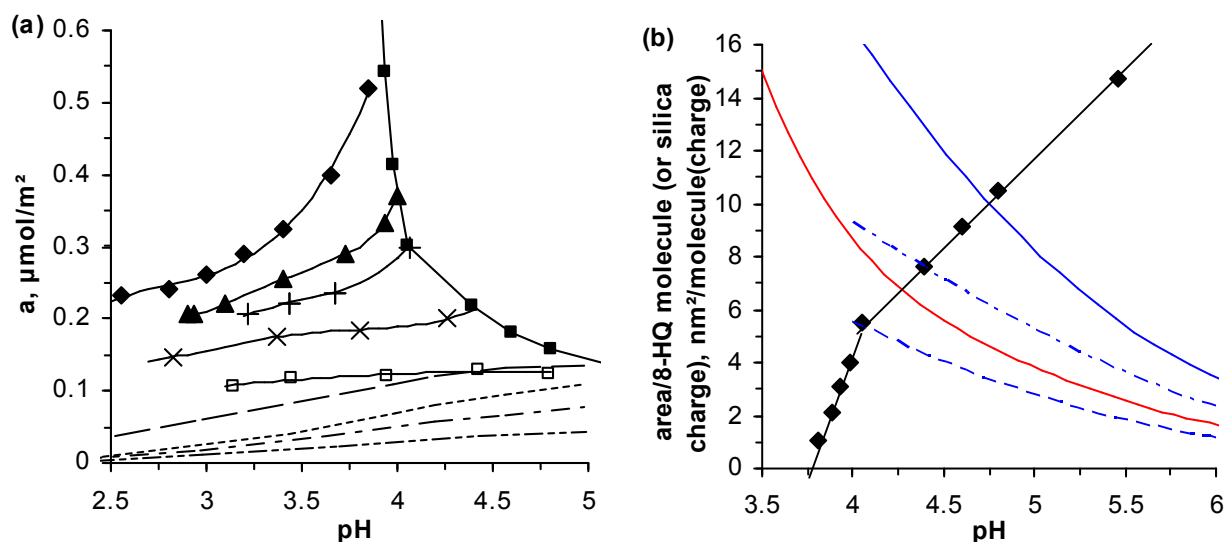


**Figure 27.** (a) adsorbed amount of 8-HQ per silica surface area vs. pH for different 8-HQ concentrations in water: saturated solution ( $\blacksquare$ ), 10 mM ( $\square$ ), 25 mM ( $\times$ ), 50 mM ( $+$ ), 100 mM ( $\blacktriangle$ ), 250 mM ( $\blacklozenge$ ), dashed lines represent data from the literature<sup>133</sup> for different 8-HQ concentrations: from the bottom up 1.2 mM, 2.4 mM, 4.8 mM, 9.5 mM. (b) Area per adsorbed 8HQ molecule in saturated aqueous solutions ( $\blacklozenge$ ). The straight lines with different slopes are drawn to denote the two adsorption regimes. For comparison: the areas per dissociated silanol group for different NaCl concentrations are also given (long dashed 1mM, short and long dashed 10 mM, continuous 100 mM NaCl) from the literature (red Tadros<sup>118</sup>, blue Bolt<sup>117</sup>).

First, the adsorption in a saturated solution is discussed, which is represented by the restricting line on the right side in the diagram of Figure 27(a). This curve has a sharp transition between  $4 < \text{pH} < 4.3$ , which results from the dramatically increased aqueous concentration of 8-HQ shown in Figure

23. As the aqueous concentration of 8-HQ increases strongly the adsorbed amount seems to follow this trend. In Figure 27(b) this curve is transformed to an area per 8-HQ molecule on the silica surface. Also the areas per silanol charge, obtained by two different groups are included for comparison. The area per adsorbed 8-HQ molecule was calculated with the specific surface area of the silica particles (BET measurement, 134 m<sup>2</sup>/g) and decreases almost linearly with a decrease in pH. However, below pH 4 the slope of the straight lines increases, representing another adsorption regime. The data for the areas per dissociated silanol group differ when comparing different works, since it is difficult to obtain precise values by potentiometric titrations at the low silica charge densities in this pH region, and also the different silica-powders that were used in these works might play a role. However, for all curves there exists an intersection point with the line for the area per adsorbed 8-HQ molecule. Above these intersection points, more 8-HQ molecules are adsorbed, than negative charges are present on the surface. This indicates that beside the electrostatically driven adsorption, an additional cooperative adsorption takes place.

Next, the adsorption for constant 8-HQ concentrations is discussed. For the comparably low concentration of 10 mM (corresponding to the solubility at pH 5) the adsorbed amount decrease gradually with decreasing pH. This decay can be explained with the decreasing silanol group dissociation on the surface of the silica particles, which effectively reduces the amount of negatively charged adsorption sites. An increase of the 8-HQ concentration up to 50 mM (corresponding to the solubility at pH 4.1) results in (i) a significant increase in adsorbed amount and (ii) an increased gradient of the adsorption curve above pH 4. This change in the gradient possibly indicates the cooperative adsorption of 8-HQ molecules, as depicted in Scheme 7, in line with the reversal of the sign of the  $\zeta$ -potential seen in Figure 26. The increased gradient of the adsorption curve can still be considered as an effect of the change of the silica charge density with pH. With a decrease in pH, electrostatically adsorbed 8-HQ molecules desorb alongside their associated molecules, increasing the rate of desorption.

With further increasing concentration of 8-HQ the adsorbed amount increases drastically. Also the increase of the gradient in the adsorption curves becomes more pronounced, thereby indicating increasing association between 8-HQ molecules in the adsorption layer.

Comparing the adsorption curve of this work at 10 mM 8-HQ with the adsorption curve obtained by Ferreiro and Bussetti<sup>133</sup> at 9.5 mM onto silica-gel show good agreement above pH 4. However upon a decrease of the pH below pH 4 the adsorption onto silica-gel decreases stronger. A possible explanation might be a different charge density dependence on pH for silica-gel.

It should be recognized, that the adsorption curve for the saturated 8-HQ solution depends also on the concentration of 8-HQ in the DEP phase, which was used for the saturation of water. As mentioned in section 3.3.1.2 the partitioning of 8-HQ between water and DEP is given by the law of Nernst, thus lower 8-HQ concentrations in DEP lower also the adsorbed amount on the silica.

The BET isotherm model considers cooperative adsorption and gave, applied to the adsorption data of 8-HQ on silica a reasonable fit as shown in Figure 28.

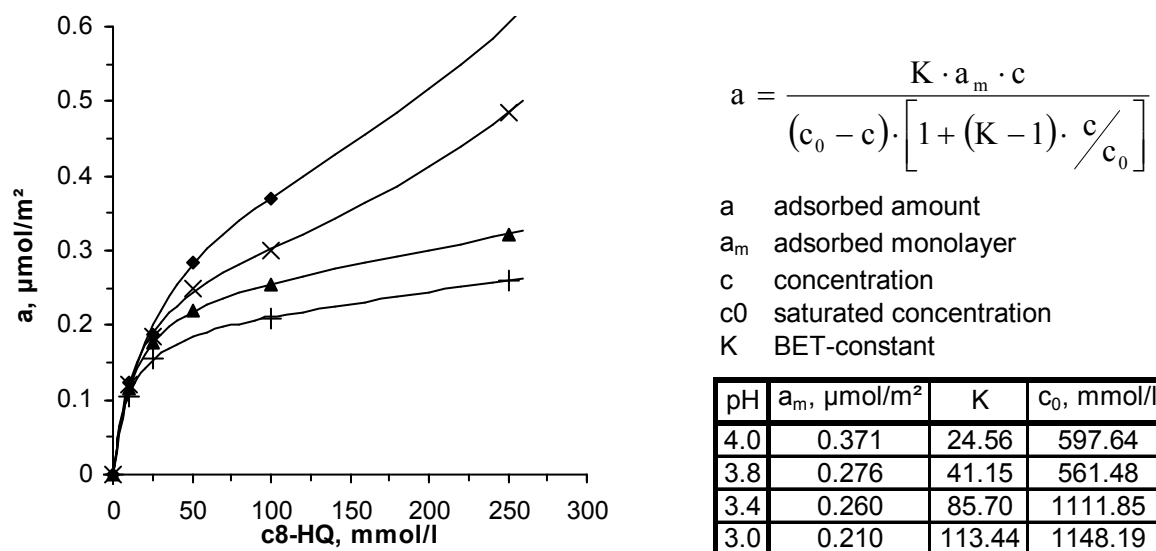


**Figure 28.** Left: Adsorption isotherms of 8-HQ on silica for different pH values: pH 4.0 (◆), pH 3.8 (×), pH 3.4 (▲), pH 3.0 (+). Curves represent the BET-adsorption model numerical fitting of the measurement data. Right: BET-adsorption model and tabulated obtained parameters from the fit.

The obtained values for the saturation concentrations  $c_0$  are higher than the measured values shown in Figure 23 but still of the same magnitude. The adsorbed monolayer quantity decreases with decreasing pH, which is reasonable because of the decreasing charge density on silica. The BET constant increases with decreasing pH, which can be interpreted as less favourable adsorption at low pH values.

### 3.3.3 Characterization of nanoparticle stabilized emulsions

#### 3.3.3.1 Contact angle of DEP droplets on 8-HQ modified glass-plates

Although a glass surface is chemically not completely identical with the surface of the silica particles (70 % SiO<sub>2</sub>, impurities like Na<sub>2</sub>O, B<sub>2</sub>O<sub>3</sub>) it can be used to show qualitatively the wettability changes of the particles, which follow from the adsorption of 8-HQ molecules. Thus, the

measurement of the contact angle of a DEP droplet (16.5 wt-% 8-HQ) on glass under 8-HQ saturated aqueous solutions helps to understand the behaviour of the particles at the oil water interface, discussed in the next section. The measured  $\theta$  for different pH values are shown in Figure 29.

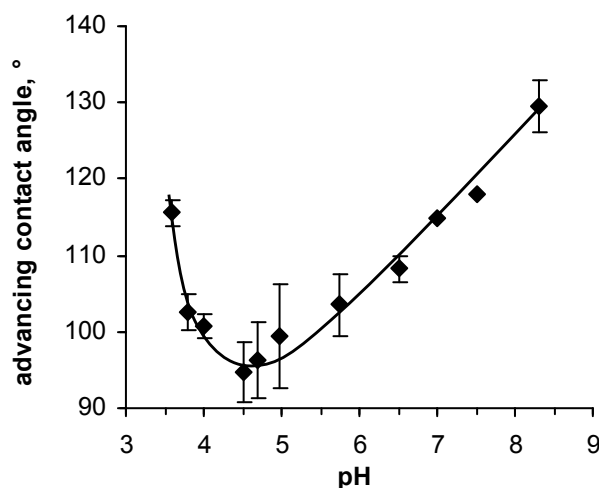
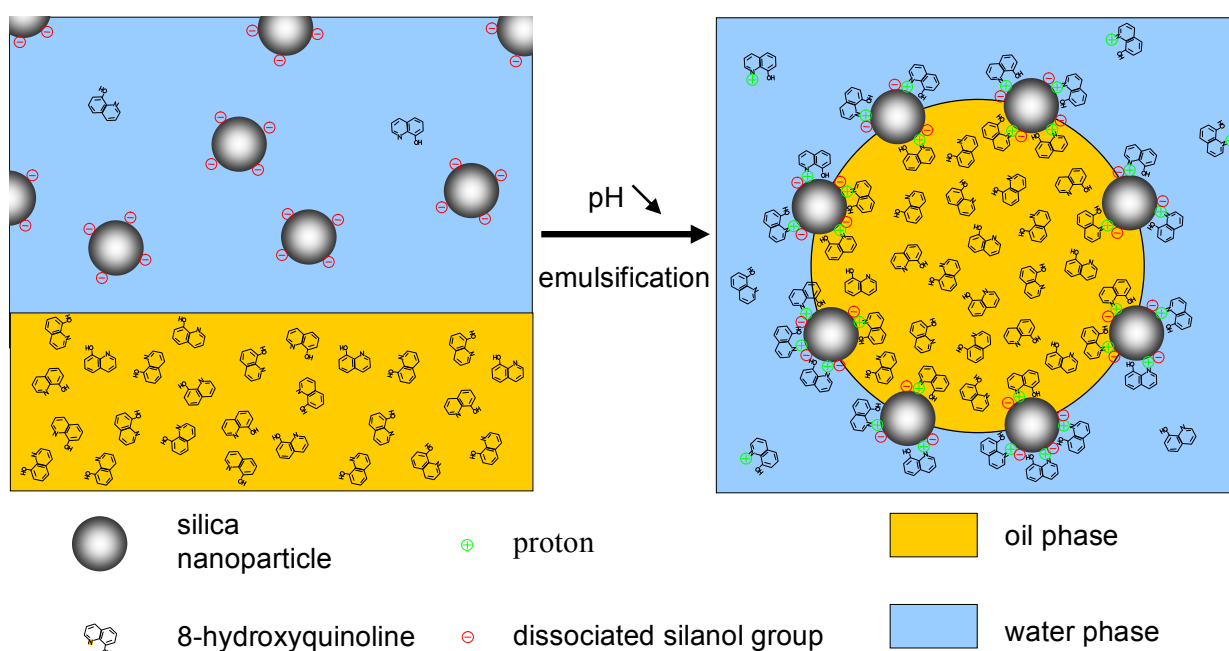


**Figure 29.** Advancing contact angles of DEP droplets on glass under 8-HQ saturated water at different pH-values. Line is drawn to guide the eye.



**Scheme 9.** Principle of lowering the pH value for stabilization of o/w emulsions by silica nanoparticles. Partitioning of 8-HQ is mainly in the oil phase for neutral pH, decreasing pH value leads to protonation of 8-HQ, solubilization in the aqueous phase and simultaneously adsorption onto the silica nanoparticle surface. 8-HQ modified silica nanoparticles then act as oil emulsifiers.

By decreasing the pH value from 8.5 downwards, also the contact angle of the DEP droplet decreases, which represents an improved wettability of DEP on the glass plate. As shown before, the pH decrease is accompanied by the increase of the aqueous concentration of protonated 8-HQ and this in turn increases the adsorbed amount of 8-HQ on silica. Since the aromatic parts of the 8-HQ molecules on the surface are exposed towards the outer fluid phase, the surface becomes more wettable for nonpolar liquids like DEP. After a minimum at pH 4.5, the contact angle increases drastically upon further pH reduction, in line with the adsorption of 8-HQ. Hence, the proposed adsorbed 8-HQ aggregates rehydrophilize the surface, probably due to their polar groups oriented towards the fluid phase as depicted in Scheme 8.

Based on the findings described in the previous sections, the behaviour of silica particles (suspended in water) in a mixture of water and DEP (16 wt-% 8-HQ) upon pH reduction and emulsification can be predicted. This behaviour is illustrated in Scheme 9.

#### 3.3.3.2 Sedimentation behaviour of emulsions

The appearance of DEP emulsions in water containing 16.5 wt % 8-HQ and stabilized by 25 g/L Ludox TMA at different pH values is shown in Figure 30. Above pH 7 emulsions coalesce rapidly forming a lower clear DEP and an upper slightly turbid water phase. Silanol groups are mainly negatively charged rendering the particles hydrophilic. Between pH 7 and 9 the concentration of 8-HQ in water is below 4 mM and the protonated fraction is negligible. The amount of 8-HQ adsorbed on the silica nanoparticles should therefore be small in this region. Above pH 9 the concentration of 8-HQ increases rapidly but only negatively charged molecules with deprotonated hydroxyl groups are dissolved in the aqueous phase. Electrostatic repulsion between these and the silica surface disfavours adsorption in this case.

The emulsions show long-term stability between pH 4 and 5.5. As shown in Figure 4a, the  $\zeta$ -potential of the silica particles possesses values between -20 and +10 mV in this pH range as a result of the 8-HQ adsorption and high ionic strength. The particles are weakly flocculated, more hydrophobic, and therefore able to act as emulsifiers. From pH 5.7 to 4.4, the sediment height increases. According to Figure 25 in this pH range pronounced aggregation of silica particles occurs. Consequently, the sediment consists of flocculated droplets and particles, which have a lower packing density compared to unflocculated droplets. At pH 4.5 also no turbidity in the aqueous phase can be recognized, indicating the complete aggregation and association of the silica particles with the sedimented emulsion phase. Below pH 4 again, only unstable emulsions can be

formed revealing coalescence after minutes. The stability of the emulsions agrees well with the dependence of the contact angle shown in Figure 29.

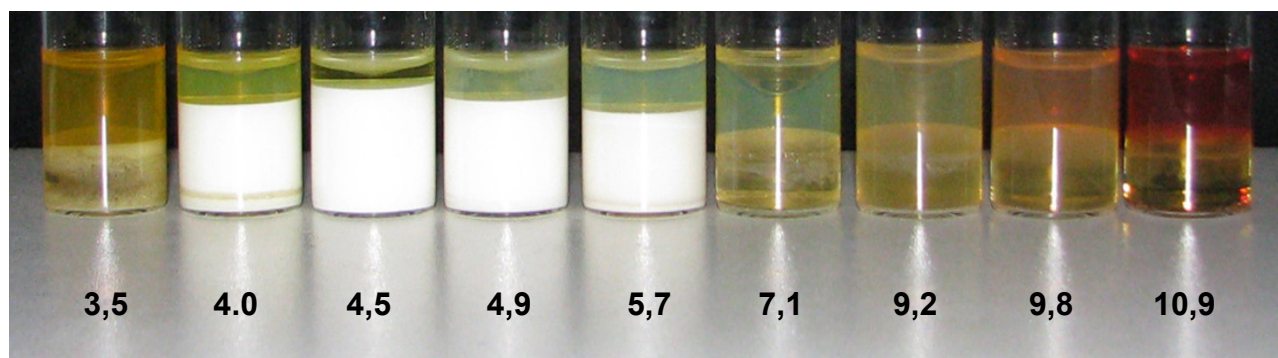


**Figure 30.** Emulsions of 50 vol-% DEP (16,5 wt-% 8-HQ) in water for different pH values after 2 weeks (pH value denoted below the vessels). The white sediment corresponds to the emulsified DEP-phase. The upper clear (or slightly turbid) liquid corresponds to the aqueous phase, whereby the color ranging from yellow to orange corresponds to the 8-HQ content.

### 3.3.3.3 Droplet-size distributions and quantification of particle attachment onto the oil-water interface

Figure 31(a) shows volumetric droplet size distributions for different pH values. At pH 5.6, the monomodal distribution (maximum of 12  $\mu\text{m}$ ) changes, via bimodal distributions, to another monomodal distribution (pH 4.8, maximum 4  $\mu\text{m}$ ). Under mechanical stress (e.g., stirring, centrifugation) 12  $\mu\text{m}$  droplets at pH 5.6 can release DEP and coalesce to bigger droplets. However, 4  $\mu\text{m}$  droplets formed below pH 5 are very stable and can survive centrifugations at  $\text{RCF} \geq 1000$ .

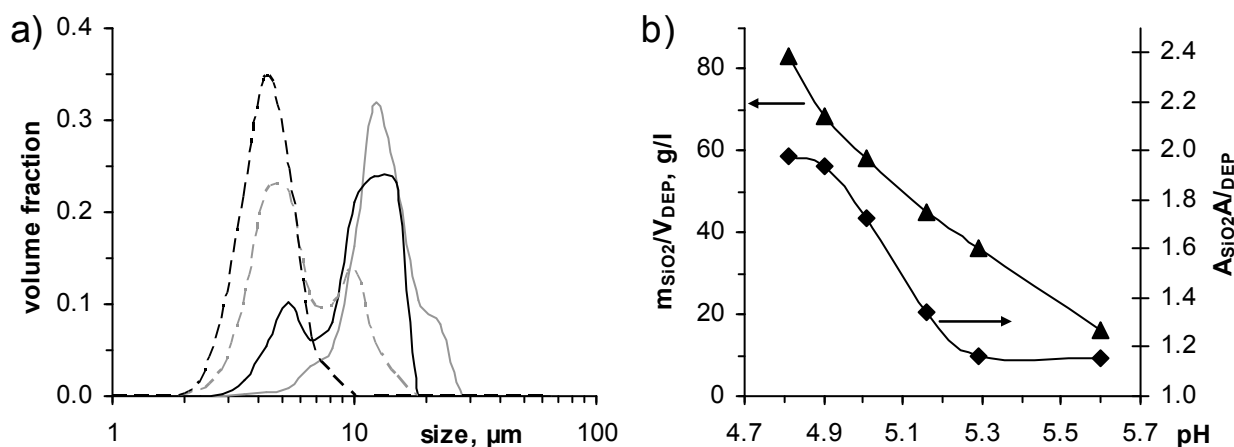


**Figure 31.** (a) Volumetric size distribution of DEP droplets for different pH values (key to lines: grey continuous: pH 5.6, black continuous: pH 5.3, grey dashed: pH 5.1, black dashed: pH 4.8) (b)

Amount of silica nanoparticles attached onto the DEP/water interface as function of pH. Left ordinate: mass per oil volume ( $\blacktriangle$ ), right ordinate: Apparent silica cross section area per total interfacial area ( $\blacklozenge$ ),  $A_{\text{SiO}_2}$  corresponds to total equatorial cross section area of all attached 20 nm spheres;  $A_{\text{Interface}}$  corresponds to total interfacial area of DEP droplets according to the size distribution in Figure 31a.

To determine the silica amount required for the emulsification of a given oil volume, measurements based on the mass balance for the silica particles were done. The results for different pH values are displayed in Figure 31(b) and show a steadily increasing amount of silica from pH 5.6 to 4.8. This can be attributed to the higher demand of particles due to decreasing size of the emulsion droplets and correspondingly due to the increasing interfacial area (Figure 31a). To allow for this effect, the particle attachment is also displayed in terms of total cross section area of attached silica spheres per total interfacial area of the emulsion. For the case where the ratio equals unity, monolayer coverage of emulsion droplets by particles is observed. However, even at pH values above 5.3 more than a monolayer seems to exist on the droplet surface. This observation and the increase of the ratio up to a double monolayer value at pH 4.8 can be attributed to aggregated particle domains on the droplet surface. Below pH 4.8 the requirements of the experimental strategy are not fulfilled because particle aggregation takes place and impedes the separation of droplets and excess particles.

#### 3.3.3.4 Cryo-SEM characterization of the nanoparticle shell

To visualize the droplets shell morphology and to obtain further insights into particle attachment in the pH range below pH 4.8 (Figure 31(b)), Cryo SEM measurements were performed. The images of Figure 32(a) at pH 4.7 clearly show aggregated silica structures on the droplet surface, which are postulated from the particle attachment curve in Figure 31(b). Droplets at pH 4.2 (Figure 32(b)) show incomplete monolayer coverage with some unoccupied regions on the DEP/water interface. Here, the particle hydrophobicity is already insufficient due to the formation of an 8-HQ bilayer and particles begin to repel each other. Hence, the particle attachment curve can be extended at least in qualitative terms. After reaching a maximum between pH 4.8 and 4.5 the amount of attached silica per DEP volume decreases again and the ratio  $A_{\text{SiO}_2}/A_{\text{Interface}}$  decreases below unity slightly above pH 4.2.

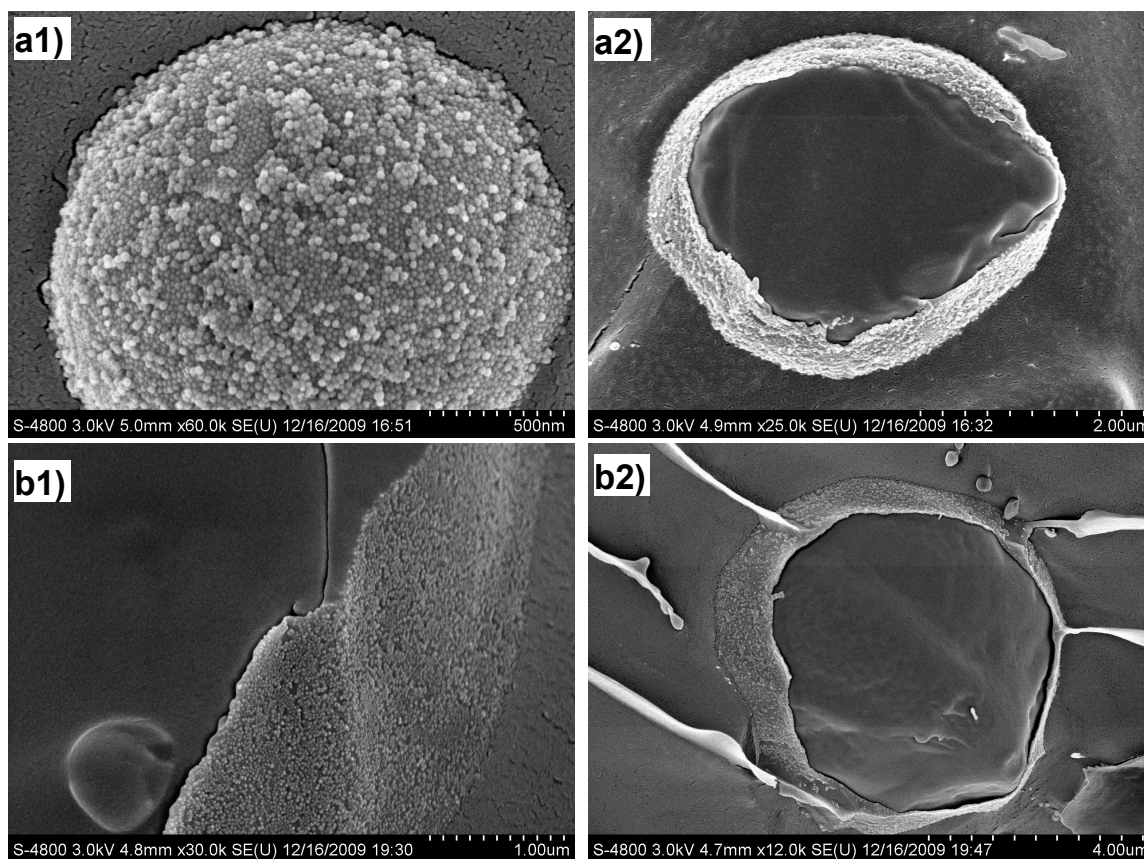


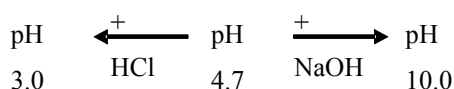
**Figure 32.** Cryo SEM images of silica stabilized DEP droplets (16,5 wt-% 8-HQ) at a1, a2) pH 4.7, b1, b2) pH 4.2. Cross-sectional views onto the droplets are a consequence of the freeze fracture sample preparation.

### 3.3.3.5 pH responsive stability of emulsions

The work explored the pH window in which an emulsion stabilized by silica particles can be prepared. The formed emulsions are stable for at least 1 year (for pH 4.5) of laboratory storage without any observation of coalescence. Another important question is whether the destabilization of a stable emulsion can be triggered by a change in pH. Figure 33 shows that upon addition of strong acid or base in amounts sufficient to shift the pH value significantly our stable emulsion can be destabilized and the formation of two separate phases (DEP and water) is observed. This process does not occur immediately, but after stirring for 1 h both separated phases are obtained.



**Figure 33.** Destabilization of a stable emulsion by either adding acid or base



## 3.3.3.6 Polyelectrolyte deposition on emulsion droplets

The idea of polyelectrolyte multilayer (PE-ML) deposition on the particle stabilized emulsion of diethylphthalate-8HQ in water is motivated by the aim to control the 8-HQ release behaviour. The combination of a weak polyelectrolyte (e.g. PAH, PMAA) with another weak or a strong polyelectrolyte (e.g. PSS, PDADMAC) has been found to show a pH sensitive permeability for macromolecules, probably due to the formation of pores at pH extremes.<sup>134-136</sup> In the present work, the combination of the weak polycation PAH with the weak polyanion PAA was chosen for the experiment. At acidic pH values the primary amines of the PAH carry positive charges, while the carboxylic acids remain uncharged. On the contrary at alkaline pH the amine groups remain uncharged, while the carboxylic groups are strongly charged. Due to the excess charges in the layers (positive at low pH, negative at high pH) a swelling of the multilayers can have an effect on its permeability for 8-HQ at acidic as well as alkaline pH, while at neutral pH the relatively balanced charge ratio leads to a more compact polyelectrolyte film with reduced permeability. However, also the charging of the amphoteric 8-HQ should be considered in this concept. When the PE-ML is positively charged at acidic conditions, also 8-HQ is positively charged while the opposite is true for alkaline pH values. The  $\zeta$ -potential dependence on the layer number and scanning electron micrographs for the polyelectrolyte coated and particle stabilized emulsion droplets are shown in Figure 34.

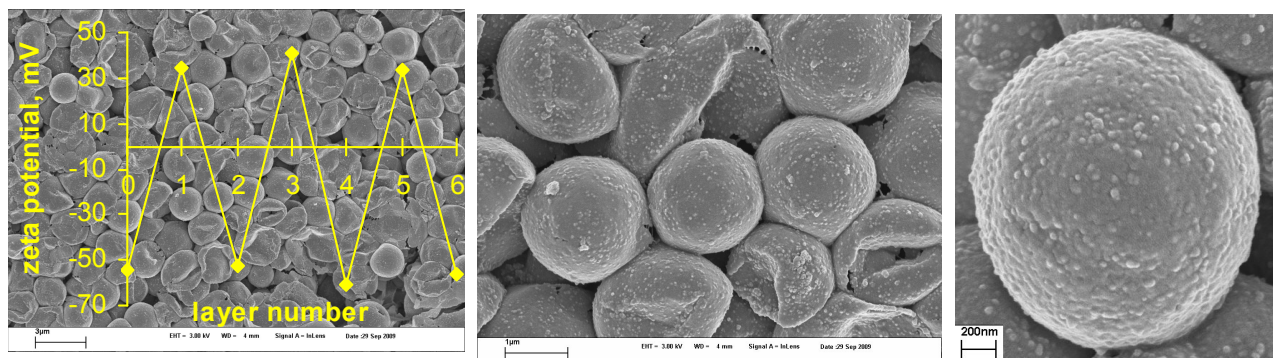


**Figure 34.** Z-potential “zig-zag” diagram for the polyelectrolyte deposition steps and scanning electron micrographs of particle stabilized emulsion droplets after deposition of 3 alternating bilayers of PAH and PAA.

After each polyelectrolyte deposition step the  $\zeta$ -potential of the emulsion droplets was reversed, confirming the successful deposition. It is important to mention, that it is required to maintain the hydrophobicity of the silica particles by keeping the pH value between 4 – 5 during the PE-

deposition (and thereby maintain the adsorption of 8-HQ on silica). If this is not the case, the DEP phase coalesces and complete phase separation occurs during the centrifugation step. However, after the deposition of 3 – 4 single-layers, this becomes less important and the emulsion is also stable at pH values outside the stability range of the uncoated PSE, probably due to the cross-linkage of particles with polyelectrolytes and thereby an improved cohesion of the shell.

The scanning electron micrographs show clearly the change of morphology of the droplet-shell after the PE-deposition (compare Figure 32a1). Also the particle structure can be recognized below the covering PE-ML by dents on the surface. Some of the capsules have collapsed during the drying procedure in vacuum for the SEM preparation. Others retain their spherical framework, probably due to the mechanical rigidity of the aggregated particle skeleton below the PE-ML. It is worthy mentioning, that such a rigidity has not been observed for hollow PE-ML capsules, whether chemically cross-linked<sup>137, 138</sup> or not<sup>134, 139</sup>. Some of the PE-ML coated PSE-droplets have clefts and seem to have bursted during the evaporation of the internal DEP. In the literature also other attempts of polyelectrolyte coated particle stabilized emulsion droplets have been published, but to the knowledge of the author comparable drastic changes of the shell morphology have not been shown.<sup>140, 141</sup>

However, the idea to use PE-ML on PSE for the controlled release of the corrosion inhibitor 8-HQ was not further investigated for several reasons. (i) preliminary experiments showed, that 8-HQ was released irrespective of the pH value, which is in agreement with the results of other researchers, who showed, that PE-ML can only delay the release of small molecules (in the range of tens of seconds)<sup>142, 143</sup>, but not prevent the release totally whether swollen or unswollen. (ii) The anticorrosive action of 8-HQ takes only place at neutral pH values. In its uncharged form it chelates  $Al^{3+}$  ions, but when positively charged itself (at low pH), this chelation does not take place. A pH sensitive release at acidic conditions is thus not necessary. (iii) For the production of the PE-ML coated PSE containing 8-HQ huge volumes of 8-HQ saturated washing water are required. Therefore, a waste-water problem results. Additionally the time consuming procedure make the whole process economically rather unattractive.

One interesting feature of the PE-ML coated PSE droplets is shown in Figure 35. When the outermost layer consists of PAA and the pH value is between 4 – 5 (8-HQ saturated water), the PSE droplets deposit on huge DEP droplets in densely packed arrangements to create an emulsion droplet stabilized emulsion.

It was tested whether this is also possible for PE-ML covered PSE in the absence of 8-HQ. To prove this, a DEP emulsion was stabilized with hexyltrimethylammonium bromide modified silica

particles and subsequently coated with 3 bilayers of PAH and PAA (or PMAA), according to the same procedure as before. After addition of the DEP phase to this PE-ML coated PSE the pH was lowered to 4 and the mixture was shaken for several minutes. The DEP phase was emulsified and coalescence did not take place, also after several hours. But the inspection under the optical microscope did show only sparsely coated huge emulsion droplets. However, by addition of 0.5 mM  $C_{16}TAB$  again the dense arrangement of PE-ML coated PSE-droplets on huge droplets was observed. It can therefore be concluded, that the outermost PAA (PMAA) layer alone does not provide sufficient hydrophobicity at low charge densities (in contrary to chapter 3.2), but the electrostatic interaction with a cationic organic molecule (8-HQ,  $C_{16}TAB$ ) enables the interfacial activity of PE-ML coated PSE-droplets. One interesting question is, if it is possible to observe a mass-transfer of e.g. dissolved fluorescent dyes between the oil-phase of the big and the small emulsion droplets. For this maybe the PE-ML shell must be modified to become more hydrophobic to enable permeability for hydrophobic dyes (e.g. by copolymers with polyelectrolyte and hydrophobic groups or subsequent chemical modification of the PE-ML with hydrophobic moieties).



**Figure 35.** PE-ML coated PSE-droplets attached to DEP droplets. **(b)** two droplets were probably coated during coalescence, the left side of the droplet is attached to the 8-HQ hydrophobized microscopic glass coverslip **(c)** dark field micrograph of a droplet. Scale bar always 20 $\mu$ m

#### 3.3.3.7 Wrecks of particle shells

At the beginning of the project about the 8-HQ encapsulation in a PSE it was not realized that 8-HQ itself can be used for the silica hydrophobization. Thus, another strategy to increase the interfacial activity of the silica particles was pursued. Lanthanum chloride was used to reduce the effective charge of the silica by specific adsorption. However, similar to  $Al^{3+}$ , dissolved  $La^{3+}$  is being chelated by 8-HQ. Thereby in the presence of sufficient 8-HQ the pH value drops from neutral to

around 5.2 until 8-HQ is sufficiently positively charged to become inactive as a chelating agent. The remaining unchelated  $\text{La}^{3+}$  and the positively charged 8-HQ coexist after that in the solution.

In a typical experiment the oil phase DEP-HQ was mixed with an aqueous silica suspension containing 2 mM  $\text{LaCl}_3$ . Immediately the formation of a yellowish precipitate took place. Because the experimenter did not understand the process behind that in this early stage of the work, the precipitate was removed and the emulsion was prepared with the remaining components. Highly stable DEP-HQ in water emulsions were obtained after sonication for several minutes, which partly consisted of grotesque shaped emulsion droplets. After sedimentation of the emulsion droplets, the aqueous supernatant remained turbid for several weeks. The size distribution of the particles in the turbid supernatant was measured by DLS and the result is shown in form of the dashed line in Figure 36(a).

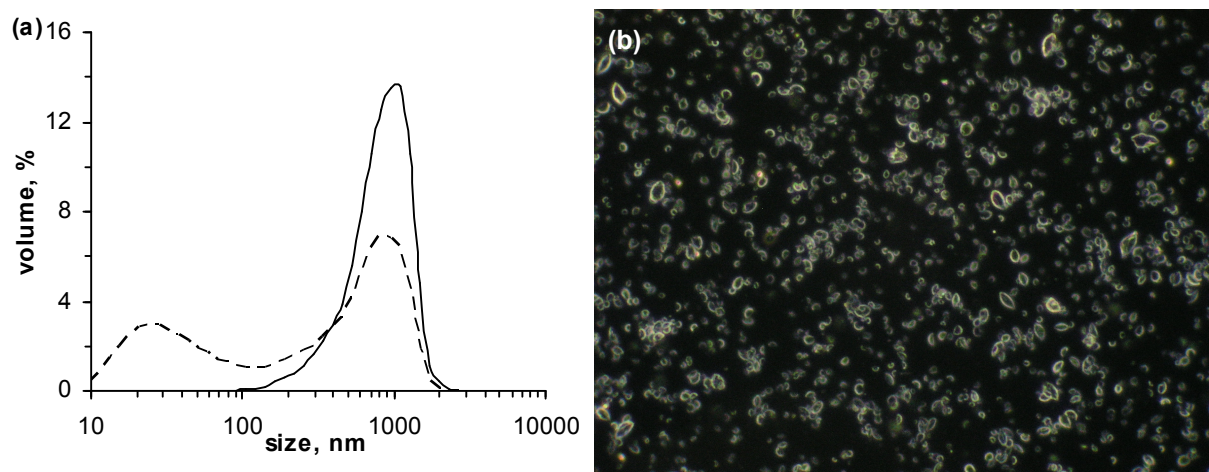


**Figure 36.** (a) Size distribution of the supernatant of a silica PSE (for details see text) before (dashed) and after removal of excess silica nanoparticles by centrifugation (b) dark-field micrograph of silica shell wrecks

The first maximum below 100 nm corresponds to the excess silica particles while the second maximum between 100 nm and 2000 nm corresponds to the mysterious objects shown in the dark-field micrograph in Figure 36(b). It was realized later, that the coaction of positively charged 8-HQ and  $\text{La}^{3+}$  enables strong interfacial aggregation of the silica particles. Under vigorous ultrasonication shell compartments of droplets were thrown back to the aqueous phase, which can be seen in Figure 36(b). Interestingly with an Ultraturrax (rotor-stator-mixer,  $14000 \text{ min}^{-1}$ ) such wrecks were not found, which shows that the heavy impact of cavitation on the particle shells is capable to detach them from their deep energy well at the oil-water interface. Also the formation of grotesque droplet shapes can be understood with the strong interfacial aggregation.

### 3.4 Inhibitor loaded silica/polymer composites

After the properties of the 8-HQ modified silica particles and their emulsification behaviour were studied, the application of the concept for the development of corrosion inhibitor filled reservoirs in anti-corrosive coatings was further developed. But for the application of the 8-HQ filled PSE-droplets in a water-borne coating essential problems remained. The stability of the emulsion is only maintained, when sufficient 8-HQ is dissolved in the water and when the pH value ensures enough positively charged 8-HQ molecules. In the aqueous phase of a water-based resin both conditions are usually not fulfilled and hence the PSE breaks in this environment. Another problem is the high internal stress inside a drying film, which can lead to a breakdown of the PSE-droplets. To compensate for this, it is advantageous to increase the mechanical rigidity of the 8-HQ filled capsules.

It has been shown by Tiarks et al.<sup>48</sup>, that mixtures of styrene and 4-vinylpyridine (4-VP) can be emulsified with silica particles and subsequently polymerized by radical initiation. In this case the interfacial activity of the silica particles is enabled due to an acid-base interaction with 4-VP. In their work, the addition of hexadecane to the monomer-phase enabled also the formation of submicrometer-sized polymer-silica composite particles by the suppression of Ostwald-ripening as mentioned in chapter 1.1.3. In the following this concept is extended to the 8-HQ modified silica PSE and another PSE containing the corrosion inhibitor mercaptobenzothiazol (MBTA). However, the idea of encapsulating materials into such polymerized miniemulsion-droplets is not new and has been developed for many different materials.<sup>144</sup>

#### 3.4.1 Bulk polymerization of the 8-HQ and MBTA concentrated monomer-solution

The solubility of 8-HQ in styrene lies above 20 wt-%, probably due to the chemical similarity of the aromatic molecules. When heating a bulk mixture of styrene containing 18 wt-% 8-HQ, 4 wt-% hexadecane (HD), 0.8 wt-% azo-bis-(isobutyronitril) (AIBN) up to 70°C, AIBN radical initiated polymerization of styrene takes place. After one hour the formation of a few transparent droplets (size  $\approx$  1 mm) is observed. These droplets consist of either of hexadecane or nitrogen from the AIBN decomposition, which can be confirmed by the observation, that they remain transparent (liquid) after cooling to room temperature (also 8-HQ is liquid at 70°C but would crystallize and become opaque upon cooling). After 24 hrs the polymer-melt is still transparent (but slightly

yellowish due to the dissolved 8-HQ). Cooling in an ice bath leads then to the formation of a very light turbidity, which shows also some Rayleigh scattering when transilluminated by light. Some of the initially dissolved 8-HQ seems to nucleate in the form of very small crystals. 8-HQ is better soluble at 70°C, probably also due to its liquid form at this temperature. The optical appearance of the bulk-polymer did not change, also after one month.

MBTA is only very slightly soluble in styrene (< 1wt-%) but well soluble in 4-VP (> 25 wt-%). A mixture of 2:1 (styrene to 4-VP) is capable to dissolve 20 wt-% MBTA. Hence 4-VP has excellent qualities to act as a cosolvent for MBTA in styrene. When polymerizing a mixture of 51 wt-% styrene, 26 wt-% 4-VP, 18 wt-% MBTA, 4 wt-% HD and 0.8 wt-% AIBN again the formation of hexadecane droplets takes place after one hour. After longer time the polymerizing melt becomes opaque and deeply red. In this case the MBTA seems to precipitate also in the polymer-melt.

#### 3.4.2 Polymer and particle size distributions

In the following mainly the development of silica-PS-8HQ composite particles will be discussed, while the silica-PS-4VP-MBTA system will only be mentioned aside. For the preparation of the emulsions the monomer-phases had the same composition as for the bulk polymerization experiments. In the water phase only the mass-fraction of silica particles was varied (for the detailed experimental procedure see chapter 2.9). It is important to recognize that the higher temperature during the polymerization leads also to a higher solubility of 8-HQ in water and thereby losses of encapsulated 8-HQ. With UV-vis spectroscopy the concentration of 8-HQ in water was determined to be 2.2 g/l at pH 4.9 and 70°C (1.4 g/l at pH 4.9 and RT). The losses are therefore small compared to the high content inside the polymer-capsules and can potentially be further reduced by increasing the volumetric fraction of the monomer-phase in the emulsion. However, it is important to prevent crystallisation of the dissolved excess 8-HQ in water during cooling to RT in the presence of the polymer-capsules, because a subsequent separation is difficult (see experimental section, chapter 2.9). By gel-permeation-chromatography (GPC) the molecular weight distribution of the polystyrene from the miniemulsions was measured and the averaged results are shown in

Table 1.

As can be seen in Table 1, in the presence of 18 wt-% 8-HQ the weight average molecular mass ( $M_w$ ) of PS is significantly lowered, while the number average molecular mass ( $M_n$ ) is approximately the same with and without 8-HQ. As a consequence the polydispersity (PDI) decreases because the formation of high molecular mass PS seems to be inhibited in the presence of 8-HQ. The decrease in  $M_w$  could possibly be explained by a chain-growth stopping reaction by 8-

HQ. 8-HQ molecules could react with the radical end of a polymer-chain and become covalently attached to the end of the chain. This would mean a consumption of 8-HQ and thereby a reduction of the content of active molecules per polymer-particle. An estimation of the 8-HQ loss is given in the following calculation. When per PS molecule one 8-HQ molecule gets attached, the fractional decrease of the initial 8-HQ amount equals

$$\frac{\Delta n_{\text{HQ}}}{n_{\text{HQ}}} = 1 - \left( \frac{n_{\text{HQ}} - n_{\text{PS}}}{n_{\text{HQ}}} \right) \quad (3.19)$$

with  $n_{\text{HQ}}$  the initial amount of 8-HQ molecules and  $n_{\text{PS}}$  the amount of polystyrene molecules.

$100 \cdot m_{8\text{-HQ}} / m_{\text{Oil-total}}$	$m_{\text{Particle}} / V_{\text{Oil}}$	$M_{\text{W}}$	$M_{\text{N}}$	PDI
wt-%	g/ml	g/mol	g/mol	-
18	0.064	96010	41550	2.3
18	0.320	85720	41190	2.1
0	0.064	152000	37260	4.1
0	0.320	196500	47630	4.1

**Table 1.** Molecular masses of emulsion polymerized PS,  $M_{\text{N}}$  - number average,  $M_{\text{W}}$  - weight average,  $\text{PDI} = M_{\text{W}}/M_{\text{N}}$  - polydispersity index.  $m_{8\text{-HQ}}/m_{\text{Oil-total}}$  denotes the mass fraction of 8-HQ in the monomer-phase,  $m_{\text{particle}}/V_{\text{Oil}}$  denotes the particle-mass per monomer-volume.

With the expressions  $n_{\text{HQ}} = m_{\text{Oil-total}} \cdot w_{\text{HQ}} / M_{\text{HQ}}$ ,  $n_{\text{PS}} = m_{\text{Oil-total}} \cdot w_{\text{Sty}} / M_{\text{N,PS}}$ , equation (3.19) can be rewritten to

$$\frac{\Delta n_{\text{HQ}}}{n_{\text{HQ}}} = 1 - \left( \frac{w_{\text{HQ}} / M_{\text{HQ}} - w_{\text{Sty}} / M_{\text{N,PS}}}{w_{\text{HQ}} / M_{\text{HQ}}} \right) \quad (3.20)$$

with  $M_{\text{HQ}}$ , the molecular mass of 8-HQ,  $M_{\text{N,PS}}$  the number averaged molecular mass of PS,  $w_{\text{HQ}}$  and  $w_{\text{Sty}}$  the respective mass-fractions of 8-HQ and styrene in the initial monomer-phase mixture. By inserting the numbers ( $w_{\text{HQ}} = 0.18$ ,  $w_{\text{Sty}} = 0.77$ ,  $M_{\text{N,PS}}$  from Table 1)  $\Delta n_{\text{HQ}}/n_{\text{HQ}}$  can be calculated to approximately 0.015 or 1.5 % of the initial 8-HQ, which could possibly become attached to the PS-molecules. It can therefore be concluded that, if this mechanism takes place, it is not capable of considerably lowering the content of active 8-HQ in the polymer-capsules.

In the studied range the silica particle mass per initial monomer volume (and thereby the polymer-particle size, see next section) does probably not influence  $M_{\text{W}}$  neither  $M_{\text{N}}$ . It is not clear if the increase of  $M_{\text{W}}$  in the absence of 8-HQ follows from the increase of  $m_{\text{particle}}/V_{\text{Oil}}$ , because the same effect is not observed in the presence of 8-HQ. It can be concluded, that also in the presence of 8-

HQ polymerization takes place and PS molecules with molecular masses  $> 40000$  g/mol or  $> 400$  styrene monomer units per PS-molecules can be obtained.

The shape of the polymer-silica composite particles is spherical and their size lies in the colloidal range. Because of that, dynamic light scattering is a well suited technique for the measurement of their size distribution. Figure 37(a) shows the measured size-distributions of the polymer-silica composite particles for different initial aqueous silica mass-fractions.

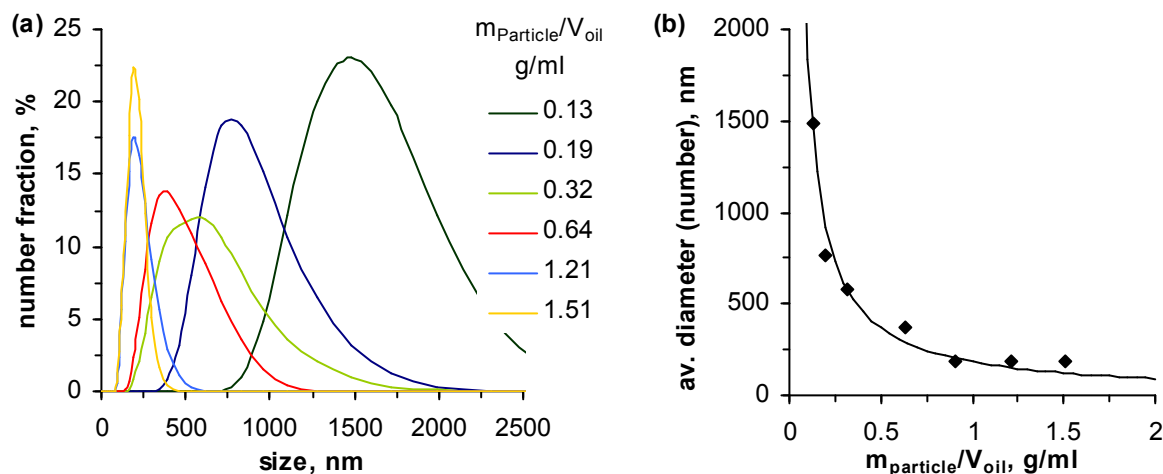


**Figure 37.** (a) Size distribution of silica-polystyrene-8HQ composite particles for different ratios of silica-mass to styrene-8HQ volume. (b) Maximum of the size distributions vs. ratio of silica-mass to styrene-8HQ volume. Diamonds represent measured values, continuous line represents the obtainable size for dense hexagonally packed silica particles on the polymer-surface.

The presence of hexadecane (HD) in the monomer phase enables the formation of droplets with sizes below  $3 \mu\text{m}$ , which maintain their size after polymerization. In the absence of HD the lower droplet-size limit is in the range  $2 - 3 \mu\text{m}$  (see Figure 16 and Figure 31). By increasing the silica particle mass fraction the droplet size can be lowered and the size distributions get less broad. Ultrasonication is capable to create submicrometer sized oil-droplets and the more silica particles are present, the higher the interfacial area that can be occupied by them. The lower limit of the size of the silica-polymer composite particles is around  $200 \text{ nm}$  ( $1.21 \text{ g}_{\text{Silica}}/\text{ml}_{\text{Oil}}$ ). Interestingly this is even smaller than the diameter obtained from equation (1.11) in chapter 1.1.3.2 of  $327 \text{ nm}$ . The droplets might thus not be at their equilibrium size before polymerization.

By the centrifugation of the silica-polymer suspension the silica-polymer composite particles were obtained as the sediment. The supernatant was dried after that and by differential weighing no solids

could be found in it. Therefore, it can be concluded, that all silica nanoparticles are attached to the polymer-particles.

It should be mentioned, that for silica-mass to oil-volume ratios below 0.19 g/ml some 8-HQ crystals were found in the sediment, although the centrifugation occurred at 70°C, and a crystallisation of dissolved 8-HQ in water should not take place. Probably in submicrometer-sized droplets the nucleation of parts of the 8-HQ during the styrene polymerisation leads to losses of the encapsulated inhibitor.

A simple estimation of the obtainable droplet-size for a given amount of particles can be derived. When monodisperse droplets are considered, the mass of particles required to coat the oil-water interface of these droplets equals  $m_p = \rho_{\text{silica}} \cdot V_p \cdot N_p \cdot N_D$  with  $\rho_{\text{silica}}$  the silica density,  $V_p$  the volume per particle,  $N_p$  the number of particles per drop and  $N_D$  the number of droplets. For a  $\theta$  of 90°, spherical droplets and particles,  $N_p$  equals the division of the surface of a spherical droplet (reduced by the packing factor  $\vartheta$ ) with the cross-sectional area of one particle  $N_p = \vartheta \cdot 4 \cdot \pi \cdot R_D^2 / (\pi \cdot r^2)$  and  $N_D$  equals the total oil volume  $V_{\text{oil}}$  divided by the volume of one droplet  $N_D = V_{\text{oil}} / (4/3 \cdot \pi \cdot R_D^3)$  with  $R_D$  the droplet radius and  $r$  the particle radius. By inserting these relations to the equation for the particle-mass and rearrangement for the droplet diameter,  $D$  can be written as

$$D = 2R_D = \left( m_p / V_{\text{oil}} \right)^{-1} \vartheta \cdot r \cdot 8 \cdot \rho_{\text{silica}} \quad (3.21)$$

Thus, the droplet diameter depends reciprocally on the particle mass to oil volume ratio. In Figure 37(b)  $D$  from equation (3.21) is plotted versus  $m_p/V_{\text{oil}}$  for the parameters of the silica particles  $r = 11$  nm,  $\rho_p = 2.2$  g/ml and the hexagonal packing factor  $\varphi = 0.907$ .<sup>‡</sup> Also the average diameters from the measured number distribution are included for comparison. Remarkable agreement between measurement and the simple calculation can be found. This finding confirms the attachment of all silica particles to the polymer-particles.

Figure 38 shows SEM micrographs of the silica-polystyrene-8HQ composite particles for different initial ratios of  $g_{\text{Silica}}/\text{ml}_{\text{Oil}}$ .

Similar to the cryogenic SEM pictures (Figure 19, Figure 32) the silica particles are densely packed on the surface of the polymer-particles. But the silica particles seem to be less aggregated, compared e.g. with the particles on the droplet of Figure 32(a). Important to recognize is, that the

---

<sup>‡</sup>  $N_p$  and  $N_D$  can be expressed by considering the curvature of the droplets, which was done by Kralchevsky<sup>37</sup>. The calculation of the dependency of  $D$  for particles with  $\theta = 60^\circ$  on  $m_p/V_{\text{oil}}$  yielded practically the same curve as in Figure 37(b).

silica particles don't seem to separate from the polymer-core, also when the pH value is increased to the alkaline range. Accordingly, after polymerization the intermediation of 8-HQ between the silica particles and the polymerized core is no longer the reason for the adhesion between both. Because experimental evidence is missing, only speculations can be done about the adhesive force between the silica particles and the PS. Due to the shrinkage of the styrene core during polymerization ( $\rho_{\text{styrene}} = 0.91 \text{ g/ml}$ ,  $\rho_{\text{PS}} \approx 1.05 \text{ g/ml}$ ) the silica particles might have approached close enough to irreversibly aggregate due to the short ranged but strong van der Waals force. The shrinking process during the polymerization might have also resulted in an incorporation of the silica particles into the polymer-matrix by mechanical forces. Finally, also a chemical interaction with the PS might be present and bond the silica particles to the PS. The silica shell enables colloidal stability of the polymer-particles in water due to the negatively charged silanol groups.

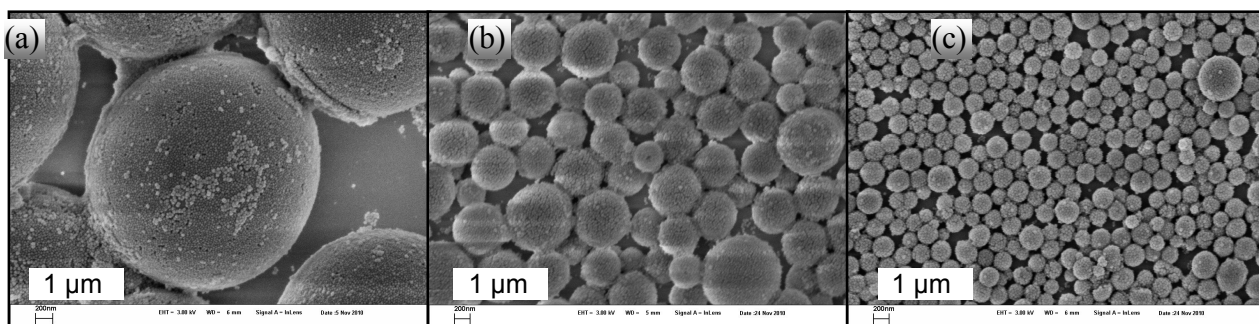


**Figure 38.** SEM images of silica-polystyrene-8-HQ composite particles with different silica-mass to oil-volume ratios: (a) 0.09, (b) 0.32 and (c) 0.91 g/ml. Scale bars correspond to 200 nm.

Similar particles have been obtained for the copolymerization of styrene and 4-VP with dissolved MBTA (18 wt-%) in the monomer mixture. The ability of the silica particles to stabilize this emulsion is owing to an acid-base interaction between 4-VP and silica.<sup>48</sup> It should be highlighted, that the present further development of the already established system of the silica-styrene-4VP emulsion-copolymerization makes not only use of the ability of 4-VP to interact with the silica particles, but also to act as a cosolvent for MBTA. SEM micrographs of the silica-poly(styrene-co-4VP)-MBTA nanocomposite particles are shown in Figure 39.

Also for the composite particles of poly(styrene-co-4VP)-MBTA-silica densely packed silica nanoparticles are found on the surface of the copolymer-particles. One remarkable difference between the system silica-8HQ and silica-4VP seems to be the different wettability. Silica particles modified with 8-HQ are capable of stabilizing foams and emulsion droplets up to sizes in the millimetre-range whereas by shaking a suspension of silica particles modified with 4-VP no foam is

generated at all and also the styrene-4VP-MBTA phase is not emulsified by shaking. Only when very small droplets are generated by ultrasonication, stable emulsions of styrene-4VP-MBTA stabilized with the silica particles can be obtained. It seems that a certain curvature of the emulsion droplets is required to let the silica particles become efficient stabilizers here.

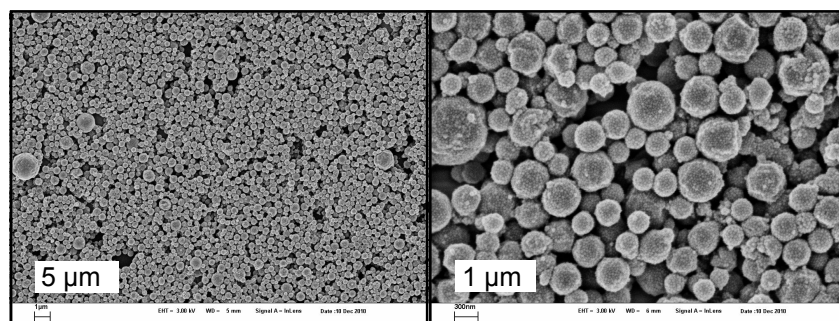


**Figure 39.** Micrographs of poly(styrene-co-4VP)-MBTA-silica nanocomposite particles with two magnifications. The ration  $m_{\text{particle}}/V_{\text{oil}}$  equals 1.21 g/ml.

### 3.4.3 8-hydroxyquinoline release in aqueous solution

The ability of the polymer-particles to release the incorporated 8-HQ into aqueous solution is essential for their later application in an inhibitive anti-corrosive-coating. Therefore, release kinetics of 8-HQ in water were measured by UV-vis spectroscopy. Different particle sizes were examined, to investigate, whether there is an effect of the different diffusion-lengths that 8-HQ molecules have to overcome in the polymer-particles with varying size. The release takes place in a stirred ultra-filtration cell and the transport of 8-HQ at the particle-solution interface should therefore be fast. The mass-concentration of polymer-silica-composite particles was selected so that the available amount of 8-HQ corresponded to 1.2 times the solubility in the given volume of the aqueous phase. Figure 40 shows the measured release kinetics.

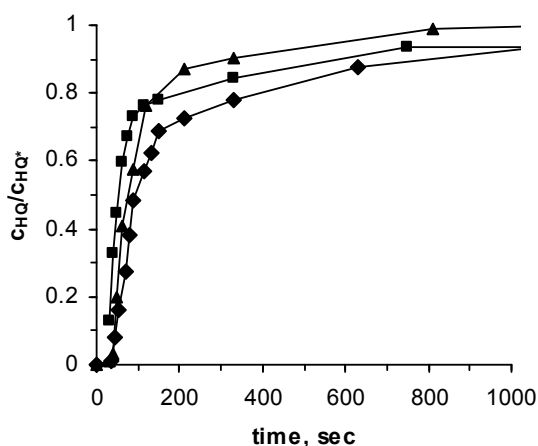


**Figure 40.** Release kinetics of 8-HQ from silica-polystyrene composite particles in aqueous solution at pH 7 (expressed with the ratio of measured 8-HQ concentration  $c_{\text{HQ}}$  and saturation concentration  $c_{\text{HQ}^*}$ ) for different silica-mass to oil-volume ratios: 0.09 (■), 0.32 (▲), 0.64 (◆) g/ml

As can be seen from Figure 40, the release up to approximately 70 - 80 % of the aqueous 8-HQ solubility is taking place in about 2 minutes, almost irrespective of the polymer-particle size. The approach towards the 8-HQ saturation in water is then prolonged asymptotically. The important output of this experiment is the demonstration that the 8-HQ release takes place, but permeation through the inside of the PS core does not seem to limit release.

### 3.4.4 Incorporation of the particles in a water-based alkyd resin

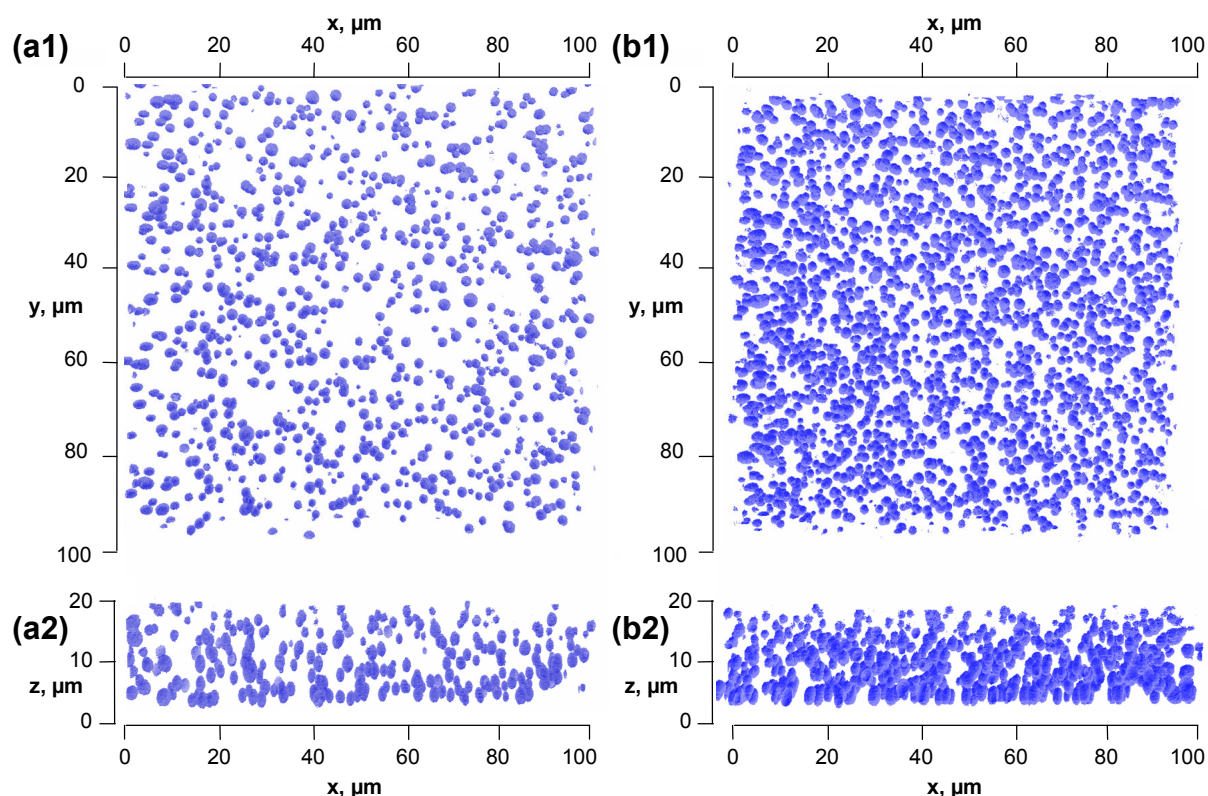


**Figure 41.** CSLM micrographs of silica-PS-8HQ composite particles ( $m_{\text{particle}}/V_{\text{oil}} = 0.13\text{g/ml}$ ) in a dry film of an alkyd-resin on a microscope slide. (a1) & (b1) top-view, (a2) & (b2) side-view, (a) corresponds to 5 wt-% and (b) to 10 wt-% of silica-PS-8HQ composite particles in the dry film. The side view reaches only 25 $\mu\text{m}$  into the y-direction to prevent overcrowding. Important to recognize is that the coordinate  $z = 0$  does not represent the surface of the substrate.

One important decision for the application of the inhibitor filled silica-polymer composite particles is the selection of the resin. Organic solvent based resins cannot be used, because the PS and also the inhibitor molecules would dissolve. Furthermore the colloidal stability could not be provided by the silica-shell and an additional surface modification would be required. Therefore, water-based

resins neither dissolve PS nor big extents of 8-HQ or MBTA. Moreover the dispersability of the silica-polymer composite particles is possible. However, also for water-based resins the particles have limitations. For instance, the particles can be well dispersed in an epoxy-resin emulsion in water, as was tested in this work. But the addition of the amine-hardener leads to a substantial problem. The amine solution shifts the pH value of the mixture to the alkaline region and thereby increases the solubility of 8-HQ or MBTA in water (for 8-HQ see Figure 23). Consequently the amphoteric inhibitors will become negatively charged and distribute freely in the coating matrix. Better compatibility is provided e.g. by an alkyd-resin emulsion in water, which is hardened at neutral pH simply by the oxidation in air. Figure 41 and Figure 42 show the distribution of the silica-PS-8HQ particles in such a resin after dispersion and drying measured with confocal scanning laser microscopy (CSLM).

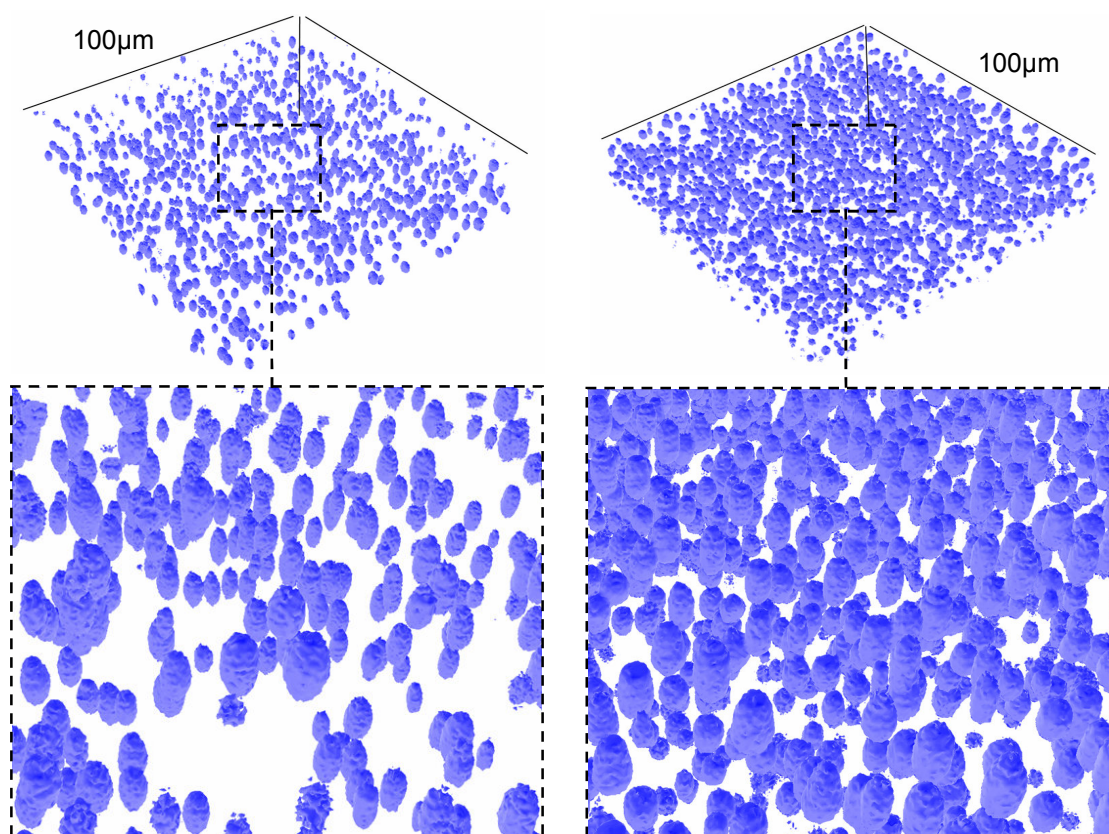


**Figure 42.** Isometric projections of the silica-PS-8HQ particle distribution in the dry film. Left: 5 wt-%, right 10 wt-% of particles. The two zoomed cutouts in the dashed frames have only approximately the same scale.

In Figure 41 & Figure 42 the particles appear egg-shaped from the side-view, which results from the “fluorescence-shadow” that the particles show by scanning vertically through the sample. In fact

the particles are spherical as shown in Figure 38. The particles are well dispersed in the film but by examining Figure 41(a2) and (b2) it can be seen that the particle concentration is increased at  $z \approx 5\mu\text{m}$ . This can be interpreted as a result of sedimentation during the film drying (the particle size is around  $1 - 3 \mu\text{m}$ ). Quantitative information about the film thickness can be obtained from the micrographs, which lies at approximately  $15\mu\text{m}$  for both particle concentrations (the polymer-film might be even thicker, since here only the region with capsules is seen). It is worthy mentioning that the oil soluble fluorescence dye did not leave the polymer particles, although the particles were enclosed by coalescing alky-emulsion droplets during the drying process.

### 3.4.5 Estimation of the percentage of 8-HQ dissolved in the water-phase of the resin

In the following an estimation of the losses of 8-HQ to the aqueous phase of the alkyd-resin emulsion is given. It is first considered that the mass fraction of 8-HQ per capsule does not equal the initial mass fraction in the monomer-mixture, because (i) the additional silica mass on the polymer-particle has to be accounted for and (ii) the squeezing out of hexadecane decreases the total mass. The mass fraction of 8-HQ in a capsule is defined as  $w_{\text{HQ}} = m_{\text{HQ}} / m_{\text{caps}}$  and the mass of a capsule  $m_{\text{caps}} = m_{\text{PS}} + m_{\text{HQ}} + m_{\text{silica}}$  with  $m$  the respective masses. With the number of particles per droplet (polymer-particle)  $N_p$  (section 3.4.2) the silica mass per polymer-particle can be written as  $m_{\text{silica}} = N_p \cdot V_p \cdot \rho_{\text{silica}} = 16/3 \cdot \vartheta \cdot R_D^2 \cdot \pi \cdot r \cdot \rho_{\text{silica}}$ . The mass of the organic core equals  $m_{\text{PS}} + m_{\text{HQ}} = 4/3 \cdot \pi \cdot R_D^3 \cdot \rho_M$  and the therein contained mass of HQ  $m_{\text{HQ}} = (m_{\text{PS}} + m_{\text{HQ}}) \cdot w_{\text{HQ,org}}$  with the PS-8HQ composite density  $\rho_M$  and the mass fraction of 8-HQ in the organic phase  $w_{\text{HQ,org}}$ . Combining the previous equations yields

$$w_{\text{HQ}} = \frac{w_{\text{HQ,org}}}{1 + \left[ 4 \cdot \vartheta \cdot r \cdot \rho_{\text{silica}} / (R_D \cdot \rho_M) \right]} \quad (3.22)$$

By considering that after squeezing out HD the masses of HQ and styrene did not change and that the mass of styrene equals the mass of PS one can write  $w_{\text{HQ,org}} = m_{\text{HQ}}^0 / (m_{\text{Sty}}^0 + m_{\text{HQ}}^0) = w_{\text{HQ}}^0 / (w_{\text{PS}}^0 + w_{\text{HQ}}^0)$  for the mass fraction of 8-HQ in the organic phase. The index 0 denotes the state before polymerization. The density of the polymer-core is approximated by the binary composite density of PS and 8-HQ  $\rho_M = \rho_{\text{HQ}} \cdot \rho_{\text{PS}} / (w_{\text{HQ}}^1 \cdot \rho_{\text{PS}} + (1 - w_{\text{HQ}}^1) \rho_{\text{HQ}})$ .

The mass fraction of capsules in the dried film is defined as  $w_{\text{caps}} = m_{\text{caps}} / (m_{\text{caps}} + m_{\text{resin}})$ , while the initial water content in the resin equals  $w_{\text{H}_2\text{O}} = m_{\text{H}_2\text{O}} / (m_{\text{H}_2\text{O}} + m_{\text{resin}})$ . The soluble mass of 8-HQ in

water equals  $m_{\text{HQ}}^* = m_{\text{H}_2\text{O}} \cdot w_{\text{HQ}}^*$  and the available mass of 8-HQ equals  $m_{\text{HQ}} = w_{\text{HQ}} \cdot m_{\text{caps}}$  with  $w_{\text{HQ}}^*$  the solubility of 8-HQ in water. Combining these relations, one can obtain

$$\frac{m_{\text{HQ}}^*}{m_{\text{HQ}}} = \frac{w_{\text{HQ}}^* w_{\text{H}_2\text{O}} (1 - w_{\text{caps}})}{(1 - w_{\text{H}_2\text{O}}) w_{\text{HQ}} w_{\text{caps}}} \quad (3.23)$$

for the ratio of the in the capsules dissolved vs. available 8-HQ.

The solubility of 8-HQ at neutral pH equals 0.6 g/l ( $w_{\text{HQ}}^* = 6.12 \cdot 10^{-4}$  g<sub>HQ</sub>/g<sub>H<sub>2</sub>O</sub>),  $w_{\text{H}_2\text{O}} = 0.58$ ,  $\rho_{\text{silica}} = 2.2$  g/ml,  $\rho_{\text{PS}} = 1.05$  g/ml,  $\rho_{\text{HQ}} = 1.03$  g/ml,  $w_{\text{HQ}}^0 = 0.18$ ,  $w_{\text{PS}}^0 = 0.771$ ,  $r = 11$  nm,  $\vartheta = 0.907$ . For this set of parameters inserted into equation (3.22) and equation (3.23) Figure 43(a) and (b) respectively are obtained.

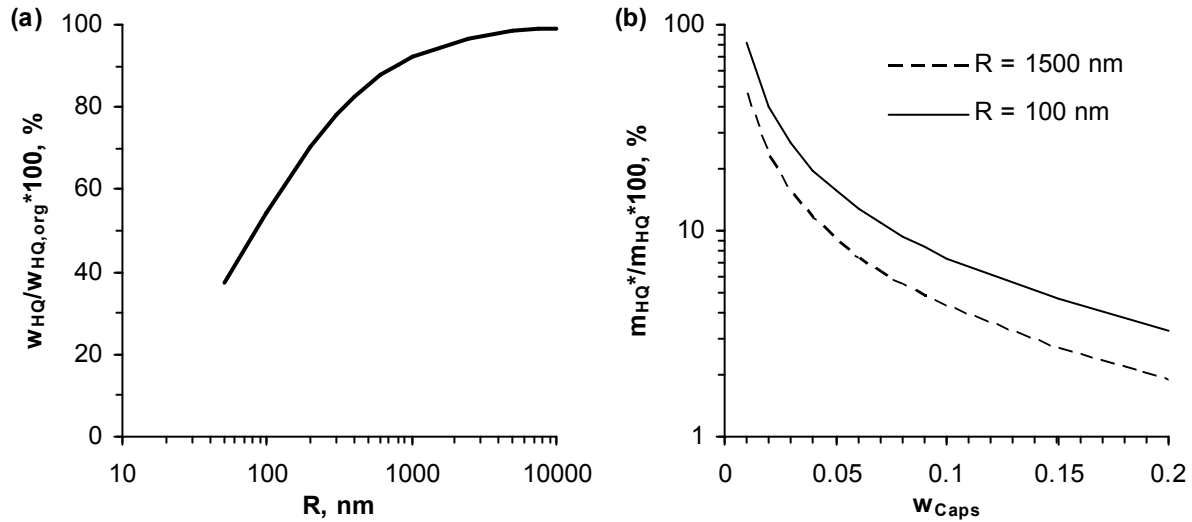


**Figure 43.** (a) Calculated ratio of the 8-HQ mass fraction in silica-nanoparticle covered PS particles vs. the 8-HQ mass fraction in the polymer-matrix ( $w_{\text{HQ}}$  decreases with particle size due to the increasing silica mass fraction). (b) Percentage of 8-HQ losses from the capsules to the aqueous phase of the water-based resin in dependence of the mass-fraction of capsules in the dry film of the resin for two capsule sizes and  $w_{\text{HQ,org}} = 0.189$ .

For big capsule sizes ( $R > 4000$  nm) the contribution of the silica nanoparticle shell is negligible and  $w_{\text{HQ}} \approx w_{\text{HQ,org}}$ , while especially for the submicrometer-size  $w_{\text{HQ}}$  decreases significantly and reaches approximately half of  $w_{\text{HQ,org}}$  for particles with a diameter of 200 nm. The losses of 8-HQ from the capsules to the aqueous phase of the resin are less than 10 % for  $w_{\text{caps}} > 5$  wt-% and for capsules with a diameter of 3  $\mu\text{m}$ , while for capsules with a diameter of 200 nm  $w_{\text{caps}}$  must be bigger than 8 % to maintain 90% of the initial 8-HQ in the capsules.

### 3.4.6 Passive anticorrosive properties

For tests of the anticorrosive properties of alkyd-coatings containing silica-PS-8HQ particles, the average number-diameter of the particles was chosen to be  $1.5 \mu\text{m}$  ( $m_{\text{particle}}/V_{\text{oil}} = 0.13 \text{ g/ml}$ , see Figure 37), because of the ratio  $w_{\text{HQ}}/w_{\text{HQ,org}}$  being close to unity (see Figure 43(a)).

By electrochemical impedance measurements Bode-plots for two alkyd-films containing 10 wt-% of silica-PS-8HQ particles ( $w_{\text{8HQ,org}} = 0.189$ ) on planar plates of the aluminium alloy AA-2024 in 0.1 M NaCl were set up for a period of 10 days. Figure 44(a) shows the importance of a high degree of dispersy of the silica-PS-8HQ particles in the film.

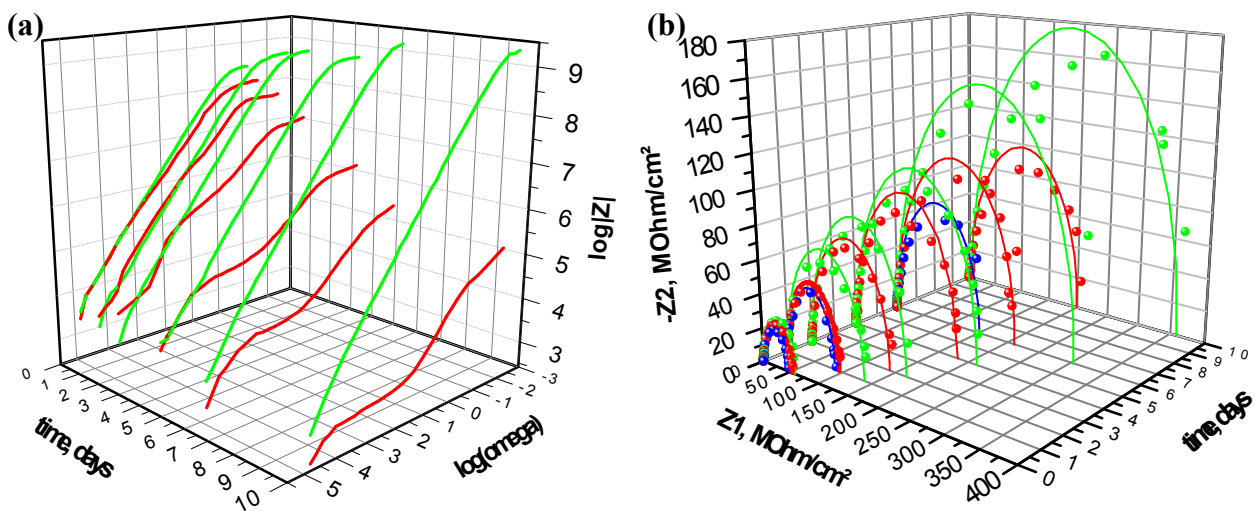


**Figure 44.** (a) Comparison of the impedance of a coating with defects (red) and a homogeneous defect-free coating (green) with both 10 wt-% containers in the Bode Plot. (b) Nyquist Plot of a coating containing 5 wt-% containers without (red) and with (green) hydroxyquinoline. Blue curves represent the blank coating. Points represent measured and continuous lines modelled impedances.

While the green curves represent a film with highly disperse silica-PS-8HQ particles, the red curves represent the effect of aggregated particle domains in the film. On the first day both films have approximately the same values for the impedance. But with time the impedance of the defect-free coating increases, while it falls for the film with defects. Visually the film with defects showed small black spots on its surface after 2 days of immersion in 0.1 M NaCl, which grew in size with time. In these spots electrochemical corrosion of aluminium takes place and during the impedance-measurements they act as conductive areas on the coating, decreasing the overall impedance of the coating. The increase of the black coloured areas around the defects with time indicates so called

filiform corrosion, which denotes the corrosion below the film of alkyd-polymers. The defect free film did not change its morphology over the whole period of 10 days. Defects result from insufficiently dispersing the particles in the water-based resin. This can be prevented by increasing the dispersing time and the agitating speed of the rotor-stator mixing device. From the visual inspection and the electrochemical measurements it can be concluded, that the film containing the 8-HQ doped silica-PS particles is not capable to self-repair defects by the formation of insoluble complexes of 8-HQ and aluminium corrosion products.

In the following the change of the electrochemical impedance over time for defect-free coatings is further examined. The impedance-spectra of these films can also be modelled by the equivalent circuit model of resistor R1 in series with a parallel circuit of a capacitor C1 and a resistor R2 ( $R1(R2/C1)$ ) introduced in chapter 2.11. Figure 44(b), Figure 45(a) and (b) show Nyquist-plots for films containing different weight-fractions of silica-PS particles with (green) and without (red) 8-HQ in the PS capsule matrices, obtained during a period of 10 days. Herein also the comparison between the measured (points) and the modelled (continuous lines) impedance data can be found. For comparison also the impedance of a pure film of the alkyd-resin is included.

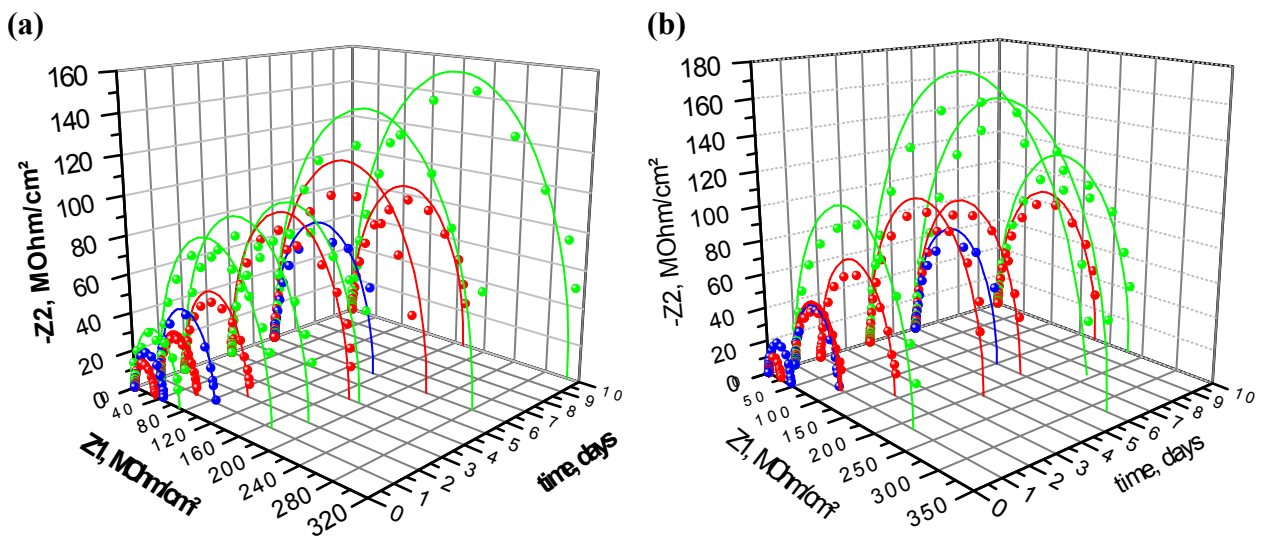


**Figure 45.** Nyquist Plots of coatings containing 10 wt-% (left) and 20 wt-% (right) containers without (red) and with (green) hydroxyquinoline. Blue curves represent the blank coating. Points represent measured and continuous lines modelled impedances.

For all films the Nyquist plots have no contribution from mass transfers, e.g. permeation of water into the films. Furthermore the impedance increases with time. This could possibly be explained by rearrangements of the alkyd-polymers in the film with time, due to a preference to reach a

conformational state of lowest energy. Another explanation might be additional cross-linking of unsaturated bonds in the fatty acid compartments of the film. The films with silica-PS particles have higher values for the impedance after 6 days compared with the blank films. There might be two reasons behind that, (i) the presence of the particles could have decreased the rate of drainage of the film due to a higher viscosity during the dip-coating process resulting in a higher film-thickness or (ii) the particles act as barrier pigments, making the transport of charges through the film a tortuous journey. However, interesting is the observation, that the films with 8-HQ doped silica-PS particles have higher impedances than the films containing silica-PS particles without 8-HQ. There might be an additional passivation on the aluminium surface due to the transport of 8-HQ to the surface. However, to confirm this assumption, the measurements have to be repeated to obtain a more statistical conclusion, since the curves here are averaged from only two measurements. However, the conclusion that the presence of well dispersed silica-polymer-inhibitor composite particles does not worsen the barrier properties of the polyalkyd-film on aluminium can be drawn. It should be recognized here also that the impedance of the alkyd-films is of the same magnitude for all mass-fractions of silica-PS-8HQ and that even mass fractions as high as 20 wt-% don't worsen the impedance of the films.

The obtained data points for the impedance resemble a short circuit appearance of a resistor in series with a parallel circuit of a second resistor and a capacitance  $R_1(C_1/R_2)$  (see chapter 2.11). By numerical fitting the measured data points with this model, corresponding Nyquist plots can be obtained, which are plotted for comparison in Figure 44(b) and Figure 45. The agreement of the model with the measurement is reasonable; deviations might be due to non-ideality. The parameters  $R_2$  and  $C_1$  obtained from the numerical fitting procedure are plotted in Figure 46 in dependence of the time.

As already recognized in the Nyquist-plots the resistance  $R_2$  of all polymer-films increases with time. However for a mass content of 20 wt-%  $R_2$  decreases after 4 days, which might be indicated as local degradation of the film. A higher resistance  $R_2$  of films containing silica-PS-HQ capsules can be observed for most of the cases. Remarkable is the increase of  $R_2$  during 10 days for 5 and 10 wt-% silica-PS-HQ capsules in the film by a factor of 7 and 3, respectively. The capacitance  $C_1$  increases with time while  $C_1$  is higher for alkyd-films containing silica-PS capsules without 8-HQ. Differences of the magnitude of the parameters  $R_2$  and  $C_1$  for films with different weight fractions of silica-PS composite particles cannot be observed. The resistance  $R_1$  is not shown in Figure 46, since its value is three orders of magnitude smaller than the resistance of the polymer-film  $R_2$  and therefore negligible.

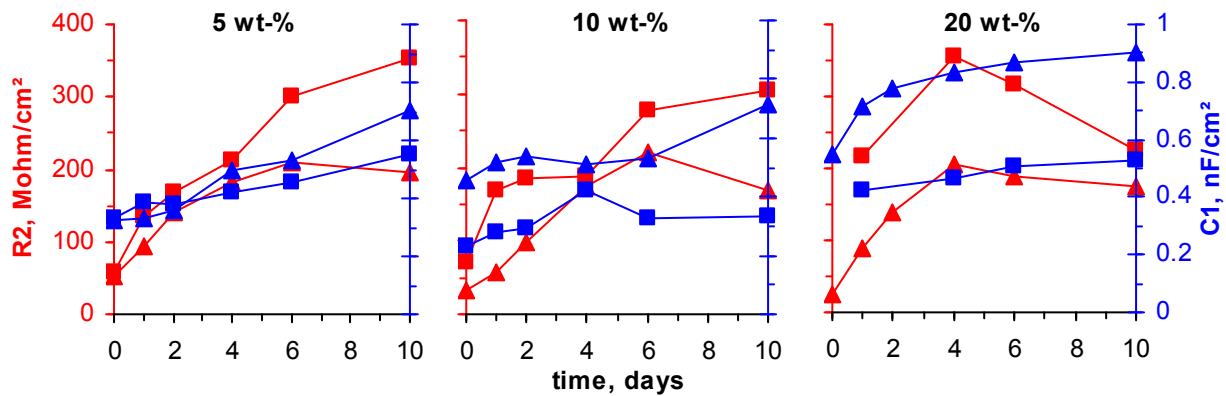


**Figure 46.** Ohmic resistance ( $R_2$ ) and capacitance ( $C_1$ ) of an alkyd polymer-film with different mass fractions of silica-PS capsules on aluminium with (■, ■) and without (▲, ▲) 8HQ in the capsules, obtained from the short circuit analysis ( $R_1(R_2/C_1)$ -circuit) of the impedance spectra shown in Figure 44(b) and Figure 45

### 3.4.7 Active Anticorrosive properties

As was already shown in Figure 44(a) and discussed in the last section, a defect in the film leads to corrosion of the aluminium below the film of alkyd-polymers. In this section the measured current densities above an artificially damaged film during the first 12 hrs after immersion of the coated aluminium plate in an electrolyte solution are discussed. The damage was introduced by scratching the film with a scalpel. For all samples visual changes in the form of black and white areas in the scratch were observed after 12 hrs. This indicates the formation of anodic and cathodic areas, as especially the white colour indicates the precipitation of the corrosion product  $Al_2O_3$  on the cathodic area. Figure 47 shows the maximum current densities, obtained by SVET measurements above the scratch area.

As can be seen for all samples, maximum current densities different from zero can be observed, indicating the formation of an anodic area in the scratch. However, the highest current densities are found for the blank coating, while the addition of 10 wt-% silica-PS-8HQ particles to the coating seems to lower the current density in average and a further reduction can be observed by increasing the mass-fraction of silica-PS-8HQ particles to 20 wt-%. Nevertheless, the scratches were introduced manually to the film. It is therefore not clear, if this method provides good reproducibility of the current density curves, since the scratch areas can differ. Furthermore, as copper inclusions play an important role during the corrosion of this aluminium alloy and their

distribution might not be homogeneous over the surface, the location of the scratch can play a role for the observed current-density curves in this work.

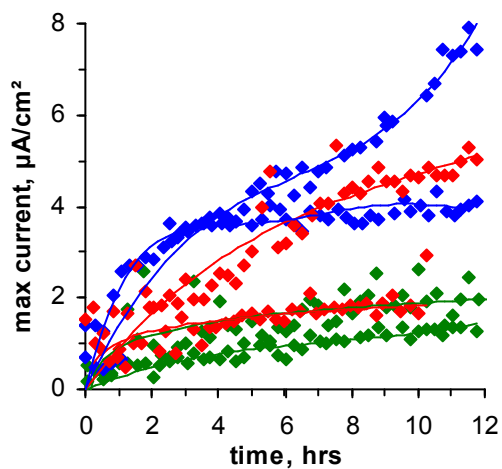


**Figure 47.** Maximum current densities obtained by SVET measurements for scratched alkyd coatings on aluminium in 0.1 M NaCl solution. Blue: blank coating (no containers), red: coating with 10 wt-% containers, green: coating with 20 wt-% containers. Lines are drawn to guide the eye.

### 4 Summary and conclusion

**Modification of the wettability of charged surfaces by the physisorption of short amphiphiles with oppositely charged headgroups.** By increasing the pH value the contact angle ( $\theta$ ) of a water droplet containing 1 mM of alkyltrimethylammonium bromides on a flat silica surface is increased under air and hexane. This results from the higher charge density of the silica surface and the accompanied higher adsorption density of the alkyltrimethylammonium bromides. Increasing the alkylchain length increases  $\theta$  at a given pH value and for a number of carbon atoms ( $n_C$ ) of 12  $\theta$  becomes larger than  $90^\circ$  at alkaline pH values. Emulsions stabilized by silica nanoparticles at these conditions are oil-in-water type, although the measured  $\theta$  on the flat surface suggests a water-in-oil emulsion. Hence, the values obtained for  $\theta$  cannot be directly assigned to nanoparticles, but show qualitatively the trend of  $\theta$  also for nanoparticles. The analysis of the involved surface energies shows that the polar component of the solid surface tension decreases, while the dispersive component increases upon alkylammonium bromide adsorption. For  $\theta < 90^\circ$  mainly the decrease of the surface energy between the silica surface and hexane or air governs the  $\theta$  upon adsorption of alkylammonium bromides, while the influence from the increase of the surface energy between the solid and water becomes pronounced at values of  $\theta$  close to  $90^\circ$ .

**Modification of the wettability of nanoparticles by the adsorption of weak polyelectrolytes (PEs) and their pH-sensitive emulsification behaviour.** The isoelectric point and the pH range of colloidal stability of particles with adsorbed weak PEs depend on the PE conformation varied via the pH during the adsorption step. A strongly coiled PE results in (i) a greater shift of the isoelectric point toward a pH value corresponding to a lower degree of PE dissociation and (ii) a broader pH stability range. Particles with adsorbed weak PEs (polycation or polyanion) can stabilize oil/water emulsions. This fact has been demonstrated for the weak polyacid PMAA on positively charged alumina and for the weak polybase PAH on negatively charged silica. The emulsification characteristics are determined by the surface wettability of the particles and thereby mainly governed by the adsorbed PE layer. Contact angle measurements showed that the wettability depends on the degree of dissociation of the PE shell. The formation of stable Pickering emulsions is possible in a pH range where the degree of dissociation of the adsorbed weak PE lies below 80%. The thickness of the adsorbed PE layer influences the properties of the emulsions with nonpolar oils, enabling for the thicker layer the formation of smaller droplets. The dependency of the droplet size on the emulsion pH value and the PE coating thickness is explained with arguments based on

the particle wetting properties, the particle aggregation state, and the oil phase polarity. There is an optimal pH window (degree of dissociation between 15 and 45%) for the emulsions where the smallest droplets can be obtained. Here, depending on the PE layer thickness, colloiddally stable particles and therefore also nonflocculated droplets can be obtained. Particles with highly charged bare surfaces carrying a totally uncharged PE layer are also able to stabilize emulsions. In this case, emulsions stable to creaming can be obtained because of the formation of a particle-droplet network. Particles that carry PEs with additional nonpolar functional groups (e.g., methyl group) have better emulsifying ability. There are numerous potential combinations of particles (oxides, nitrides, carbides, latexes, etc.) and adsorbed weak PEs (PAH, PAA, PMAA, PEI, HA, etc.) that allow Pickering emulsification.

**Emulsions stabilized by silica nanoparticles as an approach for the encapsulation of the corrosion inhibitor 8-hydroxyquinoline.** Stable o/w-Pickering emulsions with a core consisting of diethyl phthalate containing 8-hydroxyquinoline (8-HQ) stabilized by 20 nm silica particles are obtained in a narrow pH range 4.4 – 5.5. The stabilizing mechanism is based on the adsorption of 8-HQ on the surface of silica nanoparticles rendering them hydrophobic and therefore more interfacially active. Here high emulsion stability is observed with a maximum remaining concentration of 8-HQ in the emulsion droplets and a minimum droplet size. Above pH 5.5, insufficient adsorption of 8-HQ results in unstable emulsions whereas below pH 4.4 the formation of an 8-HQ bilayer on the particle surface and rehydrophilization are responsible for emulsion destabilization. Hence a situation is achieved, where the particle is sufficiently hydrophobic due to molecule attachment, but the functional molecule is to a large extent uncharged to reside predominantly in the oil phase (Scheme 9). The median droplet size for stable emulsions is shifted from 12  $\mu\text{m}$  at pH 5.6 to 4  $\mu\text{m}$  at the lower pH. For stable emulsions, solid shells around droplets are formed by densely attached particles revealing also some aggregated domains. The stability of emulsions can be broken by addition of either acid or base. The emulsions containing about 16 wt % of encapsulated corrosion inhibitor 8-HQ can act as a release system.

The LBL assembly of weak polyelectrolytes on the particle shell of the PSE-droplets was successfully applied without rupture of the soft template. Electron microscopic images show a smoothing of the particle shell. For a weak anionic outer layer and in the presence of cationic organic molecules the PE coated micrometer sized PSE-droplets become interfacially active themselves and deposit on the surface of oil droplets in water.

**Polymerization of the emulsified and 8-hydroxyquinoline enriched oil phase and application in anticorrosive coatings.** On the basis of the hydrophobization of silica particles with 8-HQ, particle stabilized emulsions of styrene containing 18 wt-% of the corrosion inhibitor 8-HQ in water can be fabricated and subsequently polymerized to obtain silica-polystyrene-8HQ composite particles. By the addition of hexadecane and the increase of the silica-nanoparticle concentration the size of the composite particles could be lowered down to 200 nm. The same could be achieved for an emulsion of styrene-4vinylpyridine-mercaptobenzothiazol in water. In aqueous solution the composite particles release 8-HQ rapidly. The composite particles could be dispersed well in a water-based alkyd-resin, as was shown 3-dimensionally by confocal fluorescence microscopy. The losses of 8-HQ from the composite particles to the aqueous phase of the resin are low, when the particles have a high concentration and sizes above 1  $\mu\text{m}$ . Electrochemical impedance measurements show that the addition of the composite particles increases the impedance of an alkyd-film on an aluminium substrate, but also that defects in the film lead to filiform corrosion. Scanning vibrating electrode measurements suggest that the corrosion rate in defects is lowered by the addition of high mass fractions of 8-HQ doped composite particles to the film.

It can be concluded, that 8-HQ doped silica-PS particles alone in the film cannot suppress corrosion totally at damaged sites of the coating, also not at high mass-fractions of the particles. Since the method of encapsulation of organic corrosion-inhibitors in particle-polymer composites is transferable also to other inhibitors, as was shown for the example MBTA, there exists a potential to test other inhibitive molecules. Also the combination of composite-particles, containing different inhibitors, e.g. cathodic and anodic corrosion inhibitors, in water-borne films on a metallic substrate shows potential.

The effective corrosion inhibition in saturated solutions of 8-HQ has been shown by several authors before.<sup>111-114</sup> Therefore, it can be concluded, that the silica-polymer particles do not provide sufficient 8-HQ molecules to prevent corrosion effectively at damaged sites of the coating at the present configuration of the film. This might be true also when the alkyd-polymer film does not provide permeability for 8-HQ molecules, so that only composite particles uncovered at the fractured area of the film supply 8-HQ. On the other hand, increasing the permeability of the film for 8-HQ (e.g. by decreasing the cross linking density) increases also the permeability for corrosive species and weakens thereby the coating. A possible solution for this problem might be a multilayered polymer-film on the metallic substrate. The first layer above the substrate consists of an impermeable film, while the second layer, containing the 8-HQ doped composite particles provides permeability for 8-HQ. To prevent release of 8-HQ to the aqueous phase in case of an

#### 4. Summary and conclusion

---

intact film, a third layer, again highly impermeable would then be required above. When the multilayered film is scratched, the supply of 8-HQ would take place from the total intermediate layer, thereby providing sufficient inhibitive molecules to suppress corrosion in the scratched area. However, economical consideration for this solution might compete with its potential effectiveness.

---

## 5 References

1. Haase, M. F.; Grigoriev, D.; Moehwald, H.; Tiersch, B.; Shchukin, D. G., Nanoparticle Modification by Weak Polyelectrolytes for pH-Sensitive Pickering Emulsions. *Langmuir*, 2011, 27, (1), 74-82.
2. Haase, M. F.; Grigoriev, D.; Moehwald, H.; Tiersch, B.; Shehukin, D. G., Encapsulation of Amphoteric Substances in a pH-Sensitive Pickering Emulsion. *J. Phys. Chem. C*, 2010 114, (41), 17304-17310.
3. Ramsden, W., "Separation of Solids in the Surface-Layers of Solutions and 'Suspensions' (Observations on Surface-Membranes, Bubbles, Emulsions, and Mechanical Coagulation). Preliminary Account." *Proc. R. Soc. London* 1903, 72, (479), 156-164.
4. Pickering, S. U., Emulsions. *J. Chem. Soc.* 1907, 91, 2001-2021.
5. Binks, B. P.; Horozov, T. S., Colloidal Particles at Liquid Interfaces: An Introduction. In *Colloidal Particles at Liquid Interfaces*, Binks, B. P., Ed. Cambridge University Press: New York, 2006; pp 1 - 74.
6. Finkle, P.; Draper, H. D.; Hildebrand, J. H., The Theory of Emulsification. *J. Am. Chem. Soc.* 1923, 45, 2780-2788.
7. Schulman, J. H.; Leja, J., Control of Contact Angles at the Oil-Water-Solid Interfaces - Emulsions Stabilized by Solid Particles (BaSO<sub>4</sub>). *Transactions of the Faraday Society* 1954, 50, (6), 598-605.
8. Gelot, A.; Friesen, W.; Hamza, H. A., Emulsification of Oil and Water in the Presence of Finely Divided Solids and Surface-Active Agents. *Colloids and Surfaces* 1984, 12, (3-4), 271-303.
9. Levine, S.; Sanford, E., Stabilization of Emulsion Droplets by Fine Powders. *Can. J. Chem. Eng.* 1985, 63, (2), 258-268.
10. Menon, V. B.; Wasan, D. T., A Review of the Factors Affecting the Stability of Solids-Stabilized Emulsions. *Sep. Sci. Technol.* 1988, 23, (12-13), 2131-2142.
11. Menon, V. B.; Nikolov, A. D.; Wasan, D. T., Interfacial Effects in Solids-Stabilized Emulsions – Measurement of Film Tension and Particle Interaction Energy. *J. Colloid Interface Sci.* 1988, 124, (1), 317-327.
12. Sullivan, A. P.; Kilpatrick, P. K., The Effects of Inorganic Solid Particles on Water and Crude Oil Emulsion Stability. *Ind. Eng. Chem. Res.* 2002, 41, (14), 3389-3404.
13. Dickinson, E., Interfacial Particles in Food Emulsions and Foams. In *Colloidal Particles at Liquid Interfaces*, Binks, B. P., Ed. Cambridge University Press: New York, 2006; pp 298 - 327.
14. Paulson, O.; Pugh, R. J., Flotation of Inherently Hydrophobic Particles in Aqueous Solutions of Inorganic Electrolytes. *Langmuir* 1996, 12, (20), 4808-4813.
15. Fuerstenau, D. W.; Rosenbaum, J. M.; Laskowski, J., Effect of Surface Functional-Groups on the Flotation of Coal. *Colloids and Surfaces* 1983, 8, (2), 153-174.
16. Gaudin, A. M.; Fuerstenau, D. W., Quartz Flotation with Cationic. *T. Am. Min. Met. Eng.* 1955, 202, (10), 958-962.
17. Levine, S.; Bowen, B. D.; Partridge, S. J., Stabilization of Emulsions by Fine Particles. 1. Partitioning of Particles between Continuous Phase and Oil-Water. *Colloids and Surfaces* 1989, 38, (4), 325-343.
18. Fujii, S.; Read, E. S.; Binks, B. P.; Armes, S. P., Stimulus-Responsive Emulsifiers Based on Nanocomposite Microgel Particles. *Adv. Mater.* 2005, 17, (8), 1014-+.

## 5. References

---

19. Ngai, T.; Behrens, S. H.; Auweter, H., Novel Emulsions Stabilized by pH and Temperature Sensitive Microgels. *Chem. Commun.* 2005, (3), 331-333.
20. Read, E. S.; Fujii, S.; Amalvy, J. I.; Randall, D. P.; Armes, S. P., Effect of Varying the Oil Phase on the Behavior of pH-Responsive Latex-Based Emulsifiers: Demulsification Versus Transitional Phase Inversion. *Langmuir* 2004, 20, (18), 7422-7429.
21. Cesarano, J.; Aksay, I. A.; Bleier, A., Stability of Aqueous Alpha-Al<sub>2</sub>O<sub>3</sub> Suspensions with Poly(Methacrylic Acid) Poly-Electrolyte. *J. Am. Ceram. Soc.* 1988, 71, (4), 250-255.
22. Hackley, V. A., Colloidal processing of silicon nitride with poly(acrylic acid) .1. Adsorption and electrostatic interactions. *J. Am. Ceram. Soc.* 1997, 80, (9), 2315-2325.
23. Lopez, M. C. B.; Rand, B.; Riley, F. L., Polymeric Stabilisation of Aqueous Suspensions of Barium Titanate. Part I: Effect of pH. *J. European Ceram. Soc.* 2000, 20, (10), 1579-1586.
24. Decher, G.; Hong, J. D.; Schmitt, J., Buildup of Ultrathin Multilayer Films by Self-Assembly Process. 3. Consecutively Alternating Adsorption of Anionic and Cationic Polyelectrolytes on Charged. *Thin Solid Films* 1992, 210, (1-2), 831-835.
25. Stamou, D.; Duschl, C.; Johannsmann, D., Long-Range Attraction Between Colloidal Spheres at the Air-Water Interface: The Consequence of an Irregular Meniscus. *Phys. Rev. E* 2000, 62, (4), 5263-5272.
26. Kralchevsky, P. A.; Nagayama, K., Capillary Interactions Between Particles Bound to Interfaces, Liquid Films and Biomembranes. *Adv. Colloid Interface Sci.* 2000, 85, (2-3), 145-192.
27. Nikolaides, M. G.; Bausch, A. R.; Hsu, M. F.; Dinsmore, A. D.; Brenner, M. P.; Weitz, D. A.; Gay, C., Electric-Field-Induced Capillary Attraction Between Like-Charged Particles at Liquid Interfaces. *Nature* 2002, 420, (6913), 299-301.
28. Koretsky, A. F.; Kruglyakov, P. M., SIBIRSKOGO OTDELENIYA AKADEMII NAUK SSSR SERIYA KHIMICHESKIKH NAUK 1971, (2), 1971.
29. Denkov, N. D.; Ivanov, I. B.; Kralchevsky, P. A.; Wasan, D. T., A Possible Mechanism of Stabilization of Emulsions by Solid Particles. *J. Colloid Interface Sci.* 1992, 150, (2), 589-593.
30. Tadros, T. F.; Vincent, B., In *Encyclopedia of Emulsion Technology*, Becher, P., Ed. New York, 1983; Vol. 1, p 129.
31. Aveyard, R.; Clint, J. H.; Horozov, T. S., Aspects of the Stabilisation of Emulsions by Solid Particles: Effects of Line Tension and Monolayer Curvature Energy. *PCCP* 2003, 5, (11), 2398-2409.
32. Aveyard, R.; Clint, J. H., Particle Wettability and Line Tension. *J. Chem. Soc.-Faraday Trans.* 1996, 92, (1), 85-89.
33. Binks, B. P., Particles as Surfactants - Similarities and Differences. *Curr. Opin. Colloid Interface Sci.* 2002, 7, (1-2), 21-41.
34. Aveyard, R.; Binks, B. P.; Clint, J. H., Emulsions stabilised solely by colloidal particles. *Adv. Colloid Interface Sci.* 2003, 100, 503-546.
35. Lopetinsky, R. J. G.; Masliyah, J. H.; Xu, Z., Solids-Stabilized Emulsions: A Review. In *Colloidal Particles at Liquid Interfaces*, Bernard P. Binks, T. S. H., Ed. Cambridge University Press: New York, 2006; pp 186 - 224.
36. Binks, B. P.; Lumsdon, S. O., Influence of Particle Wettability on the Type and Stability of Surfactant-Free Emulsions. *Langmuir* 2000, 16, (23), 8622-8631.
37. Kralchevsky, P. A.; Ivanov, I. B.; Ananthapadmanabhan, K. P.; Lips, A., On the thermodynamics of particle-stabilized emulsions: Curvature Effects and Catastrophic Phase Inversion. *Langmuir* 2005, 21, (1), 50-63.

38. Kaptay, G., On the Equation of the Maximum Capillary Pressure Induced by Solid Particles to Stabilize Emulsions and Foams and on the Emulsion Stability Diagrams. *Colloid Surf. A-Physicochem. Eng. Asp.* 2006, 282, 387-401.
39. Denkov, N. D.; Ivanov, I. B.; Kralchevsky, P. A.; Wasan, D. T., A Possible Mechanism of Stabilization of Emulsions by Solid Particles. *J. Colloid Interface Sci.* 1992, 150, (2), 589 - 593.
40. Nushtayeva, A. V.; Kruglyakov, P. M., Capillary Pressure in a Thinning Emulsion Film Stabilised by Spherical Solid Particles. *Mendeleev Commun.* 2001, (6), 235-237.
41. Nushtaeva, A. V.; Kruglyakov, P. M., Capillary Pressure in Thinning Emulsion Film Stabilized with Solid Spherical Particles. *Colloid J.* 2003, 65, (3), 341-349.
42. Lucassenreynnder.Eh; Vandentempel, M., Stabilization of Water-In-Oil Emulsions by Solid Particles. *J. Phys. Chem.* 1963, 67, (4), 731-&.
43. Binks, B. P.; Lumsdon, S. O., Stability of Oil-in-Water Emulsions Stabilised by Silica Particles. *PCCP Phys. Chem. Chem. Phys.* 1999, 1, (12), 3007-3016.
44. Tambe, D. E.; Sharma, M. M., Factors Controlling the Stability of Colloid-Stabilized Emulsions. 2. A Model for the Rheological Properties of Colloid-Laden Interfaces. *J. Colloid Interface Sci.* 1994, 162, (1), 1-10.
45. Tambe, D. E.; Sharma, M. M., Factors Controlling the Stability of Colloid-Stabilized Emulsions. 3. Measurement of the Rheological Properties of Colloid-Laden Interfaces. *J. Colloid Interface Sci.* 1995, 171, (2), 456-462.
46. Evans, D. F.; Wennerström, H., Surface Chemistry and Monolayers. In *The Colloidal Domain*, Wiley-VCH: New York, 1999; pp 66 - 67.
47. Binks, B. P.; Whitby, C. P., Nanoparticle Silica-Stabilised Oil-in-Water Emulsions: Improving Emulsion Stability. *Colloid Surf. A-Physicochem. Eng. Asp.* 2005, 253, (1-3), 105-115.
48. Tiarks, F.; Landfester, K.; Antonietti, M., Silica Nanoparticles as Surfactants and Fillers for Latexes Made by Miniemulsion Polymerization. *Langmuir* 2001, 17, (19), 5775-5780.
49. Higuchi, W. I.; Misra, J., Physical Degradation of Emulsions via Molecular Diffusion Route and Possible Prevention thereof. *J. Pharm. Sci.* 1962, 51, (5), 459-&.
50. Kabalnov, A. S.; Pertzov, A. V.; Shchukin, E. D., Ostwald Ripening in 2-Component Disperse Phase Systems – Application to Emulsion Stability. *Colloids and Surfaces* 1987, 24, (1), 19-32.
51. Landfester, K., Recent Developments in Miniemulsions - Formation and Stability Mechanisms. *Macromol. Symp.* 2000, 150, 171-178.
52. Tauer, K., Stability of Monomer Emulsion Droplets and Implications for Polymerizations Therein. *Polymer* 2005, 46, (4), 1385-1394.
53. Tsugita, A.; Takemoto, S.; Mori, K.; Yoneya, T.; Otani, Y., Studies on O/W Emulsions Stabilized with Insoluble Montmorillonite-Organic. *J. Colloid Interface Sci.* 1983, 95, (2), 551-560.
54. Thieme, J.; Abend, S.; Lagaly, G., Aggregation in Pickering emulsions. *Colloid Polym. Sci.* 1999, 277, (2-3), 257-260.
55. Horozov, T. S.; Binks, B. P.; Gottschalk-Gaudig, T., Effect of Electrolyte in Silicone Oil-in-Water Emulsions Stabilised by Fumed Silica Particles. *PCCP* 2007, 9, (48), 6398-6404.
56. Ashby, N. P.; Binks, B. P.; Paunov, V. N., Bridging Interaction Between a Water Drop Stabilised by Solid Particles and a Planar Oil/Water Interface. *Chem. Commun.* 2004, (4), 436-437.
57. Stancik, E. J.; Fuller, G. G., Connect the drops: Using Solids as Adhesives for Liquids. *Langmuir* 2004, 20, (12), 4805-4808.

## 5. References

---

58. Evans, D. F.; Wennerström, H., *The Colloidal Domain*. 2 ed.; Wiley-VCH: New York, 1999.
59. Lyne, M. P.; Bowen, B. D.; Levine, S., Double-Layer Interaction between Parallel Solid Cylinders Partially Immersed in an Oil-Water. *J. Colloid Interface Sci.* 1992, 150, (2), 374-385.
60. Fernández-Toledano, J. C.; Moncho-Jordá, A.; Martínez-López, F.; Hidalgo-Álvarez, R., Theory for Interactions between Particles in Monolayers. In *Colloidal Particles at Liquid Interfaces*, Binks, B. P., Ed. Cambridge University Press: New York, 2006; pp 108 - 151.
61. Robinson, D. J.; Earnshaw, J. C., Initiation of Aggregation of Colloidal Particle Monolayers. *Langmuir* 1993, 9, (5), 1436-1438.
62. Aveyard, R.; Clint, J. H.; Nees, D.; Paunov, V. N., Compression and Structure of Monolayers of Charged Latex Particles at Air/Water and Cctane/Water interfaces. *Langmuir* 2000, 16, (4), 1969-1979.
63. Horozov, T. S.; Aveyard, R.; Clint, J. H.; Binks, B. P., Order-disorder Transition in Monolayers of Modified Monodisperse Silica Particles at the Octane-Water Interface. *Langmuir* 2003, 19, (7), 2822-2829.
64. Israelachvili, J., Solvation Forces and Liquid Structure, as Probed by Direct Force Measurements. *Accounts Chem. Res.* 1987, 20, (11), 415-421.
65. Israelachvili, J. N.; Pashley, R. M., Measurement of the Hydrophobic Interaction between 2 Hydrophobic Surfaces in Aqueous-Electrolyte Solution. *J. Colloid Interface Sci.* 1984, 98, (2), 500-514.
66. Levine, S.; Bowen, B. D.; Partridge, S. J., Stabilization of Emulsions by Fine Particles. 2. Capillary and Van der Waals Forces between Particles. *Colloids and Surfaces* 1989, 38, (4), 345-364.
67. Tambe, D. E.; Sharma, M. M., Factors Controlling the Stability of Colloid-Stabilized Emulsions. 1. An Experimental Investigation. *J. Colloid Interface Sci.* 1993, 157, (1), 244-253.
68. Tambe, D. E.; Sharma, M. M., The Effect of Colloidal Particles on Fluid-Fluid Interfacial Properties and Emulsion Stability. *Adv. Colloid Interface Sci.* 1994, 52, 1-63.
69. Leja, J.; Schulman, J. H., Flotation Theory – Molecular Interactions between Frothers and Collectors at Solid-Liquid-Air Interfaces. *Transactions of the American Institute of Mining and Metallurgical Engineers* 1954, 199, (2), 221-228.
70. Fuerstenau, D. W., Effect of pH on Adsorption of Sodium Dodecane Sulfonate at Alumina-Water Interface. *Faraday Discuss.* 1975, 59, 157-168.
71. Manne, S.; Gaub, H. E., Molecular-Organization of Surfactants at Solid-Liquid Interfaces. *Science* 1995, 270, (5241), 1480-1482.
72. Binks, B. P.; Rodrigues, J. A.; Frith, W. J., Synergistic Interaction in Emulsions Stabilized by a Mixture of Silica Nanoparticles and Cationic Surfactant. *Langmuir* 2007, 23, (7), 3626-3636.
73. Binks, B. P.; Rodrigues, J. A., Enhanced stabilization of emulsions due to surfactant-induced nanoparticle flocculation. *Langmuir* 2007, 23, (14), 7436-7439.
74. Wang, J.; Yang, F.; Li, C. F.; Liu, S. Y.; Sun, D. J., Double Phase Inversion of Emulsions Containing Layered Double Hydroxide Particles Induced by Adsorption of Sodium Dodecyl sulfate. *Langmuir* 2008, 24, (18), 10054-10061.
75. Fuerstenau, D. W.; Jia, R. H., The adsorption of Alkylpyridinium Chlorides and their Effect on the Interfacial Behavior of Quartz. *Colloid Surf. A-Physicochem. Eng. Asp.* 2004, 250, (1-3), 223-231.

## 5. References

---

76. Cui, Z. G.; Shi, K. Z.; Cui, Y. Z.; Binks, B. P., Double Phase inversion of emulsions stabilized by a mixture of CaCO<sub>3</sub> nanoparticles and sodium dodecyl sulphate. *Colloid Surf. A-Physicochem. Eng. Asp.* 2008, 329, (1-2), 67-74.
77. Binks, B. P.; Rodrigues, J. A., Double inversion of emulsions by using nanoparticles and a di-chain surfactant. *Angew. Chem.-Int. Edit.* 2007, 46, (28), 5389-5392.
78. Gonzenbach, U. T.; Studart, A. R.; Tervoort, E.; Gauckler, L. J., Ultrastable particle-stabilized foams. *Angew. Chem.-Int. Edit.* 2006, 45, (21), 3526-3530.
79. Akartuna, I.; Studart, A. R.; Tervoort, E.; Gonzenbach, U. T.; Gauckler, L. J., Stabilization of oil-in-water emulsions by colloidal particles modified with short amphiphiles. *Langmuir* 2008, 24, (14), 7161-7168.
80. Megias-Alguacil, D.; Tervoort, E.; Cattin, C.; Gauckler, L. J., Contact angle and adsorption behavior of carboxylic acids on alpha-Al<sub>2</sub>O<sub>3</sub> surfaces. *J. Colloid Interface Sci.* 353, (2), 512-518.
81. Li, J.; Stover, H. D. H., Doubly pH-Responsive Pickering Emulsion. *Langmuir* 2008, 24, (23), 13237-13240.
82. Ashby, N. P.; Binks, B. P., Pickering emulsions stabilised by Laponite clay particles. *PCCP Phys. Chem. Chem. Phys.* 2000, 2, (24), 5640-5646.
83. Wu, W.; Giese, R. F.; Vanoss, C. J., Linkage between Sigma-Potential and Electron Donicity of Charged Polar Surfaces. 1. Implications for the Mechanism of Flocculation of Particle Suspensions with Plurivalent Counterions. *Colloid Surf. A-Physicochem. Eng. Asp.* 1994, 89, (2-3), 241-252.
84. Amalvy, J. I.; Armes, S. P.; Binks, B. P.; Rodrigues, J. A.; Unali, G. F., Use of sterically-stabilised polystyrene latex particles as a pH-responsive particulate emulsifier to prepare surfactant-free oil-in-water emulsions. *Chem. Commun.* 2003, (15), 1826-1827.
85. Binks, B. P.; Rodrigues, J. A., Inversion of emulsions stabilized solely by ionizable nanoparticles. *Angew. Chem.-Int. Edit.* 2005, 44, (3), 441-444.
86. Evans, D. F.; Wennerström, H., Polymers in Colloidal Systems. In *The Colloidal Domain*, second ed.; Wiley-VCH: New York, 1999; p 361.
87. Fixman, M., The Flexibility of Poly-Electrolyte Molecules. *J. Chem. Phys.* 1982, 76, (12), 6346-6353.
88. Forster, S.; Schmidt, M., Polyelectrolytes in Solution. In *Physical Properties of Polymers*, Springer-Verlag Berlin: Berlin 33, 1995; Vol. 120, pp 51-133.
89. Harris, F. E.; Rice, S. A., A Chain Model for Polyelectrolytes.1. *J. Phys. Chem.* 1954, 58, (9), 725-732.
90. Borkovec, M.; Koper, G. J. M., Ising-Models of Polyprotic Acids and Bases. *J. Phys. Chem.* 1994, 98, (23), 6038-6045.
91. Hall, H. K., Correlation of the Base Strengths of Amines. *J. Am. Chem. Soc.* 1957, 79, (20), 5441-5444.
92. Fang, M. M.; Kim, C. H.; Saupe, G. B.; Kim, H. N.; Waraksa, C. C.; Miwa, T.; Fujishima, A.; Mallouk, T. E., Layer-by-layer growth and condensation reactions of niobate and titanoniobate thin films. *Chem. Mat.* 1999, 11, (6), 1526-1532.
93. Kilpatrick, M.; Morse, J. G., The Dissociation Constants of Acids in Salt Solutions. 6. Carbocyclic Carboxylic Acids. *J. Am. Chem. Soc.* 1953, 75, (8), 1854-1856.
94. Gregor, H. P.; Frederick, M., Potentiometric Titration of Polyacrylic and Polymethacrylic Acids with Alkali Metal and Quarternary Ammonium Bases. *J. Polym. Sci.* 1957, 23, (103), 451-465.
95. Kirwan, L. J.; Papastavrou, G.; Borkovec, M.; Behrens, S. H., Imaging the coil-to-globule conformational transition of a weak polyelectrolyte by tuning the polyelectrolyte charge density. *Nano Lett.* 2004, 4, (1), 149-152.

## 5. References

---

96. Evers, O. A.; Fleer, G. J.; Scheutjens, J.; Lyklema, J., Adsorption of Weak Polyelectrolytes from Aqueous Solution. *J. Colloid Interface Sci.* 1986, 111, (2), 446-454.
97. Vandesteeg, H. G. M.; Stuart, M. A. C.; Dekeizer, A.; Bijsterbosch, B. H., Polyelectrolyte Adsorption – A Subtle Balance of Forces. *Langmuir* 1992, 8, (10), 2538-2546.
98. Dobrynin, A. V.; Deshkovski, A.; Rubinstein, M., Adsorption of polyelectrolytes at oppositely charged surfaces. *Macromolecules* 2001, 34, (10), 3421-3436.
99. Sorensen, P. A.; Kiil, S.; Dam-Johansen, K.; Weinell, C. E., Anticorrosive coatings: a review. *J. Coat. Technol. Res.* 2009, 6, (2), 135-176.
100. Restriction of Hazardous Substances Directive. In Directive 2002/95/EC, Union, E., Ed. [eur-lex.europa.eu](http://eur-lex.europa.eu), 2003; pp 19 - 23.
101. Sutton, R. Chromium-6 in U.S. Tap Water; Environmental working group Washington, 2010.
102. Mahdavian, M.; Attar, M. M., Investigation on zinc phosphate effectiveness at different pigment volume concentrations via electrochemical impedance spectroscopy. *Electrochim. Acta* 2005, 50, (24), 4645-4648.
103. Vippola, M.; Ahmaniemi, S.; Keranen, J.; Vuoristo, P.; Lepisto, T.; Mantyla, T.; Olsson, E., Aluminum phosphate sealed alumina coating: Characterization of microstructure. *Mater. Sci. Eng. A-Struct. Mater. Prop. Microstruct. Process.* 2002, 323, (1-2), 1-8.
104. Deya, M. C.; Blustein, G.; Romagnoli, R.; del Amo, B., The influence of the anion type on the anticorrosive behaviour of inorganic phosphates. *Surf. Coat. Technol.* 2002, 150, (2-3), 133-142.
105. Kuznetsov, Y. I., *Organic Inhibitors of Corrosion of Metals*. Plenum Press: New York, 1996.
106. Twite, R. L.; Bierwagen, G. P., Review of alternatives to chromate for corrosion protection of aluminum aerospace alloys. *Prog. Org. Coat.* 1998, 33, (2), 91-100.
107. Fix, D.; Andreeva, D. V.; Lvov, Y. M.; Shchukin, D. G.; Moehwald, H., Application of Inhibitor-Loaded Halloysite Nanotubes in Active Anti-Corrosive Coatings. *Adv. Funct. Mater.* 2009, 19, (11), 1720-1727.
108. Skorb, E. V.; Fix, D.; Andreeva, D. V.; Moehwald, H.; Shchukin, D. G., Surface-Modified Mesoporous SiO<sub>2</sub> Containers for Corrosion Protection. *Adv. Funct. Mater.* 2009, 19, (15), 2373-2379.
109. Shchukin, D. G.; Zheludkevich, M.; Moehwald, H., Feedback active coatings based on incorporated nanocontainers. *J. Mater. Chem.* 2006, 16, (47), 4561-4566.
110. Borisova, D.; Moehwald, H.; Shchukin, D. G., Mesoporous Silica Nanoparticles for Active Corrosion Protection. *ACS Nano* 5, (3), 1939-1946.
111. Casenave, C.; Pebere, N.; Dabosi, F., An electrochemical impedance study of the corrosion inhibition of a 2024 aluminum alloy in neutral chloride solutions. *Mater. Sci. Forum* 1995, 192-194, 599-610.
112. Garrigues, L.; Pebere, N.; Dabosi, F., An investigation of the corrosion inhibition of pure aluminum in neutral and acidic chloride solutions. *Electrochim. Acta* 1996, 41, (7-8), 1209-1215.
113. Szunerits, S.; Walt, D. R., Aluminum surface corrosion and the mechanism of inhibitors using pH and metal ion selective imaging fiber bundles. *Anal. Chem.* 2002, 74, (4), 886-894.
114. Lamaka, S. V.; Zheludkevich, M. L.; Yasakau, K. A.; Montemor, M. F.; Ferreira, M. G. S., High effective organic corrosion inhibitors for 2024 aluminium alloy. *Electrochim. Acta* 2007, 52, (25), 7231-7247.
115. Isaacs, H. S., The Measurement of the Galvanic Corrosion of Soldered Copper Using the Scanning Vibrating Electrode Technique. *Corrosion Sci.* 1988, 28, (6), 547-558.
116. Pawley, J. B., *Handbook of Biological Confocal Microscopy*. Springer: Berlin, 2006.

117. Bolt, G. H., Determination of the Charge Density of Silica Sols. *J. Phys. Chem.* 1957, 61, (9), 1166-1169.
118. Tadros, T. F.; Lyklema, J., Adsorption of Potential-Determining Ions at Silica-Aqueous Electrolyte Interface and Role of Some Cations. *J. Electroanal. Chem.* 1968, 17, (3-4), 267-&.
119. Abendrot, R., Behaviour of a Pyrogenic Silica in Simple Electrolytes. *J. Colloid Interface Sci.* 1970, 34, (4), 591-&.
120. Wängnerud, P.; Jönsson, B., Adsorption of Ionic Amphiphiles as Bilayers on Charged Surfaces. *Langmuir* 1994, 10, 3268-3278.
121. Wangnerud, P.; Jonsson, B., Ionic Surfactants at the Charged Solid/Water Interface – Significance of Premicellar Aggregation. *Langmuir* 1994, 10, (10), 3542-3549.
122. Fowkes, F. M., Additivity of Intermolecular Forces at Interfaces. 1. Determination of Contribution to Surface and Interfacial Tensions of Dispersion Forces in Various Liquids. *J. Phys. Chem.* 1963, 67, (12), 2538-&.
123. Owens, D. K.; Wendt, R. C., Estimation of Surface Free Energy of Polymers. *J. Appl. Polym. Sci.* 1969, 13, (8), 1741-&.
124. Tamai, Y.; Makuuchi, K.; Suzuki, M., Experimental Analysis of Interfacial Forces at Plane Surface of Solids. *J. Phys. Chem.* 1967, 71, (13), 4176-&.
125. Binks, B. P.; Clint, J. H., Solid wettability from surface energy components: Relevance to pickering emulsions. *Langmuir* 2002, 18, (4), 1270-1273.
126. Jasper, J. J., The Surface Tension of Pure Liquid Compounds. *J. Phys. Chem. Ref. Data* 1972, 1, (4), 841-1114.
127. Arditty, S.; Whitby, C. P.; Binks, B. P.; Schmitt, V.; Leal-Calderon, F., Some general features of limited coalescence in solid-stabilized emulsions. *Eur. Phys. J. E* 2003, 11, (3), 273-281.
128. Binks, B. P.; Whitby, C. P., Silica particle-stabilized emulsions of silicone oil and water: Aspects of emulsification. *Langmuir* 2004, 20, (4), 1130-1137.
129. Melle, S.; Lask, M.; Fuller, G. G., Pickering emulsions with controllable stability. *Langmuir* 2005, 21, (6), 2158-2162.
130. Golemanov, K.; Tcholakova, S.; Kralchevsky, P. A.; Ananthapadmanabhan, K. P.; Lips, A., Latex-particle-stabilized emulsions of anti-Bancroft type. *Langmuir* 2006, 22, (11), 4968-4977.
131. Petrov, A. I.; Antipov, A. A.; Sukhorukov, G. B., Base-acid equilibria in polyelectrolyte systems: From weak polyelectrolytes to interpolyelectrolyte complexes and multilayered polyelectrolyte shells. *Macromolecules* 2003, 36, (26), 10079-10086.
132. Albert, A.; Hampton, A., Analogues of 8-Hydroxyquinoline having Additional Cyclic Nitrogen Atoms. 2. Further Preparations, and some Physico-Chemical Properties. *J. Chem. Soc.* 1954, (FEB), 505-513.
133. Ferreiro, E. A.; Debussetti, S. G.; Helmy, A. K., Sorption of 8-Hydroxyquinoline by Some Clays and Oxides. *Clay Clay Min.* 1988, 36, (1), 61-67.
134. Antipov, A. A.; Sukhorukov, G. B.; Leporatti, S.; Radtchenko, I. L.; Donath, E.; Mohwald, H., Polyelectrolyte multilayer capsule permeability control. *Colloid Surf. A-Physicochem. Eng. Asp.* 2002, 198, 535-541.
135. Sukhorukov, G. B.; Fery, A.; Brumen, M.; Mohwald, H., Physical chemistry of encapsulation and release. *PCCP* 2004, 6, (16), 4078-4089.
136. Tong, W. J.; Gao, C. Y.; Mohwald, H., Stable weak polyelectrolyte microcapsules with pH-responsive permeability. *Macromolecules* 2006, 39, (1), 335-340.

## 5. References

---

137. Mauser, T.; Dejugnat, C.; Sukhorukov, G. B., Balance of hydrophobic and electrostatic forces in the pH response of weak polyelectrolyte capsules. *J. Phys. Chem. B* 2006, 110, (41), 20246-20253.
138. Tong, W. J.; Gao, C. Y.; Mohwald, H., Manipulating the properties of polyelectrolyte microcapsules by glutaraldehyde cross-linking. *Chem. Mat.* 2005, 17, (18), 4610-4616.
139. Radtchenko, I. L.; Sukhorukov, G. B.; Leporatti, S.; Khomutov, G. B.; Donath, E.; Mohwald, H., Assembly of alternated multivalent ion/polyelectrolyte layers on colloidal particles. Stability of the multilayers and encapsulation of macromolecules into polyelectrolyte capsules. *J. Colloid Interface Sci.* 2000, 230, (2), 272-280.
140. Akartuna, I.; Tervoort, E.; Studart, A. R.; Gauckler, L. J., General Route for the Assembly of Functional Inorganic Capsules. *Langmuir* 2009, 25, (21), 12419-12424.
141. Li, J. A.; Stover, H. D. H., Pickering Emulsion Templated Layer-by-Layer Assembly for Making Microcapsules. *Langmuir* 26, (19), 15554-15560.
142. Qiu, X. P.; Donath, E.; Mohwald, H., Permeability of ibuprofen in various polyelectrolyte multilayers. *Macromol. Mater. Eng.* 2001, 286, (10), 591-597.
143. Antipov, A. A.; Sukhorukov, G. B.; Donath, E.; Mohwald, H., Sustained release properties of polyelectrolyte multilayer capsules. *J. Phys. Chem. B* 2001, 105, (12), 2281-2284.
144. Landfester, K.; Weiss, C. K., Encapsulation by Miniemulsion Polymerization. In *Modern Techniques for Nano- and Microreactors/-Reactions*, Springer-Verlag Berlin: Berlin, Vol. 229, pp 1-49.